DEVELOPMENT OF AN ACID DEPOSITION MODEL FOR THE SOUTH COAST AIR BASIN

Final Report

Prepared for

California Air Resources Board and the

California Environmental Protection Agency

Contract # 92-311

by

California Institute of Technology

January 28, 1997

Fredrick W. Lurmann

Anthony S. Wexler

Spyros N. Pandis

Stefan Musarra

Naresh Kumar

Susanne V. Hering

John H. Seinfeld (Principal Investigator)

The statements and conclusions in this Report are those of the contractor and not necessarily those of the California Air Resources Board. The mention of commercial products, their source, or their use in connection with material reported herein is not to be construed as actual or implied endorsement of such products.

Table of Contents

		Page
Disclaimer		i
Abstract		iv
Executive Summary		v
1.	**Introduction**	1
2.	**The Aerosol Module**	4
	2.1 Primary Physical and Chemical Processes	4
	2.2 Aerosol General Dynamic Equation	10
	2.3 The Aerosol Module	20
	2.4 Recapitulation of Numerical Methods	25
3.	**Fog and Cloud Processes**	32
	3.1 Aqueous Phase Equilibria	32
	3.2 S(IV) to S(VI) Transformation and Sulfur Chemistry	34
	3.3 Summary	39
4.	**The UAM-AERO Acid Deposition**	40
	4.1 Overview of the Model	40
5.	**Simulation of a Summer Episode**	68
	5.1 Episode Selection	68
	5.2 Meteorological and Air Quality Conditions	68
	5.3 Emissions	70
	5.4 Model Results	71
	5.5 Model Performance	73
	5.6 Deposition	79
6.	**Simulation of a Fall Episode**	173
	6.1 Episode Selection	173
	6.2 Meteorological and Air Quality Conditions	173
	6.3 Emissions	175
	6.4 Model Results	175
	6.5 Model Performance	177
	6.6 Deposition	181
7.	**Sensitivity to Emission Changes**	261
	7.1 Sensitivity to Emission Changes under Summer Conditions	261
	7.2 Sensitivity to Emission Changes under Fall Conditions	267
Conclusions		292

Chapter 1 References 293

Chapter 2 References 294

Chapter 3 References 299

Chapter 4 References 302

Chapter 5 References 307

Chapter 6 References 308

Appendix A Station Plots for the June 23-25, 1987 Episode 309

Appendix B Station Plots for the December 10 and 11, 1987 Episode 327

Appendix C Bimodal Character of Accumulation Mode Aerosol Mass Distributions in Southern California 341

Appendix D Systematic Bias in the Measurement of $PM_{2.5}$ 353

Appendix E EQUIL2.1 User's Guide 383

Appendix F Modelling Urban and Regional Aerosols - I. Model Development 401

The statements and conclusions in this Report are those of the contractor and not necessarily those of the California Air Resources Board. The mention of commercial products, their source, or their use in connection with material reported herein is not to be construed as actual or implied endorsement of such products.

Abstract

A three-dimensional urban acid deposition model has been developed. The model incudes a size- and chemically-resolved aerosol model coupled to a photochemical air quality model. The model is capable of predicting deposition of acidic aerosol species as a function of particle size. The model has been applied to simulate gas and particulate air quality during two episodes of the Southern California Air Quality Study (SCAQS). Simulation results are deemed to be generally good, although uncertainties in key particulate emissions lead to model prediction uncertainties that will need to be sharpened in the future when more accurate emissions inventories can be developed.

Executive Summary

A three-dimensional gas/aerosol atmospheric model is presented that predicts the size-resolved concentrations of all major primary and secondary components of atmospheric particulate matter (PM), including sulfate, nitrate, ammonium, chloride, sodium, elemental carbon, organic carbon, water, and crustal material. Aerosol size resolution is based on a sectional representation, typically extending from 0.01 to 10 μm for aerosols and from 0.01 to 30 μm when fog is present. The model is based on an internally mixed aerosol, wherein all particles in a specific size range are assumed to have the same chemical composition. Gas/aerosol equilibrium is computed based on the SEQUILIB algorithm of Pilinis and Seinfeld. An empirical fog model is included that approximates the effect of fogs on gas-phase photolysis rates, on aqueous-phase chemical reactions of sulfate and nitrate, and on the growth and shrinkage of the aerosol/fog droplet size distribution. The model is applied to simulate atmospheric conditions in the South Coast Air Basin of California during the 24-25 June 1987 and 10-11 December 1987 episodes of the Southern California Air Quality Study (SCAQS). The sensitivity of predicted aerosol levels to changes in source emissions is investigated.

The emissions sensitivity studies illustrate several noteworthy features of the relationship between emissions and ambient concentrations for summer conditions. Reductions in NMOC emissions alone are predicted to lower ozone concentrations by larger amounts than equivalent reductions in NMOC and NO_x. Reductions in NO_x emissions are predicted to reduce aerosol nitrate concentrations by small amounts in the NH_3-limited regions and by close to proportional amounts in NO_x-limited regions. Similarly, reductions in NH_3 emissions are predicted to more effectively reduce aerosol ammonium concentrations in the NO_3-limited regions than in the NO_x-limited regions. The regions where ammonium nitrate formation appears to be NO_3-limited are western, central, and northern portions of the SoCAB. Downwind of the large ammonia sources in the eastern portion of the basin, ammonium nitrate formation is predicted to be NO_x-limited (or HNO_3 limited) and the highest ammonium nitrate concentrations are almost always

predicted to occur in this high ammonia area. Because large portions of the basin are probably NH_3-limited, on average, reductions in ammonia emissions are the next most effective method of lowering PM mass concentrations after direct reductions in primary PM emissions. However, reductions in NO_x emissions are more effective than reductions in NH_3 emissions at the Riverside station. Reductions in SO_2 emissions are predicted to lower ambient sulfate concentrations by significant amounts across the air basin and cause corresponding increases in aerosol nitrate in the NO_3-limited regions. Reductions in NMOC emissions are predicted to slow down the photochemistry and lower both the organic aerosol loadings and ammonium nitrate concentrations. NMOC emissions reductions are predicted to have a larger effect on ammonium nitrate levels than on secondary organic aerosol levels at most locations. The coupling between gaseous emissions and aerosol species concentrations, and the nonlinear nature of the relationships should be considered the design of air quality control strategies for urban areas like the SoCAB.

1. Introduction

Air pollution and acidic deposition in the basins of California are the result of complex gas-, aerosol-, and droplet-phase processes. Our chemical and physical understanding of these processes is embodied in three-dimensional mathematical models that predict the effect of emission changes on airborne pollutant levels and on dry and wet deposition of species.

A number of comprehensive photochemical air quality models have been developed in the last 20 years to predict source attribution of ambient ozone concentrations. They simulate fully 3-dimensional transport and dispersion in an Eulerian reference frame and have a series of scientific modules to simulate emissions, gas-phase chemistry, advection and turbulent diffusion, and dry deposition. Examples include the Urban Airshed Model (UAM), the California Institute of Technology/Carnegie Institute of Technology (CIT) model, the Regional Oxidant Model (ROM), the Regional Acid Deposition Model (RADM), the Acid Deposition and Oxidant Model (ADOM), and the Sulfur Transport Eulerian Model (STEM) (U.S. Environmental Protection Agency, 1994).

The UAM, CIT, and ROM models were initially developed as gas-phase photochemical models to simulate ozone formation over urban (UAM, CIT) and regional (ROM) areas. They include scientific modules for gas-phase chemistry of the NO_x/VOC/ozone photochemical system and dry deposition of gases. The RADM, STEM, and ADOM models were developed to address acid deposition on the regional scale. These regional acid deposition models include treatments of aqueous-phase chemistry, cloud processes, dry deposition of gases and particles, and wet deposition of gases and particles, in addition to gas-phase photochemistry. Sulfate and nitrate are included empirically as aerosol species, but without any detailed aerosol processes or prediction of size distribution.

The most fundamental and rigorous approach to an atmospheric aerosol model is one based on solution of the general dynamic equation of aerosols (Seinfeld, 1986). Such an approach yields an explicit, multicomponent, size-resolved model of atmospheric aerosols. Coupled to a three-dimensional gas-phase photochemical air quality model, the aerosol model produces a fully comprehensive simulation of coupled atmospheric gas/aerosol dynamics. The approaches of Pilinis and Seinfeld (1988), Pandis et al. (1993), and Wexler et al. (1994) fall in this category.

Particulate matter (PM) air quality has long been a critical issue in California; Rubidoux experiences routinely the highest PM_{10} values in the nation and the San Joaquin Valley has frequent PM episodes. As a result of numerous field campaigns, largely conducted in California, the complexity of airborne particulate matter is evident. A three-dimensional model capable of predicting the spatial and temporal distribution of both size- and chemically-resolved aerosols is the subject of the present project. Initial tests of predicted levels of sulfate, nitrate, ammonium, and organics, together with total $PM_{2.5}$ and PM_{10}, in the South Coast Air Basin for the Southern California Air Quality Study (SCAQS), presented in this report, are promising. As might have been expected, predictions are sensitive to assumptions concerning the particulate emissions inventory. In fact, the results obtained as part of this study are the first to demonstrate quantitatively the sensitivity of predicted ambient $PM_{2.5}$ and PM_{10} levels to particulate emissions. The model developed herein can be used by ARB staff in examining PM control strategies.

The third component of the atmospheric aerosol/acid deposition system, after gases and aerosols (sub-10 μm diameter), is droplets. In a real sense, droplet chemistry depends intimately on both gas- and aerosol-phase processes. Droplets, whether fog or cloud, are formed by activation of aerosol particles in supersaturated air, and thus the initial chemical composition of the droplet is that of the activated aerosol. After being formed, droplets function as microscopic aqueous-phase reactors, in which gases dissolve and react. Upon evaporation, a residual aerosol particle remains that reflects the composition of the initial activated particle plus material

generated *in situ* during the droplet's lifetime. To predict the acidity and composition of droplets requires that one model the processes of droplet formation, heterogeneous chemical reaction, and evaporation. This submodel is intimately coupled to models for the gas and aerosol phases. Initial development of a droplet model, coupled to a three-dimensional gas/aerosol model, is reported here. The model was developed to simulate fog formation and fog chemistry in the SoCAB, as previous work has demonstrated conclusively that sulfate levels in the SoCAB can be strongly influenced by the presence of fog (Pandis et al., 1992). However, the fog treatment here falls far short of what is ultimately required - a first - principles treatment of aerosol/cloud microphysics and aqueous-phase chemistry. Time and resources did not permit the development of such a detailed sub-model in the present project. Nevertheless, we are able to draw some preliminary conclusions about the effect of fog processing in the South Coast Air Basin.

The aerosol model "sits atop" a three-dimensional gas-phase air quality model, and is solved simultaneously with it. For the present model, the Urban Airshed Model (UAM) was selected as the host gas-phase air quality model. The UAM is extensively documented in the literature and other than those aspects that are specifically related to the aerosol model, it is not described here.

Chapter 2 is devoted to the science underlying the aerosol submodel. Chapter 3 is a brief discussion of fog modeling. The comprehensive gas/aerosol model is described in Chapter 4. Chapters 5 and 6 present the results of applications of the model to summer and fall SCAQS episodes, respectively. Chapter 7 reports on sensitivity studies with the model. This report includes several appendices. Appendices A and B contain the figures of predicted and observed concentrations at the SoCAB monitoring stations for the summer and fall episodes, respectively. Appendix C is an analysis of the measured SCAQS aerosol size distributions which is relevant to the analysis of model predictions. Appendix D addresses some PM measurement issues. Finally, Appendix E contains the User's Guide for the gas/aerosol thermodynamic model embedded in the aerosol model.

2. The Aerosol Module

2.1 Primary Physical and Chemical Processes

Atmospheric aerosols are generated by a diverse range of physical and chemical processes and can have widely varying chemical compositions. Individual aerosol particles may be solid, liquid, or a mixture of the two. Once in the atmosphere, aerosols undergo a wide variety of chemical and physical processes. Just like gaseous species, they are transported and mixed by the atmospheric flow. Evaporation and condensation of volatile materials cause particles to shrink and grow, whereas coagulation results in the formation of larger particles from smaller ones. Formation of new particles can occur by nucleation of supersaturated vapors. In the presence of supersaturated water vapor, particles exceeding a critical size can become activated to form fog and cloud droplets. Gravitational settling of relatively larger particles can lead to a net vertical transport toward the surface, and dry and wet deposition are the ultimate removal processes for particles in the atmosphere.

2.1.1 Particle Formation and Growth

Condensation and evaporation processes are important in altering particle composition and size in the atmosphere since a significant fraction of atmospheric aerosols consists of volatile compounds. Condensation and evaporation of volatile species occur as a result of super- or sub-saturation of chemical compounds in the gas phase. For some species (e.g., sulfuric acid), with sufficiently low vapor pressure evaporation is insignificant, whereas for others (e.g., water, ammonium nitrate), condensation or evaporation may occur depending on the meteorological conditions and gas-phase concentrations.

The process whereby new particles are formed from supersaturated vapor molecules is nucleation. Nucleation may take place with a single species, termed homomolecular nucleation, or with more than one species, termed heteromolecular nucleation. In addition, when nucleation occurs in the absence of foreign surfaces or material, the process is termed homogeneous nucleation; in the presence of foreign surfaces or material, the process is called heterogeneous nucleation. Particles can be introduced into the atmosphere by two paths: emissions from sources and in situ nucleation. For nucleation of a single species to occur, the vapor concentration of the species must be supersaturated. When sufficient foreign surfaces are present, such as primary particles emitted by sources, condensation of the species may occur on the pre-existing sites, preventing the accumulation of the vapor concentration to the supersaturations required for nucleation to occur. Binary nucleation can take place when the concentrations of both of the two species are below saturation.

Coagulation of particles in the atmosphere can result from differential settling, turbulence, and Brownian motion. Time constants for coagulation as a result of these processes under usual urban ambient conditions are on the order of days for coagulation from differential settling, years for coagulation from turbulence, and the order of hours for Brownian diffusion. Under the most extreme aerosol loadings in the South Coast Air Basin of California (SoCAB), for example, Brownian coagulation may have a small effect on the ambient aerosol size distribution, but other processes such as emissions, deposition, and condensation/evaporation generally dominate as a result of their much shorter time scales. In the San Joaquin Valley, Brownian coagulation time scales are expected to be sufficiently long such that coagulation can be neglected as a factor in shaping the atmospheric aerosol size distribution.

2.1.2 Chemical Transformation

The chemical composition of atmospheric aerosols is complex. The following major aerosol components can generally be expected to be present, in varying amounts, depending on the

source and history of the air mass involved: carbonaceous material (elemental and organic); nitrate; sulfate; ammonium; soil-related material; sea-salt material (for regions near the sea); and water. In addition, aerosol chemical composition is known to vary significantly with particle size. For example, most of the sulfate, ammonium, organic and elemental carbon are in particles of diameters less than 2 μm, while most of the crustal material resides in larger particles. Nitrate may occur in both small and large particles.

Ambient aerosol particles contain water and water-soluble inorganic compounds, elemental carbon, organic compounds and crustal material. The source of NaCl, elemental carbon, crustal material and a portion of the organics is typically direct emission. Most of the ammonium and nitrate, and the remaining organic compounds derive from gas-to-particle conversion processes. Aerosol-phase sulfate is derived from condensation of gas-phase sulfuric acid or from oxidation of dissolved SO_2 in fog droplets. Production of gas-phase sulfuric acid is primarily a daytime occurrence because it is formed by the oxidation of emitted SO_2 by OH radicals. The primary loss mechanisms for sulfuric acid vapor are nucleation, condensation on pre-existing particles, and dry deposition. Loss by condensation on pre-existing particles is significant if the particle loading is high. Typically, locations that have substantial SO_2 emissions, but also lower particle mass loadings, cooler temperatures, and higher relative humidities, are candidates for H_2SO_4 nucleation (Wexler, et al., 1994).

Organic carbon (OC) can either be emitted directly by sources (primary OC) or can be the result of the condensation of low vapor pressure products of the gas-phase reactions of hydrocarbons (secondary OC). For example, organic carbon aerosol accounted for roughly 65% of the fine particulate carbonaceous aerosol on an annual average basis for 1982 in the Los Angeles area (Gray et al., 1986), and 33% of the fine aerosol mass during summer midday periods (Larson and Cass, 1989).

Relative to the levels of any gaseous or particulate pollutants, water vapor is at a high concentration in the atmosphere. Liquid water, in the form of clouds and fog, is frequently

present. Small water droplets can, themselves, be viewed as microscopic chemical reactors into which gaseous species are absorbed, reactions take place, and species evaporate back to the gas phase. Droplets themselves do not always leave the atmosphere as precipitation; more often than not, cloud droplets evaporate before coalescing to a point where precipitation can occur. In terms of atmospheric chemistry, droplets can both alter the course of gas-phase chemistry through the uptake of vapor species and act as a medium for production of species that otherwise would not be produced in the gas phase or would be produced by different paths at a lower rate in the gas phase.

The chemistry that occurs in cloud and fog droplets in the atmosphere has been shown, in the last decade or so, to be highly complex. Most atmospheric species are soluble to some extent, and the liquid phase reactions that are possible lead to a diverse spectrum of products. The aspect of atmospheric aqueous-phase chemistry that has received the most attention is that involving dissolved SO_2. Sulfur dioxide is not particularly soluble in pure water, but the presence of other dissolved species such as H_2O_2 or O_3 displaces the dissolution equilibrium for SO_2, effectively enhancing the solubility of SO_2. Once dissolved, SO_2 can be oxidized to sulfate, a principal contributor to acidic deposition.

2.1.3 Interphase Equilibria

Chemical constituents of aerosols can be classified as nonvolatile or volatile. The inert nonvolatile species form a core upon which other chemical species may condense. For example, sodium and sulfate have such low vapor pressures that they can be considered nonvolatile. NaCl in the aerosol phase reduces the equilibrium vapor pressure of nitric acid, while increasing the vapor pressure of HCl. Both NaCl and H_2SO_4 shift the equilibrium concentrations of the active and volatile species, which affects aerosol mass. Ammonium, sulfate, nitrate, sodium, and chloride typically account for 25% to 50% of the non-water atmospheric aerosol mass. The mass of these inorganics in an aerosol particle, the ambient temperature, and the relative humidity

determine the mass of water in the aerosol. Under conditions of low relative humidity, little or no water may exist in atmospheric aerosol, but under conditions of high relative humidity, water may comprise over half of the total aerosol mass (Pilinis et al., 1989). Ammonia, chloride, nitrate, and water are the primary volatile chemical species in atmospheric aerosols. The inorganics (ammonia, chloride, and nitrate) react with each other and with the two nonvolatile active species (sodium and sulfate) to form ammonium and sodium salts. If the relative humidity is sufficiently high, the aerosol inorganics will form a pure aqueous solution. If the relative humidity is sufficiently low, the aerosol inorganics will form solid salts, and water may be present only in salt hydrates. For intermediate relative humidities, the aerosol may form an aqueous solution in equilibrium with one or more salts. The volatile organic species consist of primary and secondary volatile organic compounds. These species condense if their saturation vapor pressure is exceeded in the gas phase, but they are not expected to undergo significant chemical reaction in the aerosol phase.

The most prevalent approach to modeling the gas/aerosol distribution of volatile species assumes that volatile species in the gas (air) and aerosol phases are in chemical equilibrium (Stelson and Seinfeld, 1982a, b; Bassett and Seinfeld, 1983, 1984; Saxena et al., 1986; Pilinis and Seinfeld, 1987; Watson et al., 1994b). In some cases the time needed to achieve equilibrium is long compared with that in which the local air and particles are in contact, and this is not a good approximation (Wexler and Seinfeld, 1990; Meng and Seinfeld, 1996). An equilibrium model of atmospheric aerosols is an essential tool in analyzing ambient aerosol data and in predictive modeling of atmospheric aerosols. Such a model can calculate important equilibrium properties that are difficult to measure, such as the water content and acidity of the particles. Water can always be assumed to be in equilibrium and content is critical to estimating particle mass, size, and optical properties. The acidity of aerosols is important in possible health effects of inhaled particles.

2.1.4 Deposition

Deposition to the earth's surface is the way in which the atmosphere cleans itself. There are two types of deposition mechanisms: dry deposition, i.e., the uptake at the Earth's surface (soil, water, or vegetation), and wet deposition, consisting of two components: rainout, in which aerosol particles act as cloud condensation nuclei (CCN), form cloud droplets, and are removed when cloud droplets form rain drops and fall to the ground; and washout, in which rain drops remove aerosol particles by impaction as they fall through the air. Wet deposition can be measured conveniently by sampling precipitation; dry deposition is a slower process that cannot be easily measured. It is possible, however, to measure the downward flux of airborne materials by micrometeorological methods that do not interfere with the natural characteristics of the surface.

Fogs and clouds contribute to both production and removal of aerosols. Precipitating clouds provide an important removal mechanism for particles (wet deposition). Nonprecipitating clouds can also dramatically affect the aerosol size distribution through activation of aerosol as cloud condensation nuclei (CCN). Aerosol activation (i.e., the growth of particles when their critical saturation ratio is less than the ambient saturation ratio of water) depends on the cooling rate and on the number, size distribution, and composition of the particles. Typically (depending on the cloud's maximum supersaturation), particles larger than 0.06-0.16 μm in diameter can be activated to grow to cloud droplets. Upon evaporation of the cloud, a new aerosol spectrum results from the particles formed from the non-volatile material in the cloud drops. The nucleation scavenging process described above dominates all other in-cloud scavenging mechanisms for aerosols.

2.2 Aerosol General Dynamic Equation

Due to limitations in current instrumentation little information is available about the degree of mixing of aerosol particles. A few investigators (Covert and Heitzenberg, 1984; McMurry and Stolzenburg, 1989) have shown that ambient aerosol particles are not externally mixed with respect to water. However, due to lack of further information and computational cost, it is prudent for the purposes of model development to assume that aerosol particles are internally mixed. That is, the particle composition is only a function of particle size. The general dynamic equation that describes the evolution of such an aerosol over time is

$$
\begin{aligned}
&\frac{\partial q_i(m,z,t)}{\partial t} \quad (\textit{local rate of change}) \\
&+(V(z,t)-V_s(m)\,k)\cdot\nabla q_i(m,z,t) \quad (\textit{advection, settling}) \\
&=H_i(m,z,t)\,q(m,z,t)-\frac{\partial(mq_iH)}{\partial m} \quad (\textit{cond./evap.}) \\
&+\int_0^m \beta(m',m-m',z,t)\,q_i(m',z,t)\,\frac{q(m-m',z,t)}{m-m'}\,dm' \quad (\textit{coag. in}) \\
&-q_i(m,z,t)\int_0^\infty \beta(m',m,z,t)\,\frac{q(m',z,t)}{m'}\,dm' \quad (\textit{coag. out}) \\
&+\nabla\cdot(K(z,t)\ \nabla q_i(m,z,t)) \quad (\textit{spatial diffusion}) \\
&+E_i(m,z,t) \quad (\textit{primary emissions}) \\
&+R_i(m,z,t) \quad (\textit{chemical reaction}) \\
&+N_i(m,z,t) \quad (\textit{nucleation})
\end{aligned}
\tag{2.1}
$$

where $q(m, z, t)$ is the total mass distribution such that $q_i(m, z, t)\,dm$ is the mass concentration of species i (there are s species) in the mass range $[m, m+dm]$ and $q=\Sigma q_i$, m_i is the mass of species i in a particle of total mass $m = \Sigma m_i$, $H_i=(1/m)dm_i/dt$ is the

inverse of the characteristic time for particle growth due to condensation or evaporation, $H = \Sigma H_i$, $\beta(m, m') = \beta(m', m)$ is the binary coagulation coefficient, z is the spatial coordinate, t is the temporal coordinate, V is the wind velocity vector, V_s is the settling velocity, k is the unit vector in the vertical direction, $K(z, t)$ is the turbulent diffusion tensor, E is the emission rate, R_i is the rate of mass change of species i due to aerosol-phase chemical reactions, and N_i is the nucleation rate of species i. The derivations of the condensation/evaporation and coagulation terms have been derived by Pilinis (1990). The spatial advection and spatial diffusion terms are stated in Pilinis and Seinfeld (1988).

The above equation, referred to as the internally-mixed aerosol dynamic equation (IMADE), describes the processes that affect the size and composition of aerosol particles in the atmosphere. Ambient aerosol particles contain water and water soluble inorganic components including Na^+, H^+, NH_4^+, Cl^-, NO_3^-, and SO_4^{2-}, elemental carbon, organic compounds, and crustal material. The source of NaCl, elemental carbon, crustal material, and a portion of the organics (primary) is typically direct emission. Most of the ammonium and nitrate, and the remaining organic compounds are produced by gas-to-particle conversion processes. The aerosol-phase sulfate is derived from condensation of gas-phase sulfuric acid or from aqueous-phase oxidation of SO_2 in clouds and fogs. In the following paragraphs we will discuss in a little more detail the various terms of the IMADE.

2.2.1 Term-by-Term Analysis

A number of numerical methods have been proposed for the solution of the aerosol general dynamic equation. For atmospherically relevant aerosol modeling, simplifying assumptions can be employed that increase the runtime performance of the solution algorithms without significantly affecting the predictions. In particular it is instructive to examine and compare the magnitude of each term in the IMADE. Under circumstances when the effect of a term is small, we can choose not to expend additional computational effort on its evaluation.

Large Scale Spatial Transport

Particles are advected by the local wind velocity field, V, and diffuse due to atmospheric turbulence, parametrized according to K-theory using the turbulent diffusion tensor K. Aerosol-phase species advect and diffuse just as gas-phase species do, so these terms in the IMADE can be readily and efficiently solved by the same methods used for the gas-phase species as long as the particle size discretization is the same in adjoining cells. Thus fixed particle size bins are used in the model, and as with the gas-phase species operator splitting is used to separate the spatial terms from the other terms in the IMADE. The solution of the corresponding spatial diffusion and advection terms is therefore done in the gas-phase module and not in the aerosol module.

Condensation and Evaporation

Modeling of condensation and evaporation is essential in discerning the impact of the secondary aerosol species on aerosol formation. This term could be eliminated from consideration if circumstances arise such that the aerosol is mostly composed of primary species-that is, atmospheric transformation of the primary gaseous emissions does not lead to production of significant aerosol mass compared to the mass of primary emissions. Under typical conditions in inland locations of the SoCAB up to 70% of organics (Turpin and Huntzicker, 1991) and 90% of the inorganics (Eldering et al., 1991) are secondary. Thus the condensation and evaporation terms will rarely be insignificant compared to the other terms in the IMADE.

Gravitational Settling

Vertical transport of aerosol particles is governed by turbulent diffusion, advection, and gravitational settling. It is expected that for the smallest aerosol particles gravitational settling will be negligible compared to diffusion (Seinfeld, 1986), but that for sufficiently large particles gravitational settling will be significant. Gravitational settling can affect both vertical transport above the surface and deposition to the surface. Gravitational settling is significant if the settling velocity, V_s, is comparable or larger than the deposition velocity in the absence of settling, V_d. The settling velocity is given by

(Seinfeld, 1986)

$$V_s = \frac{D_p^2 \rho_g g}{18\mu} \tag{2.2}$$

where D_p is the particle diameter, ρ its density, g=9.8 m s^{-2} the gravitational constant, and μ is the viscosity of air. The deposition velocity can be estimated as

$$V_d = \frac{\kappa^2 V(z_1)}{\ln(z_1/z_0)} \; / \; (2.6 + \ln(z_1/z_0)) \tag{2.3}$$

where κ=0.4 is the von Karman's constant, $V(z_1)$ is the average wind speed at a reference height z_1 , and z_0 is the roughness height. Assuming that particle settling may affect deposition when $V_s > 0.1\ V_d$, then settling is important for the removal of particles larger than

$$D_p > \sqrt{\frac{1.8\mu}{\rho_g g} \frac{\kappa^2 V(z_1)}{\ln(z_1/z_0)} \; / \; (2.6 + \ln(z_1/z_0))} \tag{2.4}$$

For example, evaluating this expression for z_1 =10 m, z_0=2 m, $V(z_1)$=3 m s^{-1} and μ=2 10^{-5} kg m^{-1} s^{-1} , and ρ=1000 kg m^{-3} , we find that settling can be safely neglected for submicron particles, but it can accelerate the removal of particles with diameters larger than roughly 10 μm.

Gravitational settling may also affect the aerosol vertical concentration profile due to enhanced vertical transport in the bulk fluid above the surface. The ratio K/V_s defines a characteristic length over which turbulent diffusion and gravitational settling are to be compared. For atmospheric modeling the characteristic length for vertical concentration changes is the cell height, Δz. Let us assume that gravitational settling will influence the

concentration profile when $V_s > 0.1\ K/\Delta z$ or equivalently

$$D_p > \sqrt{\frac{1.8\mu}{\rho_p g}\frac{K}{\delta z}} \sim 6\ 10^{-4}\sqrt{\frac{K}{\Delta z}} \qquad (2.5)$$

Under typical daytime conditions in the SoCAB, the atmosphere below the inversion is unstable and the turbulent diffusivity is of the order of 30 $m^2\ s^{-1}$. For cell heights of the order of 500 m, only the concentrations profiles of giant particles (Dp > 100 μm) will be affected by gravitational settling. Under nighttime conditions, the atmosphere is stably stratified or neutral, and we expect turbulent diffusivity values of the order of 1 $m^2\ s^{-1}$. Using again a rather large cell height of 400 m, only the concentration profiles of particles larger than 30 μm in diameter will be affected by gravitational settling. Since we are interested in particles smaller than 10 μm in diameter, gravitational settling is considered only in the surface cells as an additional sink of particles and a contributor to the overall deposition flux. This deposition term is used as boundary condition and is not included explicitly in the IMADE.

Nucleation

It is anticipated that heterogeneous nucleation of sulfuric acid with water and possible separate nucleation of organic compounds may occur in and near plume sources of SO_2, radicals, and low volatility organics. Nucleation in the atmosphere is a significant source of aerosol particles (aerosol number), but a negligible source of aerosol mass. Since the focus of this study is on the simulation of aerosol mass and not aerosol number and detailed plume modeling is not currently included in most grid-based models, including UAM, nucleation is assumed to be negligible.

Coagulation

The coagulation of particles in an aerosol population is faster for collisions of very small particles with very large ones. The major effect of coagulation is the shaping of the aerosol number distribution by acting as a sink of the small particles. The contribution of these small particles, usually smaller than 20 nm, to the aerosol mass distribution is

negligible. The change of diameter of a large particle colliding with a small one is also negligible. Therefore, the effect of coagulation on the atmospheric aerosol mass distribution in timescales of the order of a day can be neglected. This simplification reduces drastically the computational requirements for the solution of the IMADE as one avoids the time consuming calculation of the coagulation coefficients β. This approximation introduces only a minor error in the solution of the IMADE under typical SoCAB conditions.

Aerosol-Phase Chemical Reactions

Chemical reactions in ambient aerosols have yet to be well characterized with the possible exception of the N_2O_5 to HNO_3 nighttime transformation. A parametrization of this reaction is included in the gas-phase module and will not be discussed further in this section. Several investigators have proposed that aerosols at high relative humidities may provide the reaction medium, the liquid water, for the heterogeneous oxidation of SO_2 to sulfate. While this transformation is significant in clouds and fogs having liquid water contents of the order of 0.1 g m^{-3}, our theoretical estimates (Pandis et al., 1992b) extrapolating the measured reaction rates to the concentrated aerosol solutions (liquid water less than 0.0001 g m^{-3}) suggest that the rates are negligible. Since insufficient information exists to test the validity of such an extrapolation, sulfate production in aerosols is neglected. The production of sulfate in clouds and fogs is treated by the aqueous-phase module described in Chapter 3.

2.2.2 Numerical Solution of IMADE

Neglecting the gravitational settling, coagulation, chemical reaction and nucleation terms the IMADE can be rewritten as

$$\begin{aligned} &\frac{\partial q_i(m,z,t)}{\partial t} && (local\ rate\ of\ change)\\ &+V(z,t)\cdot\nabla q_i(m,z,t) && (advection)\\ &=H_i(m,z,t)\,q(m,z,t)-\frac{\partial(mq_iH)}{\partial m} && (cond./evap.)\\ &+\nabla\cdot(K(z,t)\ \nabla q_i(m,z,t)) && (spatial\ diffusion)\\ &+E_i(m,z,t) && (primary\ emissions) \end{aligned} \tag{2.6}$$

The above equation suggests that the aerosol/size composition distribution $q_i(m, z, t)$ for the conditions of interest in the SoCAB is affected by spatial advection and diffusion, condensation/evaporation and primary emissions and deposition. Deposition is included in the boundary conditions and not in the partial differential equation itself.

Operator Splitting

In grid-based models such as UAM, operator splitting is employed to separate each of the horizontal and vertical transport terms from the gas-phase chemical reaction term so that each term may be solved independently of the others. Operator splitting significantly improves the run time performance and modularity of these models while introducing some numerical error in the calculations. By employing operator splitting on the above simplified form of the imade, the four terms may be separated from each other. The aerosol operating splitting used in the current model based on the original UAM operator splitting scheme is

$$q_i(m,z,t+\Delta t) = L_{aer}\ L_{z,emis}\ L_y\ L_x\ q_i(m,z,t) \tag{2.7}$$

where Δt is the operator timestep, L_{aer} is the aerosol operator that does the condensation/evaporation calculation, $L_{z,\,emis}$ solves for vertical transport and emissions,

L_y performs the y (north-south) transport calculation and L_x performs the x (east-west) transport calculation. Since the form of the transport operators is identical for the gas-phase and aerosol-phase species, the gas-phase spatial transport operators could be used for the solution of the corresponding terms in the IMADE. Both the gas and aerosol-phase species concentrations are dependent on time and spatial position, but in addition, the aerosol concentrations are dependent on the size parameter, m. As a result the spatial transport operators can be used to calculate the advection and diffusion of the aerosol species only if the aerosol size discretization is identical for adjacent cells. This requirement allows a straightforward integration of the aerosol module into the full 3D model.

The only term remaining for the aerosol operator, L_{aer} , is the condensation term and therefore the aerosol operator solves the condensation/evaporation equation

$$\frac{\partial q_i(m,z,t)}{\partial t} = H_i(m,z,t)\, q(m,z,t) - \frac{\partial (m q_i H)}{\partial m} \tag{2.8}$$

If the aerosol distribution is discretized into k size sections (corresponding to the parameter m) this partial differential equation can be expressed as a set of ordinary differential equations of the form

$$\frac{dq_{ik}}{dt} = \frac{2\pi D_p D_i N_k}{(2\lambda/\alpha D_p)+1}\,(C_i - C_i^{eq}) \tag{2.9}$$

where q_{ik} is the mass concentration of species i in the size section k, D_p is the particle diameter, D_i is the molecular diffusivity of the condensing or evaporating compound, i, N_k is the number concentration of particles in the k^{th} section and C_i-C_i^{eq} is the difference between the ambient concentration, C_i, and the equilibrium particle surface concentration, C_i^{eq}, α is the accommodation coefficient and λ is the mean free path of air molecules in air (Wexler and Seinfeld, 1990). The above equation states that mass of species i is

transferred between the gas and aerosol phases in an effort to establish equilibrium, that is to get the bulk gas-phase concentration equal to the concentration at particle surface, or mathematically to achieve

$$C_i = C_i^{eq} \tag{2.10}$$

This equilibrium state is achieved after a time τ_{eq}, the timescale for equilibration between the gas and aerosol phases. Most atmospheric aerosol models assume thermodynamic equilibrium for the aerosol components than can exist in both the aerosol and gas phases (nitrate, ammonium, chloride, organics, water). This assumption states that the time required for the particle to reach equilibrium, τ_{eq}, is smaller than the operator timestep Δt used in the model (usually 5-10 minutes) and therefore instead of integrating the condensation/evaporation equation one can just assume that at the end of the operator timestep thermodynamic equilibrium has been established. This is a significant simplification of the problem because one replaces the integration of a system of stiff ordinary differential equations with a system of non-linear algebraic equations that needs to be solved only once in every operator timestep.

Stelson et al. (1979) first suggested that aerosol ammonium nitrate levels could be determined from the equilibrium among ammonia, nitric acid, and aerosol ammonium nitrate. The assumption of thermodynamic equilibrium has been employed to partition the volatile compounds between the gas and aerosol phases (Stelson and Seinfeld, 1982a, b; Bassett and Seinfeld, 1983, 1984; Russell et al., 1983, 1988; Saxena et al., 1983, 1986; Russell and Cass, 1986) and to predict the aerosol size distribution (Bassett and Seinfeld, 1984; Pilinis and Seinfeld, 1987, 1988; Pilinis et al., 1988). Although the equilibrium assumption has been supported by ambient data (Doyle et al., 1979; Grosjean, 1982; Hildemann et al., 1984), other data indicate that it may introduce errors in the simulation of aerosol concentration (Cadle et al., 1982; Tanner, 1982; Allen et al., 1989).

Timescales for equilibrium

Wexler and Seinfeld (1990) have predicted that under certain atmospheric conditions, the

volatile inorganic components of atmospheric aerosol may not be in equilibrium with their gas-phase counterparts due to transport limitations. These investigators suggested that the timescale for equilibration between a monodisperse aerosol population of radius R_p and the gas phase is

$$\tau_p = \frac{\rho_p R_p^2}{3 D_i m_p} (1 + \beta_i) \qquad (2.11)$$

where ρ_p is the aerosol density, D_i is the gas-phase diffusivity of species i, m_p is the particle mass concentration, and β_i is the surface accommodation factor. This expression suggests that for small aerosol mass concentrations and large aerosol sizes (e.g conditions that could be found near the coast of a polluted area) this equilibrium timescale can be of the order of several hours and the aerosol is not necessarily in equilibrium with the surrounding gas-phase. In this case, the aerosol mass concentration is governed by transport and not thermodynamics. On the other hand when the aerosol mass concentration is high and the aerosol size small the equilibrium timescale is of the order of a few seconds and thermodynamic equilibrium is expected to be a valid assumption.

Equilibrium and aerosol distribution

Even when the aerosol is in equilibrium with the gas phase, *the size distribution* of the volatile components of atmospheric aerosols often cannot be determined from thermodynamic considerations alone, and thus mass transport has to be included to determine the size distribution of the volatile components (Wexler and Seinfeld, 1990). The inability of thermodynamics to always uniquely determine the size distribution of an aerosol population can be illustrated by a simplified example. Let us assume that our aerosol population consists of NH_4NO_3 particles of different sizes. Thermodynamic equilibrium requires that the product of the gas-phase concentrations of NH_3 and HNO_3 should be equal to a constant. Assume now that a certain amount of HNO_3 is produced in the system. Return to an equilibrium state requires the condensation of some HNO_3 and an equimolar amount of NH_3 to the aerosol particles so that the product of their gas-phase concentrations is again equal to the equilibrium constant value. But this thermodynamic

driving force is the same for all the solid ammonium nitrate particles and thermodynamic considerations alone actually result in infinite ways of distributing this ammonium nitrate among the various particles. The aerosol distribution is determined by transport considerations and as Wexler and Seinfeld (1990) point out often "thermodynamics is not enough". These authors describe several other cases where thermodynamics alone cannot assist us in determining the aerosol size distribution and suggest that in general both transport and thermodynamics should be used in our effort to predict the ambient aerosol size composition distribution.

2.3 The Aerosol Module

The aerosol module is an extension of the module developed by Pandis et al. (1993) as one of the components of the Size Resolved Secondary Organic Aerosol Model (SRSOAM). The module calculates the evolution of the aerosol size composition distribution during the transfer of aerosol species between the gas and aerosol phases.

2.3.1 Modeling the Aerosol Size Distribution

The aerosol size composition is discretized in sections, with all the particles in each section having the same size and the same chemical composition (Gelbard et al., 1980; Seigneur et al., 1986). The movement of these sections as a result of particle growth by gas-to-particle conversion is calculated using the moving section technique (Gelbard, 1990; Kim and Seinfeld, 1990). A spline interpolation technique is used for the mapping of the aerosol size/composition distribution onto the fixed size grid. Therefore, the main model maintains the aerosol size distributions for all computational cells in the same fixed size grid, facilitating the advection and turbulent transport calculations. The aerosol module internally uses a moving grid, but after the end of the timestep using spline interpolation recalculates the resulting distribution on the fixed grid and transfers it as module output to the main code.

The inorganic and organic aerosol species are distributed among the aerosol and gas phases assuming that thermodynamic equilibrium is established over timescales smaller

than the 10 min operator timestep used in the model. Stelson et al. (1979) have postulated that the sulfate-nitrate-ammonium aerosol constituents should be in thermodynamic equilibrium with the local gas phase. Particulate and gaseous pollutant concentrations at some inland Los Angeles sampling sites have been found to agree with the thermodynamic equilibrium assumption (Hildemann et al., 1984). Wexler and Seinfeld (1990) have predicted that the volatile inorganic components of atmospheric aerosol may not be in equilibrium with their gas-phase counterparts due to transport limitations under some atmospheric conditions (low temperatures, low pollution levels, etc.) and found support for their predictions in SCAQS data (Wexler and Seinfeld, 1992). Keeping in mind the uncertainties in ambient aerosol measurements and the enormous computing cost associated with a detailed mass-transfer calculation we employ the aerosol equilibrium assumption, despite the potential error introduced in certain cases. This equilibrium assumption error is expected to be small for high pollution, high temperature cases.

The inorganic multicomponent atmospheric aerosol equilibrium model of Pilinis and Seinfeld (1987) is used for the calculation of the total quantities of ammonium, chloride, nitrate and water contained in atmospheric aerosols. The model predicts the gas phase concentrations of NH_3, HCl, HNO_3 and the aerosol phase concentrations of H_2O, NH_4^+, SO_4^{2-}, NO_3^-, Na^+, C^{l-}, $HSO4^-$, H_2SO_4, Na_2SO_4, $NaHSO_4$, NaCl, $NaNO_3$, NH_4Cl, NH_4NO_3, $(NH_4)_2SO_4$, NH_4HSO_4 and $(NH_4)_3H(SO_4)_2$. The equilibrium code has been successful in predicting the concentrations of the various aerosol species in Long Beach, California (Pilinis and Seinfeld, 1987).

Thermodynamic equilibrium has been also assumed for the various condensible organic vapors. When their gas-phase concentration exceeds their vapor pressure the vapors condense to the aerosol phase in an effort to establish equilibrium. Evaporation occurs when the gas phase is subsaturated. Following Pandis and Seinfeld (1992) we have used the few available saturation vapor pressure measurements and arbitrarily assumed a temperature independent saturation concentration value of 2 ppt for the remaining

condensible species. The above authors showed that if the vapor pressure is a few ppt, as assumed in this study, the predicted secondary organic aerosol concentrations are relatively insensitive to the exact value, but if the vapor pressure is over about 0.1 ppb, the model predictions are extremely sensitive to the assumed value. Due to existing uncertainties in the corresponding physical properties of the secondary organic aerosol species, the adsorption of organic vapors on dry particles (Pankow, 1987) and their dissolution in water or in each other are not treated by the present model. The sensitivity of the model to these assumed saturation vapor pressures has been discussed by Pandis et al. (1993).

2.3.2 The Hybrid Method

Wexler and Seinfeld (1990) have shown that even if the aerosol is in equilibrium with the gas phase, the size distribution of the volatile inorganic and organic components of atmospheric aerosols often cannot be uniquely determined from thermodynamic considerations alone, and thus mass transport has to be included to predict the aerosol size composition. This is especially true for secondary organics, since the vapor pressure is assumed to be constant. To overcome these difficulties without increasing the computational cost of the aerosol module we have used the Hybrid Method originally proposed by Pandis et al. (1993). The basic idea of the method is that can calculate the total aerosol mass using the equilibrium assumption, and then calculate the size distribution using a simplified mass transfer algorithm.

The single particle flux of condensate or evaporate is given by

$$J_i = \frac{2\pi D_p D_i}{(2\lambda/\alpha D_p) + 1} (C_i - C_i^{eq}) \qquad (2.12)$$

The overall transport rate to a size section, nJi, depends on the number of particles in the section, $n(D_p)$, and the single particle transport rate. The fraction of condensate that appears in each size section, f, is given by

$$f = \frac{2n\pi D_p D_i (C_i - C_i^{eq}) / (\beta + 1)}{\int_0^{\infty} 2n\pi D_p D_i (C_i - C_i^{eq}) / (\beta + 1)\, dD_p} \qquad (2.13)$$

If equilibrium has been established, then initially all the particles have the same C_i^{eq} as all of them are in equilibrium with the same bulk gas-phase concentration of *i*. During condensation of i the chemical composition of the particles change and the equilibrium concentrations for the various particle sizes may start to deviate. We assume here that this change is slow enough so that

C_i^{eq} depends only weakly on the aerosol size or equivalently that it is independent of the diameter D_p. Since the ambient concentration, C_i, is the same for all particles, the difference $C_i - C_i^{eq}$ is independent of particle size and the above equation can be simplified to

$$f = \frac{nD_p / (\beta + 1)}{\int_0^{\infty} nD_p / (\beta + 1)\, dD_p} \qquad (2.14)$$

The quantity β is dependent on the particle size and accommodation coefficient (the fraction of the number of gas-particle collisions in which the gas molecule is taken up by water, to 10^{-4} (Pandis et al., 1993). Changes in accommodation coefficient independent of particle size change the size distribution of condensate. In the present module we assume an accommodation coefficient of 1.0, independent of particle size. Sensitivity to this selection has been discussed by Pandis et al. (1993).

To predict the size distribution of condensable compounds, the module requires as input from the main model the gas-phase concentrations of these compounds in the beginning of the aerosol operator timestep. For the inorganic compounds the total aerosol and vapor composition is used with an equilibrium code (Pilinis and Seinfeld, 1987) to determine

the equilibrium vapor composition. The amount condensed or evaporated is partitioned among the sections with the above equation. For inland location in Los Angeles, the aerosol loading is high, which gives a short time constant for equilibration (Wexler and Seinfeld, 1990), and the aerosol contains a significant amount of ammonium nitrate so that the mixing processes does not significantly alter the partial pressures (Wexler and Seinfeld, 1992). In less polluted locations, with less of an accumulation of ammonium nitrate, the assumptions employed here may increase uncertainty in the predictions. For the organic compounds, when the concentration exceeds their equilibrium vapor pressures, the excess is condensed on the particles using the above equation. When the concentration is below the equilibrium concentration, the deficit evaporates from the particles by the same equation to restore the vapor concentration to the equilibrium levels until the particulate concentration of the compound is depleted.

2.3.3 Secondary Organic Aerosol

Several organic gases emitted directly to the atmosphere have been recognized as organic aerosol precursors. During the atmospheric oxidation of these gases by OH, O_3, and NO_3, etc., low vapor pressure products are formed that can then condense to the aerosol phase as secondary organic aerosol material. Grosjean (1977) reviewed the organic aerosol forming potential of several hydrocarbons. Most paraffins do not generate aerosol, even at high concentrations. Some aerosol can be formed from the more reactive branched paraffins having more than six carbon atoms, e.g. isooctane. Acetylenics do not form aerosol. Alkenes with fewer than six carbon atoms do not form aerosol; those with six or more carbon atoms form aerosol when they yield, after rupture of the double bond, a fragment with at least five carbon atoms. For example, 1-heptene forms much more aerosol than 3-heptene, and 2,4,4-trimethyl-1-pentene (isooctene) forms more aerosol than its isomer trans-4-octane. Cyclic olefins and diolefins form more aerosol than 1-alkenes that have the same number of carbon atoms. Heavier unsaturated cyclic compounds such as indene and terpenes form even more aerosol. Carbonyl compounds (ketones, C_{1-7} aldehydes, dialdehydes) do not generate aerosol. Significant aerosol quantities are formed during the photooxidation of aromatic hydrocarbons.

Our knowledge of the chemical composition of most condensible gaseous products and the exact chemical pathways leading to their formation, including the stoichiometry and rate constants, remains incomplete. Therefore, the mechanistic description of the production of low volatility gaseous products follows the condensed gas-phase mechanisms used in urban and regional air pollution models. The atmospheric oxidation of a hydrocarbon HC by an oxidant like OH or O_3 or NO_3 is described by a single reaction that incorporates all the individual mechanistic steps

$$HC + oxidant \rightarrow a\ A + b\ B + ... + y\ G$$

where A, B, etc. are the regular gaseous products, G is a generic condensible gas that could form secondary organic aerosol and y is the corresponding stoichiometric coefficient. Pandis et al. (1992) have argued that the stoichiometric coefficient y is equal for practical purposes to the fractional aerosol yield Y of the hydrocarbon. Experimental measurements of the aerosol yields, Y, of the photooxidation of several hydrocarbons are available in the literature and the yields for the remaining reactions relevant to urban smog have been estimated by Grosjean and Seinfeld (1989) and Pandis et al. (1992). The production of the secondary organic aerosol components during the photooxidation of their precursors is modeled following the approach used by Pandis et al. (1992) in their Secondary Organic Aerosol Model (SOAM). A detailed list of the aerosol yields used are given in Table 2.1.

2.4 Recapitulation of Numerical Methods

OVERVIEW OF NUMERICAL METHODS

A significant portion of particulate matter mass is due to condensation of gas-phase species upon an existing aerosol mass created by fresh emissions. The model considers five condensable gas-phase species: ammonia (NH_3), sulfuric acid (H_2SO_4), nitric acid (HNO_3), hydrochloric acid (HCl), and a lumped species of condensable organic material (COC). In the aerosol phase, these species disassociate into their respective ions: ammonium (NH_4^+), sulfate ($SO_4^=$), nitrate (NO_3^-), chloride (Cl^-), and hydrogen ion (H^+). Condensable organic material is uncharged, and in the aerosol phase it is represented simply as organic carbon (OM). There is also condensation upon particulate matter generated by other processes such as windblown fine dust and salt particles (NaCl) generated by sea spray. But as temperatures increase during the day, some aerosol species, notably ammonium nitrate, become more volatile and are subject to evaporation from the particles causing shrinkage of particles.

The model assumes thermodynamic equilibrium exists between the gas-phase and the combined aerosol mass from all size sections. A single call to the equilibrium routine determines updated equilibrium gas-phase concentrations and the net amount of each condensable gas-phase species that should either be transported to or from the aerosol phase. The amount transported to each size section is determined by diffusional transport limitations and the number of particles in each size bin. In general, more mass is usually transported to the smallest size sections, because there is less diffusional resistance and because there are a greater number of particles (and more surface area) in those size sections. After the mass has been transported, the new equilibrium water content is calculated separately for each size section.

After mass has been transported, the new sizes of the particles are calculated. The aerosol module must then reapportion the mass into the original particle size sections, since transport and dispersion between adjacent grid squares can only be calculated for particles of the same size. To accomplish this, the size distribution for each chemical species is fitted to a cubic spline. This continuous distribution is then apportioned to each section by numerical integration.

In practice, the thermodynamic model often predicts that significant amounts of condensable gases and/or water need to be transported between the gas and aerosol phases over a 10 minute time step. Large gas-aerosol transport fluxes can significantly influence the predicted size distributions. In fact, in developing the algorithm, conditions were encountered where the predicted size of one particle section increased to more than the size of next larger size section when a single 10 minutes time step was employed. This problem of sectional overlap was solved by implementation of a multi-step transport algorithm that assures numerically stable simulation of transport. Often stable transport can be simulated with a single 10 minute time step, however, when large gas-aerosol transport fluxes occur, the algorithm uses small transport time steps to assure stability and realistic evolution of the size distribution. Between each transport step, the updated size distribution (from the moving sections) is fitted to a cubic spline and reapportioned to the original size sections.

THERMODYNAMIC EQUILIBRIUM

The composition of an aerosol particle, the relative humidity of the atmosphere, and the temperature completely determine the vapor pressure of the condensable gases. If the vapor pressure of a gas is greater than its partial pressure in the atmosphere, then a certain amount of that gas will evaporate from the particle until the vapor pressure is equal to the atmospheric partial pressure. Conversely, if the vapor pressure is less that the partial pressure, gas will condense on the particle until the partial pressure is equal to the vapor pressure.

The thermodynamic model directly calculates the partition between gas and aerosol phase for each species, rather than the actual vapor pressure. For a given total quantity of species in both phases expressed in equivalent units of ammonia (NH_3), sulfuric acid (H_2SO_4), nitric acid (HNO_3), and salt (NaCl), the model predicts the gas phase composition after equilibrium has been achieved. The final aerosol composition is determined simply by difference between the total initial amount and the final amount in the gas phase.

Before the equilibrium routine is called, a charge balance is performed on the aerosol content of each size section and then each size section is neutralized. This step is performed because thermodynamic equilibrium essentially dictates that the net ionic charge be neutral. In nature, a charge imbalance would quickly be corrected by transport of the appropriate species. This is because a charge imbalance would cause the vapor pressures to be significantly different than the partial pressures. Therefore, the aerosol would soon be neutralized by mass transport. This neutralization step transports mass between the aerosol and gas phases so that the net charges are balanced for the ionic components excluding H^+.

AEROSOL RESIZING ALGORITHM

The individual steps and logic in the aerosol module are shown schematically in Figure 1. The aerosol module consists of the following nine steps:

1. Each size section of the aerosol is neutralized.
2. The number density for each size section is calculated.
3. The thermodynamic routine is called to calculate the equilibrium composition.
4. The transport factors are calculated, which apportion mass according to the product of diffusional resistance and number of particles for each section.
5. The species are transported using the previously calculated transport factors and the difference between the equilibrium values and the initial values.
6. Each size section is neutralized a second time.
7. The equilibrium routine is called to calculate the water content for each section.
8. The new section mean diameters and cut point diameters are calculated.
9. The new size distribution is fitted to a cubic spline for each aerosol component and the distribution is reapportioned to the initial size sections using numerical integration.

If the thermodynamic routine predicts that a significant amount of mass should be transported between the phases, there is the possibility that the change in size of one section could overtake the size of the next higher section. In these situations, the transport factors are reduced and a smaller amount of mass is transported in multiple time steps. This same reduction is also applied to the fraction of water transported to achieve equilibrium. If this step is successful without sectional overlap, then the resulting distribution is fitted to a cubic spline and the aerosol mass is reapportioned to the original size sections. The transport factors are then increased and the number density for the new distribution is calculated. Then the transport step is repeated. Under extreme situations where concentrations are far from equilibrium, up to five gas-aerosol transport steps (about 2 minutes each) are need to transport the material in a numerically stable manner.

Table 2.1 Secondary Organic Aerosol Measured and Estimated Yields (Pandis et al., 1992).

Species	Aerosol yield ($\mu g\ m^{-3}\ ppm^{-1}$)
Alkanes	0
Propane	0
n-Butane	0
Isobutane	0
n-Pentane	0
Cyclopentane	0
Pentane isomers	0
n-Hexane	0
Methylcyclopentane	17
Cyclohexane	17
Hexane isomers	0
n-Heptane	7
Methylcyclohexane	120
C7-cycloparafins	120
Heptane isomers	0
n-Octane	98
Ethylcyclohexane	275
C8-Cycloparaffins	275
Octane isomers	98
n-Nonane	236
C9-Cycloparaffins	466
Nonane isomers	236
n-Decane	348
C10-Cycloparaffins	687
Decane isomers	348
n-Undecane	479
C11-Cycloparaffins	945
Undecane isomers	479
n-Dodecane	626
C12-Cycloparaffins	1100
Dodecane isomers	626
n-Tridecane	865

C13-Cycloparaffins	1265
Tridecane isomers	865
n-Tetradecane	972
C14-Cycloparaffins	1443
Tetradecane isomers	972
n-Pentadecane	1300
C15-Cycloparaffins	1717
Pentadecane isomers	1300
Alkenes	
Ethene	0
Propene	0
1-Butene	0
1-Butene isomers	0
2-Butene	0
2-Butene isomers	0
1,3 Butadiene	0
1-Pentene	0
1-Pentene isomers	0
2-Pentene isomers	0
Cyclopentene	132
1-Hexene	0
1-Hexene isomers	0
2-Hexene isomers	0
Cyclohexene	278
1-Heptene isomers	78
2-Heptene isomers	78
1-Octene isomers	227
2-Octene isomers	227
1-Nonene isomers	304
2-Nonene isomers	304
Decene isomers	470
Undecene isomers	743
Dodecene isomers	878
Tridecene isomers	1024
Tetradecene isomers	1180
Pentadecene isomers	1350

Bioalkenes	
Isoprene	0
α–Pinene	762
β-Pinene	720
Monoterpenes	762
Aromatics	
Benzene	0
Toluene	424
Ethylbenzene	440
Isopropylbenzene	334
n-Propylbenzene	138
Isobutylbenzene	334
m-Xylene	419
o-Xylene	428
p-Xylene	180
1,3,5-Trimethylbenzene	577
1,2,3-Trimethylbenzene	496
1,2,4-Trimethylbenzene	251
Naphthalene	400
2,3-Dimethylnaphthalene	600
Methylnaphthalenes	500
Tetralin	400
Other	
Methyl ethyl ketone	0
Alkyl phenols	220
Glyoxal	0
Methyl glyoxal	0
Higher aldehydes	0
Acetone	0
Higher PAN analogues	0
Aromatic aldehydes	5
Peroxy benzoyl nitrate	5
Phenols	192
Nitrophenols	285

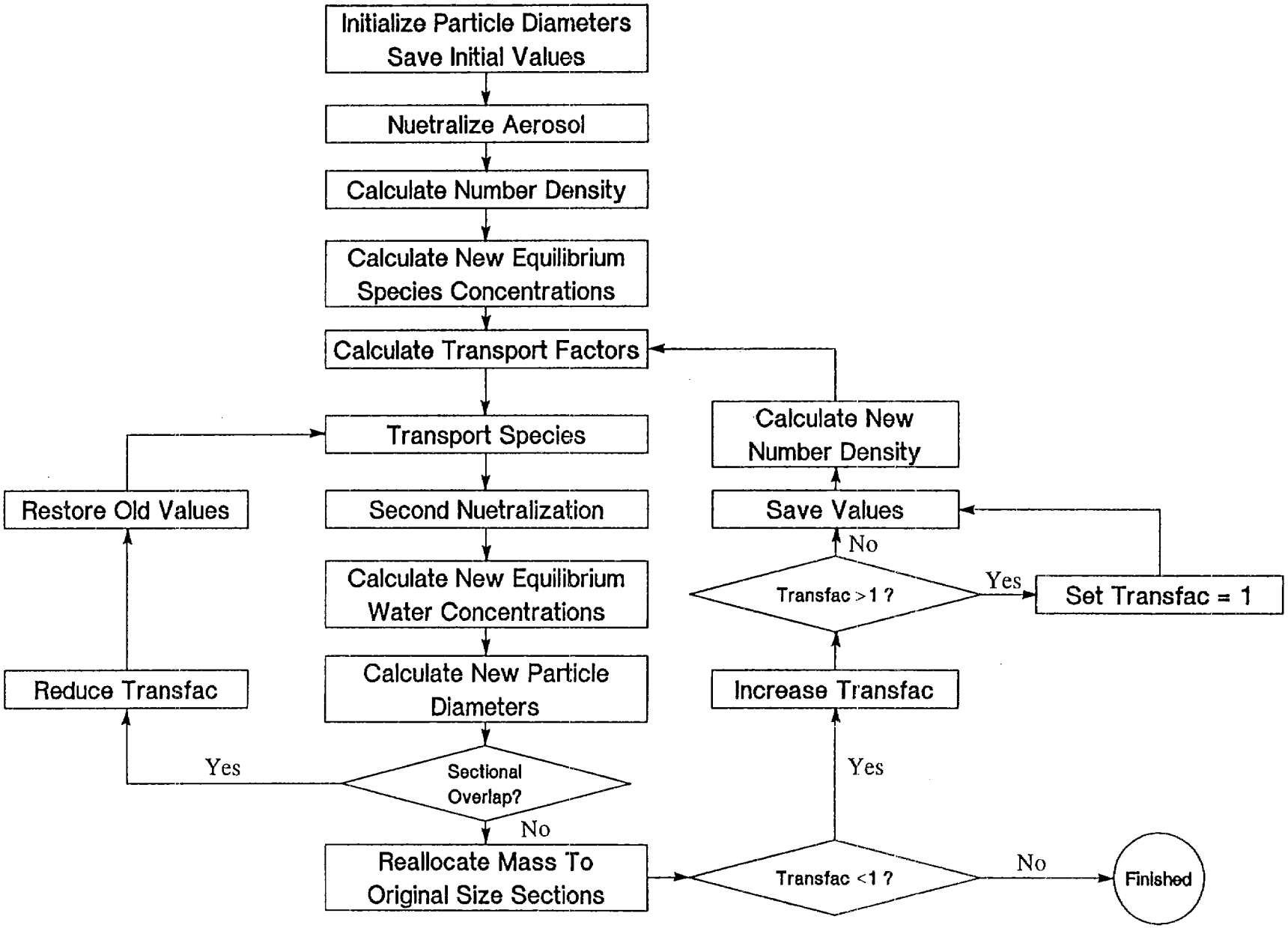

Figure 2.1 Aerosol module schematic.

3. Fog and Cloud Processes

Fog and cloud processes are predicted to have a significant effect on the chemistry of the troposphere (Lelieveld and Crutzen, 1990, 1991; Warneck, 1991, 1992). For example, the uptake of HCHO, HO_2 radicals, and N_2O_5 into cloud droplets can lead to a decrease in the production of ozone at the global scale. Removal of HCHO reduces the rate of gas-phase production of HO_2 radicals and consequent conversion of NO to NO_2, and absorption of N_2O_5 into cloud droplets can lead to a decrease in the production of ozone because the decomposition reaction to NO_2 and NO_3 is prevented. Also, aqueous-phase reactions of $H_2C(OH)_2$, the hydrated form of HCHO, lead to the formation of O_2^- , which can react with dissolved O_3 to enhance the rate of transfer of O_3 to the liquid phase over that based solely on physical solubility. Clouds and fogs promote the oxidation of SO_2 to sulfate. When present, they dominate sulfate production; in the presence of oxidants such as ozone, hydrogen peroxide, or oxygen catalyzed by trace metals, SO_2 is oxidized much more rapidly in the aqueous phase than in the gas phase. As much as 80 to 90 percent of global SO_2 oxidation is believed to occur in clouds (Lelieveld and Heintzenberg, 1992). At the urban and regional scale, aqueous-phase oxidation of dissolved SO_2 is a key process in the generation of atmospheric acidity.

3.1 Aqueous Phase Equilibria

The liquid water content of the atmosphere, w_L, is usually expressed either in g of water per m^3 of air or as a dimensionless volume fraction L (e.g., m^3 of liquid water per m^3 of air). Typical liquid water content values are:

0.1 to 1 g m^{-3}	(L= 10^{-7}- 10^{-6})	for clouds,
0.05 to 0.5 g m^{-3}	(L= 5 x 10^{-7} - 5 x 10^{-6})	for fogs,
10^{-5} to 10^{-4}g m^{-3}	(L=10^{-11}-10^{-10})	for aerosols.

For dilute solutions the equilibrium distribution of a reagent gas A between the gas and aqueous phases is given by Henry's law, $[A] = H_{Ap_A}$ where p_A is the partial pressure of A in the gas-phase, $[A]$ is the equilibrium aqueous-phase concentration of A and H_A is the Henry's law coefficient for species A. The customary units of H_A are mole l^{-1} atm^{-1}. H_A can be viewed as the equilibrium constant of the reaction $A(g) \underset{\rightarrow}{\leftarrow} A(aq)$. Henry's law coefficients generally decrease with increasing temperatures, resulting in lower solubilities at higher temperatures (Seinfeld, 1986).

Several gases, after dissolving in the aqueous-phase, ionize and establish an aqueous-phase chemical equilibrium system. For example for SO_2,

$$SO_2(g) \underset{\rightarrow}{\leftarrow} SO_2 \cdot H_2O$$

$$SO_2 \cdot H_2O \underset{\rightarrow}{\leftarrow} HSO_3^- + H^+$$

$$HSO_3^- \leftrightarrows SO_3^{2-} + H^+$$

with

$$H_{SO_2} = \frac{[SO_2 \cdot H_2O]}{p_{SO_2}},\ K_{s1} = \frac{[HSO_3^-][H^+]}{[SO_2 \cdot H_2O]},\ K_{s2} = \frac{[SO_3^{2-}][H^+]}{[HSO_3^-]}$$

K_{s1} and K_{s2} are the first and second dissociation constants for SO_2. It is convenient to consider the total dissolved sulfur in oxidation state IV as a single entity and refer to it as S(IV),

$$[S(IV)] = [SO_2 \cdot H_2O] + [HSO_3^-] + [SO_3^{2-}]$$

The three sulfur species are in rapid equilibrium and therefore [S(IV)] changes only when a transfer of SO_2 occurs between the gas and aqueous phases. The total dissolved sulfur, S(IV), can be expressed as a function of only the pH and the partial pressure of SO_2 over the solution by:

$$[S(IV)] = H_{SO_2} p_{SO_2} \left[1 + \frac{K_{s1}}{[H^+]} + \frac{K_{s1}K_{s2}}{[H^+]^2} \right]$$

The above equation can be expressed in a form similar to Henry's law as

$$[S(IV)] = H^*_{S(IV)} p_{SO_2}$$

where $H^*_{S(IV)}$ is the effective (or modified) Henry's law coefficient given for S(IV) by

$$H^*_{S(IV)} = H_{SO_2}\left[1 + \frac{K_{s1}}{[H^+]} + \frac{K_{s1}K_{s2}}{[H^+]^2}\right]$$

The modified Henry's law coefficient relates the total dissolved S(IV) (and not only $SO_2 \cdot H_2O$) with the SO_2 vapor pressure over the solution. The dissociation of dissolved SO_2 enhances its aqueous solubility and the total amount of dissolved S(IV) always exceeds that predicted by Henry's law for SO_2 alone and is quite pH dependent. The Henry's law coefficient for SO_2 alone, H_{SO_2}, is 1.23 M atm^{-1} at 298 K, while for the same temperature, the effective Henry's law coefficient for S(IV), $H^*_{S(IV)}$, is 16.4 M atm^{-1} for pH=3, 152 M atm^{-1} for pH=4 and 1524 M atm^{-1} for pH=5. Equilibrium S(IV) concentrations for SO_2 gas-phase concentrations of 0.2-200 ppb, and over a pH range 1-6 vary approximately from 0.001 to 1000 μM.

3.2 S(IV) to S(VI) Transformation and Sulfur Chemistry

The aqueous-phase conversion of dissolved SO_2 to sulfate is thought to be the most important chemical transformation in cloudwater. Dissolution of SO_2 in water results in the formation of three chemical species: hydrated SO_2 ($SO_2 \cdot H_2O$), the bisulfite ion (HSO_3^-) and the sulfite ion (SO_3^{2-}). At the pH range of atmospheric interest (pH =2-7) most of the S(IV) is in the form of HSO_3^-, whereas at low pH (pH <2), all of the S(IV) occurs as $SO_2 \cdot H_2O$. At higher pH values (pH >7), SO_3^{2-} is the preferred S(IV) state. The individual dissociations are fast, occurring on timescales of milliseconds or less . Therefore, during a reaction consuming one of the three species, $SO_2 \cdot H_2O$, HSO_3^-, or SO_3^{2-}, the corresponding aqueous-phase equilibria can be considered to be re-established instantaneously.

Several pathways for S(IV) transformation to S(VI) have been identified involving reactions of S(IV) with O_3, H_2O_2, O_2 (catalyzed by Mn^{+} and Fe^{3+}), OH, SO_5^-, HSO_5^-, SO_4^-, PAN, CH_3OOH, $CH_3C(O)OOH$, HO_2, NO_3, NO_2, N(III), HCHO and Cl_2^- (see Pandis and Seinfeld, 1989a).

3.2.1 S(IV)-O_3 Reaction

Although ozone reacts very slowly with SO_2 in the gas phase, the aqueous-phase reaction is rapid. The possible importance of O_3 as an aqueous-phase oxidant for S(IV) was first suggested by Penkett (1972),

$$S(IV) + O_3 \rightarrow S(VI) + O_2$$

Hoffmann and Calvert (1985), after a detailed investigation of existing experimental kinetic and mechanistic data, suggested the following expression for the rate of the reaction of S(IV) with dissolved ozone:

$$R_1 = -\frac{d[S(IV)]}{dt} = \left\{(k_0[SO_2 \cdot H_2O] + k_1[HSO_3^-] + k_2[SO_3^{2-}])\right\}[O_3]$$

recommending the values k_0 =2.4 x 10^4 M^{-1} s^{-1}, k_1 =3.7 x 10^5 M^{-1} s^{-1} and, k_2=1.5 x 10^9 M^{-1} s^{-1}. They also proposed that this reaction proceeds by nucleophilic attack on ozone by $SO_2 \cdot H_2O$, HSO_3^- , and SO_3^{2-}. An increase in the aqueous-phase pH results in an increase of all three, $[SO_2 \cdot H_2O]$, $[HSO_3^-]$ and $[SO_3^{2-}]$, equilibrium concentrations and therefore in an increase of the overall reaction rate. For an ozone gas-phase mixing ratio of 30 ppb, the reaction rate varies from less than 0.001 μM h^{-1} (ppb SO_2)$^{-1}$ at pH=2 (or less than 0.01% SO_2 (g) h^{-1} (g water /m^3 air)$^{-1}$) to 3000 μM h^{-1} (ppb SO_2)$^{-1}$ at pH=6 (7000% SO_2 (g) h^{-1} (g water /m^3 air)$^{-1}$). The gas-phase SO_2 oxidation rate is of the order of 1% h^{-1} and therefore the S(IV) heterogeneous oxidation by ozone is significant for pH values greater than 4. The strong positive dependence of the reaction rate on the pH renders this reaction self-limiting. The production of sulfate by this reaction lowers the pH and effectively decreases the rate of further reaction. The availability of

atmospheric ozone guarantees that this reaction will play an important role both as a sink of gas-phase SO_2 and as a cause of cloudwater acidification as long as the pH of the atmospheric aqueous phase exceeds 4.

3.2.2 S(IV)-H_2O_2 Reaction

Hydrogen peroxide, H_2O_2, is one of the most effective oxidants of S(IV) in clouds and fogs (Pandis and Seinfeld, 1989a). H_2O_2 is very soluble in water and under typical ambient conditions its aqueous-phase concentration is approximately six orders of magnitude higher than that of ozone. The proposed rate expression is (Hoffmann and Calvert, 1985)

$$R_2 = -\frac{d[\mathrm{S(IV)}]}{dt} = \frac{k[\mathrm{H^+}][\mathrm{H_2O_2}][\mathrm{HSO_3^-}]}{1+K[\mathrm{H^+}]}$$

with k=7.45 x 10^7 M^{-1} s^{-1} and K=13 M^{-1} at 298 K. Noting that H_2O_2 is a very weak electrolyte, and that $[H^+]\,[HSO_3^-] = H_{SO_2}K_{s1}p_{SO_2}$ and that for pH> 2 , $1 + K\,[H^+] \doteq 1$, one concludes that the rate of this reaction is practically pH-independent in the pH range of atmospheric interest. For a H_2O_2(g) mixing ratio of 1 ppb the rate is roughly 300 μM h^{-1} (ppb SO_2)$^{-1}$ (700% SO_2(g)h^{-1} (g water /m^3 air)$^{-1}$). The near pH independence can also be viewed as the result of the cancellation of the pH dependence of the S(IV) solubility and the reaction rate constant. The reaction is very fast and indeed both field measurements (Daum et al., 1984) and theoretical studies (Pandis and Seinfeld, 1989b) have suggested that H_2O_2(g) and SO_2(g) rarely coexist in clouds and fogs. The species with the lowest concentration before the cloud or fog formation is the limiting reactant, and is rapidly depleted inside the cloud or fog layer.

3.2.3 Metal-Catalyzed S(IV)-O_2 Reaction

The S(IV) oxidation by O_2 is known to be catalyzed by Fe^{3+} and Mn^{2+}

$$\mathrm{S(IV)} + \frac{1}{2}\mathrm{O_2} \xrightarrow{\mathrm{Mn^{2+}, Fe^{3+}}} \mathrm{S(VI)}$$

This reaction has been the subject of considerable interest (Hoffmann and Boyce, 1983; Martin, 1984; Hoffmann and Jacob, 1984; Hoffmann and Calvert, 1985; Clarke and Radojevic, 1987) and significantly different measured reaction rates, rate laws and pH dependencies have been reported (Hoffmann and Jacob, 1984). Martin and Hill (1987ab) have demonstrated that this reaction is inhibited as ionic strength increases. At present it is not known to what extent these catalytic reactions might be important in San Joaquin Valley fog and cloud water.

3.2.4 S(IV)-Free Radical Reactions

Free radicals, such as OH and HO_2, either heterogeneously scavenged by the aqueous phase or produced in the aqueous phase, participate in a series of aqueous phase reactions. Pandis and Seinfeld (1989a) proposed that under typical remote continental conditions there are two main radical pathways resulting in the conversion of S(IV) to S(VI):

$$S(IV)(+OH) \rightarrow SO_5^-(+O_2^-) \rightarrow HSO_5^-(+HSO_3^-) \rightarrow S(VI)$$
$$S(IV)(+OH) \rightarrow SO_5^- \rightarrow SO_4^-(+Cl^-, HSO_3^-) \rightarrow S(VI)$$

with the first of these two pathways typically being faster that the second.

3.2.5 S(IV)-NO_2 Reaction

Nitrogen dioxide has a low water solubility and therefore its low resulting aqueous-phase concentrations suggests that its oxidation of S(IV)

$$2NO_2 + HSO_3^- \xrightarrow{H_2O} 3H^+ + 2NO_2^- + SO_4^{2-}$$

should be of minor important in most cases. This reaction has been studied by Lee and Schwartz (1983) at pH 5.0, 5.8 and 6.4 and was described as a reaction that is first order in NO_2 and first order in S(IV), with a pH-dependent rate constant. This reaction is considered of secondary importance at the concentrations and pH values representative of clouds. However, Pandis and Seinfeld (1989b) reported that for fogs occurring in urban polluted areas with high NO_2

concentrations this reaction could be a major pathway for the S(IV) oxidation, if the atmosphere has enough neutralizing capacity, e.g. high NH_3 (g) concentrations.

3.2.6 S(IV)-HCHO Reaction

Sulfite and bisulfite can form complexes with various dissolved aldehydes. One important example is the reaction of sulfite or bisulfite with formaldehyde to produce hydroxymethanesulfonate ion (HMS) (Boyce and Hoffmann, 1984; Munger et al., 1984, 1986; Olson and Hoffmann, 1989; Faccini et al., 1992),

$$HCHO + SO_3^{2-} \leftrightarrows CH_2(O)SO_3^{2-}$$

$$HCHO + HSO_3^- \leftrightarrows HOCH_2SO_3^-$$

The HMS formed acts as a S(IV) reservoir protecting it from further oxidation, and its formation has been advanced to explain high S(IV) concentrations that have been observed in clouds and fogs. The rates of S(IV) complexation and oxidation are highly dependent on cloud pH and on the concentrations of HCHO and oxidants. Characteristic times for S(IV) depletion through complexation and oxidation can be compared for typical ranges of HCHO, H_2O_2, and pH. At pH values below about 4, the rate of these two reactions are several orders of magnitude slower than the reaction of S(IV) with dissolved H_2O_2. Thus, in this range oxidation predominates over complexation. The characteristic times of the two reactions become approximately comparable at pH around 5 so that complexation with HCHO becomes competitive with oxidation by H_2O_2. When pH exceeds 6, the reactions of S(IV) with HCHO became more important than reaction with H_2O_2. HMS formation can inhibit S(IV) oxidation if the S(IV) complexation rate is comparable to, or greater than, the S(IV) oxidation rate and the rate of SO_2 mass transport into the drop controls the rate of S(IV) oxidation. The effectiveness of HMS as a S(IV) reservoir depends critically on its resistivity to OH attack:

$$HOCH_2SO_3^- + OH \xrightarrow{O_2} SO_5^- + HCHO + H_2O$$

Jacob (1986) suggested a reaction constant of 1.4×10^9 M^{-1} s^{-1} for this reaction.

Formaldehyde is very soluble in water because it hydrates to its diol form, methylene glycol:

$$HCHO \xrightarrow{H_2O} H_2C(OH)_2$$

The equilibrium constant for this reaction is 1800, so that HCHO in cloud water is almost totally present as $H_2C(OH)_2$. Methylene glycol is rapidly oxidized by OH to produce formic acid (HCOOH).

$$H_2C(OH)_2 + OH \xrightarrow{O_2} HCOOH + HO_2 + H_2O$$

This reaction has been calculated to consume HCHO for typical continental clouds at a rate of 12% h^{-1} and therefore clouds are expected to decrease the ambient HCHO(g) concentrations and also to produce formic acid enhancing its gas-phase concentration.

3.3 Summary

As noted in the Introduction, time and resources did not permit the development of a detailed size-and chemically-resolved fog microphysical/chemical model in the present project, although such a development was an initial goal. The semi-empirical fog module incorporated into the aerosol model is described in Section 4.5. The fog treatment, given in Section 4.5, should be considered as an initial step, yet it captures in an zeroth-order manner the effect of liquid water on the processing of dissolved SO_2 to sulfate. Development of a size - and chemically - resolved version of the fog model and integration into the three-dimensional gas/aerosol model is a subject for future work.

4. UAM-AERO ACID DEPOSITION

4.1. OVERVIEW OF THE MODEL

This section provides a description of the UAM-AERO air quality model that has been used to simulate episodic air quality in the San Joaquin Valley (SJV) and the South Coast Air Basin (SoCAB) of California. As the name implies, the UAM-AERO model is based on the Urban Airshed Model (UAM-IV, SAI, 1990a,b,c,d,e). The UAM-AERO is an extension of the UAM model to treat aerosols as well as gaseous species. The UAM is a three-dimensional photochemical model that is recommended by the EPA for use in ozone attainment demonstration plans. It simulates the effects of emissions injection, horizontal and vertical transport and dispersion, dry deposition, and chemical reactions on atmospheric concentrations of pollutants. The procedures used in the UAM-AERO model to simulate horizontal transport and dispersion and emission injections are identical to those used in the standard UAM (SAI, 1990a,b,c,d,e). The formats of the input data and model running procedures are, for the most part, identical to those for the UAM; however, the UAM-AERO has additional input data requirements for aerosol species emissions and concentrations, and meteorological parameters.

The procedures used in the UAM-AERO model to simulate gas-phase chemical reactions and dry deposition of gases are similar to those in the UAM. The principle differences for gases are that the UAM-AERO model includes:

- A flexible gas-phase chemical mechanism interface that allows the chemical mechanism to be easily changed (Kumar et al., 1995). For the SJV demonstration runs, the UAM-AERO was run with the SAPRC90 chemical mechanism (Carter 1990); however, it has also been run with the Carbon Bond IV chemical mechanism (Gery et al., 1988) for South Coast Air Basin (SoCAB) runs. The list of reactions and the list of species for both mechanisms are given in Appendix A.

- Integration of the gas-phase chemical kinetics with an implicit-explicit hybrid (IEH) method employing the Livermore Solver for Ordinary Differential Equations (LSODE) solver to ensure high accuracy solutions (Sun et al., 1994; Chock et al., 1994; Kumar et al., 1995).

- Production of sulfuric acid from oxidation of sulfur dioxide.

- Production of condensable organic species from oxidation of gaseous organic compounds based on the organic aerosol yields reported by Pandis et al. (1992a).

- Calculation of the gas-phase chemical kinetic rate expressions from hourly three-dimensional temperature and water vapor concentration fields (rather than hourly two-dimensional temperature fields and hourly scalar water vapor concentration).

- An updated three-resistance dry deposition algorithm for gases based on Wesely (1989), which is comparable to that used in the SARMAP, RADM, and UAM-V models.

These features represent improvements in the model that have relatively small effects on the ozone predictions in most applications, but are scientifically more up-to-date than the features included in the standard UAM model.

The major difference between the UAM-AERO and UAM models is in the treatment of aerosol species. The UAM-AERO model includes additional algorithms to simulate physical and chemical processes important for atmospheric aerosols. The additional features included in the model are:

- Simulation of the aerosol concentrations of all the major primary and secondary components of atmospheric PM, including sulfate, nitrate, ammonium, chloride, sodium, elemental carbon, organic carbon, water, and other crustal material.
- A sectional approach for characterization of the continuous aerosol-size distribution, typically extending from 0.01 to 10 μm for aerosols and from 0.01 to 30 μm when fog droplets are present, with user-specified size bins. The model can also be applied with a single aerosol-size bin.
- The internally mixed aerosol assumption, where all particles in a specific size range are assumed to have the same chemical composition.
- An algorithm to simulate the mass transfer occurring between the gaseous and aerosol species during condensation, evaporation, and nucleation.
- An algorithm to simulate the distribution of aerosol species concentrations based on the thermodynamics of the sulfate/nitrate/chloride/ammonium/sodium/water chemical system encoded in the SEQUILIB aerosol module (Pilinis and Seinfeld, 1987; Pandis, 1996a).
- A fog module that empirically approximates the effects of fogs on gas-phase photolytic reaction rates, the effects of aqueous-phase chemical reactions occurring in fog droplets on sulfate and nitrate, and the effects of fogwater condensation and evaporation on the growth and shrinkage of the aerosol/fog droplet-size distribution.
- An algorithm to simulate particle deposition and gravitational settling for particles of various sizes.

The algorithms included in the UAM-AERO model have been partially adapted from the Size-Resolved Secondary Organic Aerosol Model (SRSOAM) developed by Pandis et al. (1993). The formulation of the modules are described below.

Numerous other small changes were made in the UAM code. One of the more significant changes was implementation of a numerical stability check and revised time step selection procedure in the vertical advection algorithm. Under conditions of sufficiently high vertical wind velocity and/or high deposition velocity, the original model became unstable, producing negative concentrations, because it used large time steps with regard to the Courrant number. The original UAM reset the negative concentrations to zero, which violates the conservation of mass principle. The revised code integrates the dry deposition and vertical advection separately and

selects a time step for vertical advection that assures numerical stability. Under conditions of high vertical wind velocities, the UAM-AERO takes numerous small time steps to complete the vertical advection integration for each time slice. Previously, it always took one step per time slice.

4.1.1. Gas Phase Chemistry

A distinguishing feature of the UAM-AERO model is its ability to predict the concentrations of secondary aerosols formed from gaseous precursor emissions. In particular, the UAM-AERO model is designed to predict the secondary sulfate, secondary nitrate, secondary ammonium, and secondary organic aerosols. Inclusion of a state-of-the-science gas-phase chemical mechanism is essential for predicting these secondary aerosol species. Under clear sky conditions, the rate-limiting process for the formation of aerosol nitrate and sulfate is often gas-phase chemical reactions. Simulation of the gas-phase chemical reactions, which convert NO_x to nitric acid and SO_2 to sulfuric acid, is essential for modeling secondary PM. Hydrocarbons and photochemistry play a key role in the atmospheric oxidation of NO_x and SO_2 and must be included as well. Furthermore, although the atmospheric chemistry is less certain, it is also desirable to simulate the formation of condensable organic species from the oxidation of VOCs.

The UAM-AERO has been designed with a flexible gas-phase chemical mechanism interface to allow the use of different chemical mechanisms. The SAPRC90 chemical mechanism (Carter, 1990) has been used for most of the UAM-AERO model development. The model has also been run with the Carbon Bond IV chemical mechanism (Gery et al., 1988). The SAPRC90 mechanism was selected for the development work because it has been evaluated extensively against environmental chamber data (Carter and Lurmann, 1991) and its VOC lumping scheme is better suited to the addition of organic aerosols than the Carbon Bond IV mechanism. In the SAPRC90 mechanism, the VOC species are lumped into the VOC classes listed in **Table 4-1**. Several aspects of the gas-phase chemistry are worth noting:

- The version of the SAPRC90 chemical mechanism used in UAM-AERO includes the gas-phase production of sulfuric acid from SO_2 via reaction with OH

$$SO_2 + OH \xrightarrow{O_2,H_2O} H_2SO_4 + HO_2 \qquad \textbf{(4-1)}$$

  Sulfuric acid produced by this reaction nucleates or condenses on existing aerosols, and is an important source of sulfate aerosols.

Table 4-1. Secondary organic aerosol yields for the SAPRC90 chemical mechanism organic classes for the 1987 SCAQS VOC emission inventory.

Species	Description	Numbers of Carbons	Aerosol Yield[a]
ALK1	Less reactive alkanes ($k_{OH} \leq 10{,}000$ ppm^{-1}min^{-1})	4.5	1.4
ALK2	More reactive alkanes ($k_{OH} > 10{,}000$ ppm^{-1}min^{-1})	7.4	144.
ARO1	Less reactive aromatics ($k_{OH} \leq 20{,}000$ ppm^{-1}min^{-1})	7.1	402.
ARO2	More reactive aromatics ($k_{OH} > 20{,}000$ ppm^{-1}min^{-1})	8.5	416.
CRES	Cresols and other alkyl phenols	7.	221.
OLE1	Less reactive alkenes ($k_{OH} \leq 75{,}000$ ppm^{-1}min^{-1})	3.7	9.5
OLE2	More reactive alkenes ($k_{OH} > 75{,}000$ ppm^{-1}min^{-1})	5.0	30.
OLE4	Biogenic C10 alkenes	10.	762.
HCHO	Formaldehyde	1.	0.
CCHO	Acetaldehyde	2.	0.
RCHO	Propionaldehyde and higher aldehydes	3.	0.
MEK	Methyl ethyl ketone and lumped higher ketones	4.	0.
MGLY	Methyl glyoxal	3.	0.
MEOH	Methanol	1.	0.
ETOH	Ethanol	2.	0.
MTBE	Methyl tertiary butyl ether	5.	0.
ETHE	Ethene	2.	0.
OLE3	Isoprene	5.	0.

[a] Aerosol yields are in $\mu g\ m^{-3}$ ppm^{-1} of aerosol mass, including carbon, hydrogen, oxygen, etc. (not just carbon). The individual component yields are from Pandis et al. (1992a). The lumped compound yields are based on the VOC composition of the 1987 regional emission inventory for the South Coast Air Basin.

- The SAPRC90 chemical mechanism includes the production of formic and acetic acids from alkenes. These products do not affect ozone production and are usually omitted from the mechanism in ozone modeling. These two organic acids are included in the mechanism for UAM-AERO because ambient data suggest they are relatively abundant in Southern California (Solomon et al., 1988; Peters et al., 1995) and they can influence the pH of fogwater. Therefore, they can influence the rate of oxidation of dissolved SO_2 by ozone and oxygen catalyzed by iron and manganese in fogwater droplets. It is assumed that Criegee bi-radicals formed in ozone-alkene reactions react solely with water vapor to form these organic acids.

- Ammonia and hydrochloric acid (HCl) are included as gas-phase species in UAM-AERO, however, they only interact with the aerosol phase. That is, the gas-phase reactions of ammonia and HCl are of negligible importance relative to their interactions with the aerosol phase.

- For this application, the SAPRC90 chemical mechanism has been extended to include production of condensable organic species from higher molecular weight (C5+) gaseous

VOCs. The condensable organic compound (COC) yields for the lumped organic compounds are obtained from the database of individual compound yields reported by Pandis et al. (1992a) and the composition of the regional VOC emission inventories. The knowledge of the chemical composition of most condensable vapor products and the exact chemical pathways leading to their formation, including the stoichiometry and rate constants, remains incomplete. Therefore, the mechanistic description of the production of low-volatility products follows the condensed gas-phase mechanisms used in regional photochemical models. The atmospheric oxidant of a hydrocarbon, HC, by an oxidant like OH, O_3, or NO_3 is described by a single reaction that incorporates all the individual mechanistic steps

$$HC + Oxidant \text{ ---> } aA + bB + ... + gG \qquad \textbf{(4-2)}$$

where A, B, etc., are the regular gaseous products, G is a generic condensable gas that forms secondary organic aerosol, and g is the corresponding stoichiometric coefficient. The stoichiometric coefficient g is approximately equivalent to the fractional aerosol yield, Y, of the hydrocarbon. Experimental measurements of the aerosol yields, Y, are available from the literature for numerous hydrocarbons and estimates of the yields of the remaining hydrocarbons are provided by Grosjean and Seinfeld (1989) and Pandis et al. (1992a). Examples of the aerosol yields from the lumped organics included in the SAPRC90 chemical mechanism for the 1987 SCAQS VOC inventory are shown in Table 2-1.

Lastly, the numerical integration of the gas-phase chemical kinetics in the UAM-AERO is performed with an IEH method. The fast-reacting chemical species are integrated with an implicit solver (LSODE, which is a GEAR technique) and the more slowly reacting species are integrated with an explicit technique. The steady-state approximation is made for fast-reacting radical species that do not react with other radical species. As shown in **Table 4-2**, the important radical species, ozone, NO, NO_2, NO_3, and N_2O_5, are treated as fast-reacting species and most of the VOCs, HNO_3, SO_2 are treated as slow-reacting species. The IEH solver has been carefully evaluated and shown to provide highly accurate solutions (Sun et al., 1994; Chock et al., 1994; Kumar et al., 1995). The IEH solver also uses substantially less CPU time than the original UAM solver for the SAPRC90 mechanism (but comparable CPU time for the Carbon Bond IV mechanism).

4.1.2. Aerosol Thermodynamics

The inorganic and organic aerosol species are distributed among the aerosol and gas phases by assuming that thermodynamic equilibrium is established over time scales smaller than the 5- to 15-minute operator-splitting time step used in the model. Stelson et al. (1979) postulated that ammonium nitrate aerosol constituents should be in thermodynamic equilibrium with the local gas phase. Hildemann et al. (1984) found that particulate and gaseous concentrations at some inland sites in the Los Angeles Basin agreed with the thermodynamic equilibrium assumption. Wexler and Seinfeld (1990) predicted that the more volatile inorganic

Table 4-2. Fast-reacting, slow-reacting, and steady-state species in the SAPRC90 mechanism.

Fast-Reacting Species	Slow-Reacting Species		Steady-State Species
O_3	ALK1	MGLY	O
NO	ALK2	AFG2	O^1D
NO_2	ETHE	-OOH	RO_2-R
NO_3	OLE1	CO	RO_2-N
N_2O_5	OLE2	HONO	R_2O_2
OH	OLE3	HNO_3	HOCOO
HO_2	OLE4	HNO_4	BZ-O
RO_2	HCHO	PAN	
CCO_3	CCHO	PPN	
C_2CO_3	RCHO	RNO_3	
CRES	ARO1	H_2O_2	
	ARO2	SO_2	
	MEK	H_2SO_4	
	COC	FACD	
		AACD	

components of atmospheric aerosols may not be in equilibrium with their gas-phase counterparts due to mass transfer limitations under some atmospheric conditions (e.g., low temperatures and low particle number concentrations) and found support for their predictions in some of the SCAQS data (Wexler and Seinfeld, 1992). Testing was performed to determine the practicality of including detailed mass transfer calculations in UAM-AERO and the results suggested the computational burden for simulating the detailed mass transfer calculation was large and impractical (Wexler et al., 1994). Thus, the gas-aerosol equilibrium assumption is employed in the model, despite the potential error introduced in certain cases.

The inorganic multicomponent atmospheric aerosol equilibrium model, SEQUILIB, of Pilinis and Seinfeld (1987) with recent updates (Pandis, 1996a) is used for the calculation of the total quantities of ammonium, chloride, nitrate, and water contained in atmospheric particles. The model predicts the gas-phase concentrations of NH_3, HCl, HNO_3, and the aerosol-phase concentrations of H_2O, NH_4^+, $SO_4^=$, NO_3^-, Na^+, Cl^-, HSO_4^-, H_2SO_4, Na_2SO_4, $NaHSO_4$, NaCl, $NaNO_3$, NH_4Cl, NH_4NO_3, $(NH_4)_2SO_4$, NH_4HSO_4, and $(NH_4)_3H(SO_4)_2$ using the equilibrium relationships shown in **Table 4-3**. It uses the Bromley method to obtain multicomponent activity coefficients (Bromley, 1973) and the Pitzer method to obtain the binary activity coefficients (Pitzer, 1979). Kim et al. (1993a,b) suggest that the Pitzer method is more accurate than the Bromley method for multicomponent activity coefficients and that the K-M method (Kusik and Meissner, 1978) may be more accurate than the Pitzer method for binary activity coefficients. Given the paucity of high-concentration laboratory data on which to evaluate their performance, the activity coefficient calculation methods originally coded in SEQUILIB were used. The water activity coefficients are obtained using the ZSR method (Stokes and Robinson, 1966). The equilibrium code has been relatively successful in

Table 4-3. Equilibrium relations in the SEQUILIB aerosol module.

Reaction	Equilibrium Constant
$NaCl(s) + HNO_3(g) \leftrightarrow NaNO_3(s) + HCl(s)$	$3.96\exp\left[5.50\left(\frac{T_o}{T}-1\right)-2.180\left(1+\ln\left(\frac{T_o}{T}\right)-\frac{T_o}{T}\right)\right]$
$NH_3(g) + HNO_3(g) \leftrightarrow NH_4^+ + NO_3^-$	$3.99\times10^{17}\exp\left[64.7\left(\frac{T_o}{T}-1\right)+11.51\left(1+\ln\left(\frac{T_o}{T}\right)-\frac{T_o}{T}\right)\right]\ mol^2Kg^{-2}atm^{-2}$
$HCl(g) \leftrightarrow H^+ + Cl^-$	$2.03\times10^{6}\exp\left[30.21\left(\frac{T_o}{T}-1\right)+19.91\left(1+\ln\left(\frac{T_o}{T}\right)-\frac{T_o}{T}\right)\right]\ mol^2Kg^{-2}atm^{-1}$
$NH_3(g) + HCl(g) \leftrightarrow NH_4^+ + Cl^-$	$2.12\times10^{17}\exp\left[65.08\left(\frac{T_o}{T}-1\right)+14.51\left(1+\ln\left(\frac{T_o}{T}\right)-\frac{T_o}{T}\right)\right]\ mol^2Kg^{-2}atm^{-2}$
$Na_2SO_4(s) \leftrightarrow 2Na^+ + SO_4^{2-}$	$0.4805\exp\left[0.98\left(\frac{T_o}{T}-1\right)+39.57\left(1+\ln\left(\frac{T_o}{T}\right)-\frac{T_o}{T}\right)\right]\ mol^3Kg^{-3}$
$(NH_4)_2SO_4(s) \leftrightarrow 2NH_4^+ + SO_4^{2-}$	$1.425\exp\left[-2.65\left(\frac{T_o}{T}-1\right)+38.55\left(1+\ln\left(\frac{T_o}{T}\right)-\frac{T_o}{T}\right)\right]\ mol^3Kg^{-3}$
$HSO_4^- \leftrightarrow H^+ + SO_4^{2-}$	$1.031\times10^{-2}\exp\left[7.59\left(\frac{T_o}{T}-1\right)+18.83\left(1+\ln\left(\frac{T_o}{T}\right)-\frac{T_o}{T}\right)\right]\ mol\,Kg^{-1}$
$HNO_3(g) \leftrightarrow H^+NO_3^-$	$3.638\times10^{6}\exp\left[29.47\left(\frac{T_o}{T}-1\right)+16.84\left(1+\ln\left(\frac{T_o}{T}\right)-\frac{T_o}{T}\right)\right]\ mol^2Kg^{-2}atm^{-1}$
$NH_4Cl(s) \leftrightarrow NH_3(g) + HCl(g)$	$1.039\times10^{-16}\exp\left[-71.04\left(\frac{T_o}{T}-1\right)+2.40\left(1+\ln\left(\frac{T_o}{T}\right)-\frac{T_o}{T}\right)\right]\ atm^{-2}$
$NH_3(g) + HNO_3(g) \leftrightarrow NH_4NO_3(s)$	$3.349\times10^{16}\exp\left[75.11\left(\frac{T_o}{T}-1\right)-13.46\left(1+\ln\left(\frac{T_o}{T}\right)-\frac{T_o}{T}\right)\right]\ atm^{-2}$
$NaNO_3(s) \leftrightarrow Na^+ + NO_3^-$	$11.971\exp\left[-8.22\left(\frac{T_o}{T}-1\right)+16.01\left(1+\ln\left(\frac{T_o}{T}\right)-\frac{T_o}{T}\right)\right]\ mol^2Kg^{-2}$
$NaCl(s) \leftrightarrow Na^+ + Cl^-$	$37.743\exp\left[-1.57\left(\frac{T_o}{T}-1\right)+16.89\left(1+\ln\left(\frac{T_o}{T}\right)-\frac{T_o}{T}\right)\right]\ mol^2Kg^{-2}$
$NaHSO_4(s) \leftrightarrow Na^+ + HSO_4^-$	$2.44\times10^{4}\exp\left[0.79\left(\frac{T_o}{T}-1\right)+4.53\left(1+\ln\left(\frac{T_o}{T}\right)-\frac{T_o}{T}\right)\right]\ mol^2Kg^{-2}$

predicting the concentrations of the various aerosol species in the SoCAB (Pilinis and Seinfeld (1987, 1988) and elsewhere (Watson et al., 1994a).

Thermodynamic equilibrium is also assumed for the condensable organic vapors. When their gas-phase concentrations exceed their vapor pressure, the vapors condense to the aerosol phase in an effort to establish equilibrium. Evaporation occurs when the gas phase is subsaturated. Following Pandis et al. (1992a), the UAM-AERO model assumes a negligibly small saturation vapor pressure (0.1 ppt), which essentially places all of the condensable organic material in the aerosol phase. Due to the physical and chemical uncertainties in the secondary

organic aerosol species, no attempt is made to estimate the amount of water absorbed or desorbed by the organic particles. Saxena et al. (1995) have shown that condensed organic species can alter the hygroscopic behavior of atmospheric particles, and alterations may be positive or negative depending on the location (nonurban or urban). These differential water absorption effects are not included in the model.

4.1.3. Modeling the Aerosol-Size Distribution

The UAM-AERO model can be exercised using one or more aerosol-size bins. In theory, simulation of the aerosol-size distribution is necessary to accurately simulate the chemical evolution of the aerosol and the aerosol removal by deposition. It is generally recommended that the model be run with at least eight sections below 10 μm and one section above 10 μm if fogs occur in the simulation period. Typical aerosol-size sections used in the model are shown in **Table 4-4**. While these sections are logarithmically spaced, the model's algorithm can accommodate arbitrarily spaced size bins.

Table 4-4. Typical aerosol-size bins used in the UAM-AERO model.

Section	Particle Size (μm)
1	$0.04^a < D_p \leq 0.08$
2	$0.08 < D_p \leq 0.16$
3	$0.16 < D_p \leq 0.31$
4	$0.31 < D_p \leq 0.62$
5	$0.62 < D_p \leq 1.25$
6	$1.25 < D_p \leq 2.5$
7	$2.50 < D_p \leq 5.0$
8	$5.00 < D_p \leq 10.0$
9	$10.0 < D_p \leq 30.0$

[a] The model requires a lower size limit on the first bin to calculate aerosol properties. The first size bin contains all particles with diameters less than 0.08 μm.

The UAM-AERO model uses the internally mixed assumption for aerosol composition. The aerosol-size composition is discretized in size sections and all particles in each section are assumed to have the same chemical composition (Gelbard et al., 1980; Seigneur et al., 1986). The movement of these sections in the size coordinate, as a result of particle growth and shrinkage (i.e., by gas-to-particle conversion, condensation, or evaporation), is initially

calculated using the moving section technique (Gelbard, 1990; Kim and Seinfeld, 1990). With the moving section technique, the number of particles in each size bin is constant during the aerosol transport step and the changes in mass due to condensation or evaporation are reflected in new mass mean diameters for the sections. In some situations where a large amount of mass is being transported between the gas and aerosol phases, multiple aerosol transport steps are taken to assure numerical stability. However, because the three-dimensional air quality model requires fixed aerosol-size bins for the advection and diffusion steps, the mass in the new size distribution is reallocated to the original size bins using a mass-conserving cubic spline-fitting procedure.

The gas-aerosol transport is calculated as follows. The single particle flux of condensate or evaporate is

$$J_i = \frac{2\pi D_p D_i (C_{ai} - C_{ei})}{1 + \beta} \tag{4-3}$$

where D_p is the particle diameter, D_i is the molecular diffusivity of the condensing or evaporating compound i, and $C_{ai} - C_{ei}$ is the difference between the ambient concentration (C_{ai}) and the equilibrium particle surface concentration (C_{ei}). Beta is defined as

$$\beta = \frac{2\lambda}{\alpha D_p} \tag{4-4}$$

where λ is the mean free path of air and α is the accommodation coefficient. In the model, gases are transported to particles of diameter D_p at a rate given by Equation 4-3. The overall transport rate to a size section (nJ_i) depends on the number of particles in the section, $n(D_p)$, and the single-particle transport rate. The fraction of condensate that appears in each size section, f, is given by

$$f = \frac{2\pi D_p D_i (C_{ai} - C_{ei}) / (1+\beta)}{\int_0^\infty 2\pi D_p D_i (C_{ai} - C_{ei}) / (1+\beta) dD_p} \tag{4-5}$$

In general, C_{ei} depends on chemical composition of the aerosol in each size section, but in the UAM-AERO model C_{ei} is determined from the aerosol equilibrium calculation on the total aerosol chemical composition. When the concentration difference ($C_{ai} - C_{ei}$) is independent of particle size, the transport factor expression reduces to

$$f = \frac{nD_p / (1+\beta)}{\int_0^\infty nD_p / (1+\beta) dD_p} \tag{4-6}$$

where β depends on the particle size and accommodation coefficient. The accommodation coefficient has been estimated to range from near unity, for water molecules condensing on water, to 10^{-4}. Changes in accommodation coefficient independent of particle size alter the size distribution of the condensate. Smaller values of the accommodation coefficient favor condensation on larger particles. Based on the work of Pandis et al. (1993), an accommodation coefficient of one is used for water and all other aerosol species in the UAM-AERO.

To predict the size distribution of the condensable compounds, the model first calculates the gas-phase concentrations of these compounds resulting from transport and chemical reactions. For the inorganic compounds, the equilibrium concentrations of the total aerosol and vapors are determined from SEQUILIB. The amount condensed or evaporated is partitioned among the sections in accordance with Equation 4-5. SEQUILIB is then used again to obtain improved estimates of the water content of each aerosol section. As a result of the condensation or evaporation, the aerosol-size sections grow or shrink. Then, the mass in the new size distribution is reallocated to the original size bins using a mass-conserving cubic spline-fitting procedure. The cubic spline reallocation procedure is numerically robust, however, it introduces some pseudo dispersion into the size distributions. That is, the predicted size distributions are somewhat smoother or broader than may exist in the ambient atmosphere. During periods of rapidly increasing or decreasing moisture, the gas-aerosol transfer and resizing is performed using small time steps to ensure the size distribution evolves in a stable manner.

It is generally recommended that the model be run with at least eight sections below 10 μm and one section above 10 μm if fogs occur in the simulation period. However, comparable (±10 percent) PM_{10} predictions have been obtained from one-section and nine-section simulations of SCAQS episodes when the particle deposition velocities for the one-section simulation were based on the average size distribution calculated for the nine-section simulation. Tests using five sections gave similar PM_{10} predictions, but poor $PM_{2.5}$ predictions compared to nine-section simulations. Fine size resolution (e.g., eight or more size bins below 10 μm) is needed if the model outputs are used for calculation of atmospheric light scattering and absorption by particles in visibility models (Richards et al., 1996).

4.1.4. Fog Module

Fogs can have significant effects on gaseous and aerosol pollutants in the atmosphere (Munger et al., 1983; Waldman, 1986; Jacob et al., 1984, 1986a, 1986b, 1987; Pandis and Seinfeld, 1989; Pandis et al., 1992b). Fogs absorb soluble gases, such as nitric acid, sulfur dioxide, hydrogen peroxide, and carbon dioxide, and fogs scavenge particles, especially those with diameters greater than about 0.3 μm. Fog droplets grow, by absorbing water and pollutants, to sizes where they deposit rapidly (compared to the deposition rates of typical atmospheric aerosols under nonfog conditions). Enhanced removal of dissolved gases and scavenged particles from the atmosphere is one of the major effects of fog on pollutant levels.

Another important effect of fogs is the production of particles, particularly sulfate aerosols, from aqueous-phase oxidation of dissolved SO_2 in fog droplets. Dissolved SO_2 is

oxidized in the aqueous phase by hydrogen peroxide, ozone, and oxygen catalyzed by iron and manganese. Aqueous-phase SO_2 oxidation rates can be fast compared to gas-phase oxidation rates (Calvert and Stockwell, 1983). The rate of aqueous-phase SO_2 oxidation depends on the amount of liquid water in the atmosphere, the amount of oxidants present, and usually the acidity (or pH) of the fogwater. SO_2 oxidation by hydrogen peroxide is fast and does not depend on the fogwater acidity. SO_2 oxidation by ozone and oxygen (catalyzed by Fe and Mn) is fast at high pH (above 6) and slow at low pH (below 4).

Fogs in the atmosphere also modify the vertical distribution of solar radiation, which in turn affect the photolytic reaction rates. Typically, fogs reduce the solar radiation intensity within the fog layer and enhance the solar radiation above the fog layer. Changes in the radiation intensity directly affect the photolytic reaction rates of gases and dissolved species. This can have an important effect on atmospheric photochemistry because the photolytic reactions are the driving force behind the atmospheric oxidation of VOCs, NO_x, and SO_2.

The effects of fogs on pollutant levels are simulated in an empirical manner in the UAM-AERO model. The time and locations of haze and fog are input to the model hourly using codes of 1 for no fog, 2 for haze, and 3 for fog (i.e., hourly gridded two-dimensional fog code fields are input to the model). When haze or fog exist, the model allows particles to grow to larger sizes (i.e., above 10 μm). Particle growth and shrinkage is determined by the amount of water transferred to and from the aerosol based on the equilibrium concentrations estimated by SEQUILIB for specific relative humidity, temperature, and aerosol chemical composition. SEQUILIB is used in the fog module to estimate the equilibrium concentrations during fogs much like during nonfog periods. Deposition of fog droplets is calculated using the same equations used for other aerosols, however, the size of the droplets are allowed to exceed 10 μm in diameter. Typically, one extra size bin (e.g., 10 to 30 μm) is used to simulate the fog droplet growth above 10 μm.

The effects of aqueous-phase kinetic reactions are simulated using the gas-phase chemistry operator. A first-order reaction of gaseous SO_2 forming sulfuric acid (H_2SO_4) and a second-order reaction of SO_2 with gaseous H_2O_2, forming H_2SO_4 are assigned nonzero rates during foggy or hazy conditions if the relative humidity is above 80 percent. An example of empirical rates of the reactions are shown in **Table 4-5**. These rates are assigned in an include file "fog.inc" which can be modified by the user (see Section 3). The rate of hydrolysis of nitrogen pentoxide (forming nitric acid) is increased by factors of 5 and 50 during hazy and foggy periods, respectively, to simulate the enhanced hydrolysis rates expected when liquid water exists for the heterogeneous reaction. Lastly, the empirical fog module reduces

Table 4-5. Chemical reactions included in the empirical fog module.

Chemical Reactions[a]	No Fog KFOG = 1	Haze & RH > 70 KFOG = 2	Heavy Fog KFOG = 3
$SO_2(g) + H_2O_2(g) \dashrightarrow H_2SO_4(g)$	k = 0 in all layers	k =0.05 $ppm^{-1}min^{-1}$ in layers 1-2 k = 0 in layers 3-5	k = 5 $ppm^{-1}min^{-1}$ in layers 1-2 k = 0 in layers 3-5
$SO_2(g) \dashrightarrow H_2SO_4(g)$	k = 0 in all layers	k = .00033 min^{-1} in layers 1-2 k= 0 in layers 3-5	k = 0.00167 min^{-1} in layers 1-2 k = 0 in layers 3-5
$N_2O_5(g) + H_2O(g) \dashrightarrow 2HNO_3(g)$	k = Original in all layers	k = 5x original in layers 1-2 k = Original in layers 3-5	k = 50x original in layers 1-2 k = Original in layers 3-5
All photolytic reactions	Clear sky rates in all layers	Clear sky rates in all layers	70% clear sky rates in layers 1-2 130% clear sky rates in layers 3-5

[a] Gaseous H_2SO_4 is rapidly transferred to the interstitial aerosol or fog droplets [$H_2SO_4(g) \dashrightarrow SO(aq) + 2H^+(aq)$].

photolytic reaction rates by 30 percent within the fog layers (assumed to be layers 1 and 2) and increases photolytic reaction rates by 30 percent above the fog layers (assumed to be layers 3-NZ, where NZ is the total number of vertical layers) to simulate effects of fogs on the solar actinic flux during fogs (not haze). The rates incorporated into the UAM-AERO fog module are empirical. The rates are plausible based on aqueous-phase kinetic data, fog microphysical data, and radiation data. However, the rates may need to be adjusted for specific areas or as more experience (empirical evidence) is gained with the model. For example, a lower rate for the first-order SO_2 reaction is usually used in late fall or winter simulations because there is typically less oxidant available to oxidize SO_2 in fogwater in that season.

4.1.5. Dry Deposition

Deposition of particles and gases is treated as a first-order removal process in UAM-AERO. The deposition velocity (v_d) is defined as a mass conductance (or inverse resistance) of the form

$$v_d = \frac{1}{r_T} = -\frac{F_c}{C_z} \qquad (4\text{-}7)$$

where r_T is the total resistance (s/m) to mass transport to the surface, F_c is the depositing mass flux ($\mu g/m^2 s$), and C_z is the time-averaged ambient concentration ($\mu g/m^3$) of the pollutant at reference height z. This formulation is identical to that included in the standard UAM. However, the similarity between the UAM and UAM-AERO deposition routine ends there. Substantial improvements were made in the methods and data used to calculate the deposition velocities in the UAM-AERO model. These were needed because the UAM model did not have an algorithm to calculate deposition velocities for particles and because the UAM procedures for calculating gas deposition velocities were out-of-date and inconsistent with current theory and practice.

Improvements in the deposition routines necessitated supplying additional input data to the model. The new gas deposition routine requires gridded land-use data that specify the predominant land use in each grid using an 11-category scheme. In addition, the routine requires the instantaneous solar radiation intensity, which is estimated in the model based on the location, date, time of day, and the clear sky assumption. The new deposition routine also uses the surface air temperature and relative humidity for each grid as well as the surface roughness, wind speed, and atmospheric stability.

4.1.5.1.Dry deposition of particles

The dry deposition of particles to surfaces may occur from diffusion, impaction, and/or gravitational settling. The dominant mechanism for particle deposition varies with the particle

size. In UAM-AERO, particle deposition velocities are calculated from the following equation recommended by Slinn and Slinn (1980)

$$v_d^i = \frac{1}{r_a + r_d^i + r_a r_d^i v_g} + v_g^i \qquad \textbf{(4-8)}$$

where
v_d^i = deposition velocity (m/s) of particles of the ith size bin
r_a = aerodynamic resistance (s/m)
r_d^i = deposition layer resistance (s/m) of particles of the ith size bin
v_g^i = gravitational settling velocity (m/s) of particles of the ith size bin

Particle diffusion in the thin, quasi-laminar deposition layer just above the surface is principally due to Brownian diffusion and inertial impaction. Particles transported through this layer are assumed to stick to the surface (Voldner et al., 1986). The resistance to diffusion through this layer (r_d) is parameterized in terms of the Schmidt number and the Stokes number. The deposition layer resistance is given by

$$r_d^i = \frac{1}{u_* (Sc^{-2/3} + 10^{-3/St})}$$

$$S_c = \frac{\nu}{D} \quad \textit{(Schmidt number)} \qquad \textbf{(4-9)}$$

$$S_t = \frac{v_g^i u_*^2}{\nu g} \quad \textit{(Stokes number)}$$

where
ν = viscosity of air
D = Brownian diffusivity
v_g^i = gravitational settling velocity (of the ith particle-size bin)
u_* = friction velocity

The gravitational settling velocity is calculated from

$$v_g = \frac{D_p^2 g C(\rho_p - \rho_g)}{18\nu}$$

$$C = 1 + \frac{2\lambda}{D_p}\left[1.257 + 0.4\exp\left(\frac{-0.55 D_p}{\lambda}\right)\right] \qquad \textbf{(4-10)}$$

where
D_p = particle diameter (m), mean diameter of particle-size bin
ρ_p = particle density (g/m^3)
ρ_g = air density (g/m^3)
g = acceleration due to gravity (m/s^2)
C = Cunningham correction factor for small particles
λ = mean free path of air (m)
ν = viscosity in g/m-s

Deposition in the constant-flux, surface layer, which is the next 10 to 20 m above the deposition layer, is a function of the atmospheric turbulence (or stability) and the surface characteristics. The aerodynamic resistance (r_a) is the same for gases and particles, and is calculated from

$$r_a = \frac{1}{k\,u_*}\left[\ln\left(\frac{z_s}{z_o}\right) - \phi_H(L, z_s)\right] \qquad \textbf{(4-11)}$$

where
z_s = reference height (m)
z_o = surface roughness height (m)
k = von Karman constant (0.4)
ϕ_H = stability correction term
L = Monin-Obukhov length (m)

Figure 4-1 shows experimental data for size dependence of particle deposition velocities. The data indicate particles with diameters less than 0.015 μm and greater than 2 μm have significant deposition velocities, while particles in the 0.015- to 2-μm range do not. The reason for this behavior is that small particles ($D_p < 0.015$ μm) behave much like gases and are efficiently transported across the deposition layer by Brownian diffusion. Brownian diffusion is not an effective transport mechanism for particles with diameters above 0.05 μm. Moderately large particles in the 2- to 20-μm-diameter range are efficiently transported across the deposition layer by inertial impaction and the deposition of even larger particles ($D_p > 20$ μm) is principally due to gravitational settling. Since the settling velocity increases with the square of the particle diameter, large particles (and fog droplets) have relatively high deposition velocities. There are no effective transport mechanisms for particles in the 0.015 to 2-μm-diameter range, the size range for most secondary aerosols in the atmosphere. The atmospheric lifetimes of these particles may be many days unless they are scavenged by fog or precipitation.

In UAM-AERO, the deposition velocities of all particles in a specific size bin are calculated using the geometric mass mean diameter of the size section. The deposition velocities are calculated at each time step (5 to 15 minutes) of the simulation. If the model is applied using only one size section, the model assumes the aerosol size is log-normally distributed for each component. It uses internally stored geometric-mass mean diameters (D_p^{mean}) and geometric standard deviations (F_d) for each chemical component to compute a mass-weighted average deposition velocity based on nine calculations of deposition velocities for diameters between $D_p^{mean} - 2\sigma_d$ and $D_p^{mean} + 2\sigma_d$. The size distributions for one-section simulations are spatially and temporally invariant; however, separate size parameters are input for each aerosol component. The default geometric mass mean diameters and geometric standard deviations of each chemical components for nonfog and fog conditions are listed in **Table 4-6**. The default size distributions were calculated from predicted size distribution from a nine-section simulation of the June 24-25, 1987 episode and may overestimate the deposition of PM_{10} in some applications. The user can input application-specific size distributions to override the default distributions.

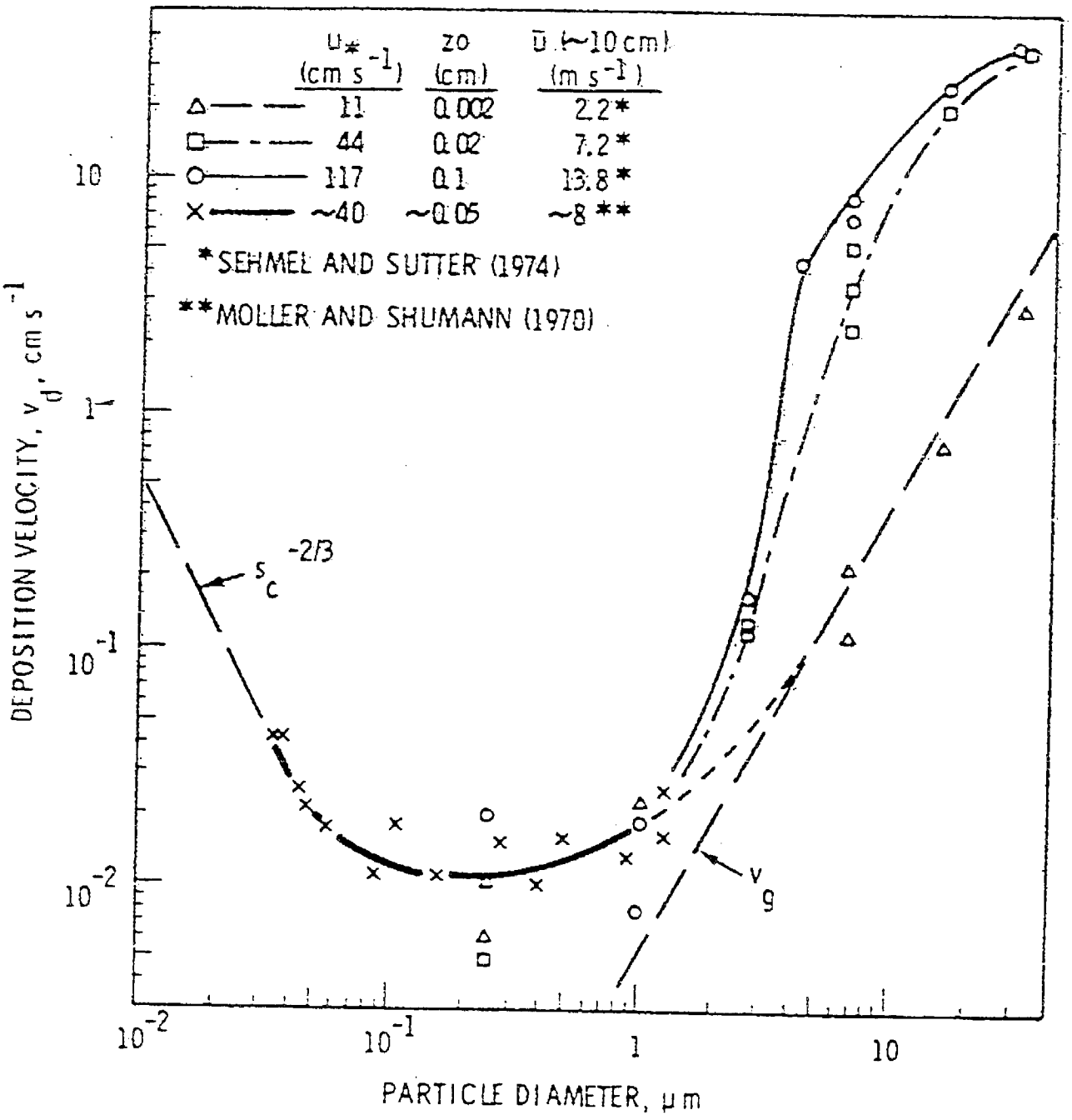

Figure 4-1. Deposition velocity as a function of particle size for particles depositing on a water surface in a wind tunnel. (Slinn et al., 1978)

Table 4-6. Default PM_{10} aerosol-size distributions used for aerosol deposition velocity calculations.

Chemical Component	Geometric Mean Diameter[a] (μm)	
	Nonfog Conditions	Foggy Conditions
$SO_4^=$	1.3	2.6
NO_3^-	1.2	2.4
NH_4^+	1.1	2.2
OC	1.8	3.6
EC	1.6	3.2
Na^+	2.4	4.8
Cl^-	1.7	3.4
H_2O	1.5	3.0
H^+	1.6	3.2
Other	2.1	4.2

[a] A geometric standard deviation of 2 is used in all cases.

4.1.5.2.Dry deposition of gases

In contrast to particles, the dry deposition of gases to surfaces depends not only on the prevailing meteorological conditions and surface roughness, but also on the nature and state of the surface and the chemical nature of the pollutant. Deposition of gases is due to a number of mass transport and uptake processes that can conveniently be divided into three serial resistances.

$$v_g^i = \frac{1}{r_a + r_d^i + r_s^i} \qquad \textbf{(4-12)}$$

The aerodynamic resistance (r_a) is the resistance to mass transport from the reference height (z) to the top of the quasi-laminar layer above the surface and it is calculated using Equation 2-11 for both gases and particles. The deposition layer resistance (r_d^i) is the resistance to mass transfer across the quasi-laminar layer and it depends on the Schmidt number and the friction velocity, as shown below (Wesely, 1989).

$$r_d^i = \frac{5(Sc_i)^{0.67}}{u_*} \qquad \textbf{(4-13)}$$

The surface resistance r_s^i represents the overall resistance to uptake of a specific pollutant at the surface or within a surface media (vegetation, soil, water, etc.). The surface resistance is the most complex term in the formulation and many different approaches are available to estimate this term (Wesely, 1989; Scire et al., 1990; Massman, 1993; Hicks et al., 1987; Sheih et al., 1986; Russell et al., 1993; Gray et al., 1991). The approach adopted for UAM-AERO is primarily based on the methodology developed by Wesely (1989) for regional modeling. The Wesely approach was selected because it addresses the most pollutants, land-use types, and seasons. Optionally, UAM-AERO can be run with a slightly different version of Wesely's approach, which is similar to that used in the UAM-V model (Gray et al., 1991) and the CALPUFF model (Scire et al., 1990).

For all land-use types, Wesely divides the surface resistance into component resistances representing specific physical processes. Again, using the analogy to electrical circuits, the surface resistance is calculated from individual bulk component resistances

$$r_s = \left(\frac{1}{r_{st} + r_m} + \frac{1}{r_{lu}} + \frac{1}{r_{dc} + r_{cl}} + \frac{1}{r_{ac} + r_{gs}} \right)^{-1} \qquad \textbf{(4-14)}$$

where the first term includes the leaf stomatal (r_{st}) and mesophyllic (r_m) resistances; the second term is outer surface resistance in the upper canopy (r_{lu}), which includes the leaf cuticular resistance in healthy vegetation and the other outer surface resistances; the third term is resistance in the lower canopy, which includes the resistance to transfer by buoyant convection (r_{dc}) and the resistance to uptake by leaves, twigs, and other exposed surfaces; and the fourth term is resistance in the ground, which includes a transfer resistance (r_{ac}) for processes that depend only on canopy height and a resistance for uptake by the soil, leaf litter, etc. at the ground surface. Wesely provides tabulated values of 7 resistance components (r_j, r_{lu}, r_{ac}, r_{gsS}, r_{gsO}, r_{clS}, r_{clO}) for 5 seasonal categories, and for 11 land-use types. The seasonal categories and land-use types are shown in **Table 4-7**. All the resistances needed to apply Equation 4-14 to an individual gas can be calculated from the baseline resistance values.

The stomatal resistance is calculated from tabulated values of r_j, the solar radiation (G, in W/m^2), and surface air temperature (T_s) using

$$r_{st} = r_j \left(1 + \left(\frac{200}{G + 0.1} \right)^2 \left(\frac{400}{T_s(40 - T_s)} \right) \right) \qquad \textbf{(4-15)}$$

in cases where the surface temperature is between 0 and 40°C. Outside of this range, the stomata are assumed to be closed and r_{st} is set to a large value. The combined minimum stomatal and mesophyll resistance is calculated from

Table 4-7. Season and land-use categories used for determining dry deposition resistances.

No.	Season Category	No.	Land-use Category
1	Midsummer with lush vegetation	1	Urban land
2	Autumn with unharvested cropland	2	Agricultural land
3	Late autumn after frost, no snow	3	Range land
4	Winter, snow on ground and subfreezing	4	Deciduous forest
5	Transitional spring with partially green short annuals	5	Coniferous forest
		6	Mixed forest including wetland
		7	Water, both salt and fresh
		8	Barren land, mostly desert
		9	Nonforested wetland
		10	Mixed agricultural and range land
		11	Rocky open areas with low-growing shrubs

$$r_{sm}^{i} = r_{st}^{i} + r_{m}^{i} = r_{s}\left(\frac{D_{H20}}{D_{i}}\right) + \left(\frac{1}{3.3\times10^{-4} H_{i}^{*} + 100 f_{o}^{i}}\right) \qquad \textbf{(4-16)}$$

where D_{H2O}/D_i is the ratio of the molecular diffusivity of water to the diffusivity of the specific gas (i), H_i^* is the Henry's Law constant (M/atm) for the gas, and f_o^i is a normalized (0 to 1) reactivity factor for the dissolved gas.

The resistance of the outer surfaces in the upper canopy for a specific gas (i) is computed from

$$r_{lu}^{i} = r_{lu}\left(\frac{1}{10^{-5} H_{i}^{*} + f_{o}^{i}}\right) \qquad \textbf{(4-17)}$$

where r_{lu} is tabulated for each season and land-use category.

The resistance r_{dc} is determined by the effects of mixing forced by buoyant convection (due to surface heating of the ground and/or lower canopy) and by penetration of winds into canopies on the hillsides. The resistance is estimated from

$$r_{dc} = 100\left(1 + \frac{1000}{G + 10}\right)\left(\frac{1}{1 + 1000\theta}\right) \quad \textbf{(4-18)}$$

where 2 is the slope of the local terrain in radians. The resistance of the exposed surfaces in the lower portions of structures (canopies or buildings) is computed from

$$r_{cl}^{i} = \left(\frac{10^{-5} H_i^*}{r_{clS}} + \frac{f_o^i}{r_{clO}}\right)^{-1} \quad \textbf{(4-19)}$$

where r_{clS} and r_{clO} are tabulated for each season and land-use category. Similarly, at the ground, the resistances are computed from

$$r_{gs}^{i} = \left(\frac{10^{-5} H_i^*}{r_{gsS}} + \frac{f_o^i}{r_{gsO}}\right)^{-1} \quad \textbf{(4-20)}$$

Table 4-8 lists the gaseous species considered in the UAM-AERO dry deposition algorithm and the relevant properties needed to calculate their deposition layer and surface resistances. Data for several species not considered in Wesely (1989) were added, including propionaldehyde, acetic acid, pernitric acid, propionacetyl nitrate, C5+ alkyl nitrates, cresols, methyl glyoxal, and hydrochloric acid. It is important to recognize that the reactivity factors assigned to the depositing species are approximate and may vary significantly with the vegetation type or state. In addition, following the approach adopted for UAM-V, the Henry's Constants are optionally adjusted for temperature using the expression

$$H(T) = H_o\left(\frac{1}{298} - \frac{1}{\max(T,250)}\right) \quad \textbf{(4-21)}$$

and adjusted for aqueous dissolution reactions assuming neutral conditions on the leaf surface. The Henry's Law constants for species that dissociate in the aqueous phase (SO_2, H_2O_2, HNO_3, NH_3, formic acid, acetic acid, pernitric acid, and methyl glyoxal) are calculated using the expressions shown in **Table 4-9**.

For deposition over water bodies, UAM-AERO calculates the surface resistance from the expression recommended by Sehmel (1980), which incorporates wind speed and air/water partitioning coefficient dependencies, rather than from Wesely's tabulated values for water bodies. The surface resistance over water is

Table 4-8. Relevant properties of gases considered in the dry deposition module.

Species	Symbol	Ratio of Molecular Diffusivities ($D_{H2O}/D_{species}$)	Henry's Law Constant (H*) (M/atm)	Henry's Law Exponent[a] (A)	Normalized Reactivity (f_o)
Sulfur dioxide	SO_2	1.89	1×10^{5}	-3020	0
Ozone	O_3	1.63	1×10^{-2}	+2300	1
Nitrogen dioxide	NO_2	1.6	1×10^{-2}	-2500	0.1
Nitric oxide	NO	1.29	2×10^{-3}	-1480	0
Nitric acid	HNO_3	1.87	1×10^{14}	-8650	0
Hydrogen peroxide	H_2O_2	1.37	1×10^{5}	-6800	1
Acetaldehyde	CCHO	1.56	15	-6500	0
Propionaldehyde	RCHO	1.8	15	-6500	0
Formaldehyde	HCHO	1.29	6×10^{3}	-6500	0
Methyl hydroperoxide	-OOH	1.6	220	-5600	0.3
Formic acid	FACD	1.6	4×10^{6}	-5740	0
Acetic acid	AACD	1.83	4×10^{6}	-5740	0
Ammonia	NH_3	0.97	2×10^{4}	-3400	0
Peroxyacetyl nitrate	PAN	2.59	3.6	-5910	0.1
Nitrous acid	HONO	1.62	1×10^{5}	-4800	0.1
Pernitric acid	HNO_4	2.09	2×10^{4}	-1500	0
Propionacetyl nitrate	PPN	2.74	3.6	-5910	0.1
C5+ Alkyl nitrates	RNO_3	2.72	3.6	-5910	0.1
Cresols	CRES	2.45	1200	-6000	0
Methyl glyoxal	MGLY	2.00	3700	-7500	0
Hydrochloric acid	HCl	1.42	2.05×10^{6}	-2020	0

[a] The exponent A is used in the expression H(T) = H exp{A[1/298 - 1/max(T,250)]} to calculate H at the surface temperature. If the Wesely option is selected, A is assumed to be zero.

Table 4-9. Aqueous dissolution reaction data for selected species.

Gaseous Species	Henry Law Expression
SO_2	H(T)*(1 + ((1.23e-2)*exp(-2010*TT))/[H^+] + ((1.23e-2)*exp(-2010*TT))*(6.6e-8)* exp(5.1e-4*TT))/([H^+][H^+]))
HNO_3	H(T)*(1 + ((2.2e-12)*exp(3730*TT))/[H^+])
NH_3	H(T)*(1 + ((1.75e-5)*exp(450*TT)*[H^+])/ (1.e-14)* exp(6710*TT))
FACD	H(T)*(1 + ((1.78e-4)*exp(150*TT))/[H^+])
AACD	H(T)*(1 + ((1.78e-4)*exp(150*TT))/[H^+])
HNO_4	H(T)*(1 + 100*/[H^+])
MGLY	H(T)*(1 + ((2.7e3*exp(-4250*TT)))

where TT = [1/298 - 1/max(T,250)] and [H^+] is in moles per liter.

$$r_s^i = \frac{1}{3.94x10^{-5} H_i^* Tu_*} \quad (4\text{-}22)$$

where T is the surface air temperature in °K and u_* is the water friction velocity (which is assumed to be equal to u_*).

Wesely (1989) recommends an alternate surface resistance equation when the surface is wet due to rain or dew. For surfaces covered with dew, the upper-canopy resistances for SO_2 and ozone are calculated from

$$\begin{aligned} r_{lu}^{SO2} &= 100 \text{ s/m} \\ r_{lu}^{O3} &= \left(\frac{1}{3000} + \frac{1}{3r_{lu}}\right)^{-1} \end{aligned} \quad (4\text{-}23)$$

When it is raining, the SO_2 and ozone upper-canopy resistance is calculated from

$$\begin{aligned} r_{lu}^{SO2} &= \left(\frac{1}{5000} + \frac{1}{3r_{lu}}\right)^{-1} \quad \textit{for nonurban land use} \\ r_{lu}^{SO2} &= 50\ s/m \quad \textit{for urban land use} \\ r_{lu}^{O3} &= \left(\frac{1}{1000} + \frac{1}{3r_{lu}}\right)^{-1} \quad \textit{for both} \end{aligned} \quad (4\text{-}24)$$

The upper-canopy resistance for other species is calculated from

$$r_{lu}^i = \left(\frac{1}{3r_{lu}} + 10^{-7} H_i^* + \frac{f_o^i}{r_{luO}}\right)^{-1} \quad (4\text{-}25)$$

when the surface is covered by rainwater or dew. Dew conditions are diagnosed in UAM-AERO from the relative humidity and wind speed and these adjustments for dew are used in the simulations. However, since UAM-AERO is rarely applied to periods with rain, it does not currently accept rainfall inputs. An internal variable currently sets the rainfall rate to zero. Nonetheless, the logic is included to adjust the resistances for rainfall in the future.

Additional adjustments are available to approximately account for vegetation stress. All of the formulas described above are for unstressed vegetation, which is the default vegetation status. Optionally, for vegetation stress due to lack of water, the model increases the stomatal resistance by a factor of 10 and for inactive vegetation (winter deciduous), the model uses a

stomatal resistance of 10,000 s/m, indicating a complete shutdown of this pathway. Currently, the vegetation stress level is internally set to the unstressed state.

4.1.6. Particle Emissions

The UAM-AERO model requires chemically-resolved and size-resolved PM emissions data corresponding to the model's chemical components of PM and the size distribution used for a particular simulation. The ARB and EPA maintain PM emission composition and size distribution data for a modest number of emission source categories. These composition/size profiles are extrapolated to cover all source categories with PM emissions. The PM emission composition data has been aggregated into the six species needed for modeling: sulfate, elemental carbon, organic carbon, crustal (or other PM species), sodium, and chloride. The nitrate and ammonium fractions are extremely small and are currently lumped with "other species" in the emissions processing. The sodium and chloride fractions for everything except sea-salt emissions are also small and lumped with other species. The ARB PM profiles split the mass into four size ranges: < 1 μm, 1 to 2.5 μm, 2.5 to 10 μm, and > 10 μm. For each species and source category, a continuous-size distribution has been estimated (see below). These distributions are subsequently divided into the size ranges (below 10 μm) used for a particular UAM-AERO simulation. Typically, the size distribution has included eight size sections below 10 μm, spaced equidistant on a log scale, with a minimum value of 0.039 μm and a maximum value of 10 μm. This minimum value places the division between the 6th and 7th bins at a diameter of exactly 2.5 μm. This approach provides reasonable size resolution for aerosol dynamics and provides 2.5- and 10-μm cut points to facilitate comparison with ambient $PM_{2.5}$ and PM_{10} observations. Emissions for particles larger than 10 μm are not input to the model in current simulations. The composition/size profiles are summarized in **Tables 4-10 and 4-11**.

The continuous-size distributions were estimated using a modified version of Twomey's algorithm for inversion of cascade impactor data to generate the size distribution. The algorithm was obtained from Walter John at the Air and Industrial Hygiene Laboratory of the California Department of Health Services, Berkeley. (The code was developed by Hwa-Chi Wang and Wolfgang Winklmayr.) The estimated distributions, although not based on precise data, provide more realistic size inputs for particles less than 1 μm and between 2.5 and 10 μm than direct use of the size distribution data in histogram format.

Twomey's inversion algorithm is nonlinear and iterative, hence the initial guess can strongly influence the final distribution. The calculation of the initial guesses were changed from a pure "saw-tooth" linear interpolation of the input data to use one-half saw-tooth and one-half a sum of four log-normal functions, where one-half the mass in each bin was used to calculate the coefficient for a log-normal function having the geometric mean diameter of the bin. The geometric standard deviation for each bin was chosen such that the function decayed to a fixed fraction of its maximum at the edge of the bin. A value of 0.3 for the fractional

Table 4-10. PM emissions size distribution data.

Profile Number	Profile Name	$PM_{<0.625}$ Fraction	$PM_{.625-2.5}$ Fraction	$PM_{2.5-10}$ Fraction	$PM_{>10}$ Fraction
110	Liquid Material Combustion	0.7907	0.1784	0.0067	0.0242
111	Fuel Combustion-Residual	0.5542	0.2097	0.1002	0.1359
112	Fuel Combustion-Distillate	0.7907	0.1784	0.0067	0.0242
113	Utility Boilers-Residual	0.7816	0.1745	0.013	0.0309
114	Stat. I.C. Engine-Liquid Fuel	0.7907	0.1784	0.0067	0.0242
115	Stat. I.C. Engine-Gasoline	0.8058	0.1806	0.0075	0.0061
116	Stat. I.C. Engine-Diesel	0.7697	0.1711	0.018	0.0412
117	Vehicular Sources-Gasoline	0.8058	0.1805	0.0075	0.0062
118	Vehicular Sources-Diesel	0.7696	0.1714	0.0179	0.0411
119	Marine Vessels-Liquid Fuel	0.7697	0.1711	0.018	0.0412
120	Gaseous Material Combustion	0.8111	0.1812	0.0077	0
121	Residential-Natural Gas	0.8111	0.1812	0.0077	0
123	Stat. I.C.Engine-Gas	0.8058	0.1806	0.0075	0.0061
125	Petroleum Heaters-Gas	0.7629	0.1707	0.015	0.0514
130	Solid Material Combustion	0.6403	0.2902	0.0658	0.0037
131	Coal/Coke Combustion	0.0167	0.14	0.2203	0.623
132	Stat. I.C. Engine-Solid Fuel	0.6403	0.2902	0.0658	0.0037
133	Wood Waste Combustion	0.6403	0.2902	0.0658	0.0037
134	Other Waste Combustion	0.6403	0.2902	0.0658	0.0037
135	Planned/Unplannd Forest Fires	0.6919	0.1627	0.0227	0.1227
136	Agricultural Burning	0.6919	0.1627	0.0227	0.1227
137	Unplanned Structural Fires	0.7165	0.2002	0.0619	0.0214
138	Fireplaces	0.7162	0.1578	0.0431	0.0829
141	Aircraft-Jet Fuel	0.0253	0	0	0.9747
151	Orchard Heaters	0.7907	0.1784	0.0067	0.0242
161	Incineration-Liquid Fuel	0.7907	0.1784	0.0067	0.0242
162	Incineration-Gaseous Fuel	0.8111	0.1812	0.0077	0
163	Incineration-Solid Fuel	0.11	0.103	0.0719	0.7151
200	Evaporation	0.7617	0.1679	0.0289	0.0415
220	Coating Material Evaporation	0.7617	0.1679	0.0289	0.0415
222	Paint Application-Oil Based	0.7617	0.1679	0.0289	0.0415
223	Paint Application-Water Based	0.5138	0.1158	0.0428	0.3276
311	Chemical Manufacturing	0.727	0.1668	0.0052	0.101
312	Chemical Fertilizer-Urea	0.777	0.1759	0.0065	0.0406
321	Agricultural Tillage Dust	0.0205	0.0815	0.322	0.576
322	Livestock Dust	0.0399	0.0477	0.3671	0.5453
324	Feed And Grain Operations	0.0013	0.0283	0.2338	0.7366
325	Grain Drying	0.2598	0.1499	0.1167	0.4736
327	Coffee Roasting	0.4833	0.111	0.0202	0.3855
328	Cotton Ginning	0.4603	0.1047	0.0372	0.3978
331	Petroleum Refining	0.4382	0.1261	0.0377	0.398
341	Asphalt Roofing Manufacture	0.7782	0.1706	0.0301	0.0211

Table 4-10. PM emissions size distribution data.

Profile Number	Profile Name	$PM_{<0.625}$ Fraction	$PM_{.625-2.5}$ Fraction	$PM_{2.5-10}$ Fraction	$PM_{>10}$ Fraction
342	Asphaltic Concrete Batch Plant	0.2725	0.0725	0.044	0.611
343	Cement Prod./Concrete Batching	0.2624	0.3622	0.2892	0.0862
344	Lime Manufacturing	0.0591	0.0658	0.153	0.7221
345	Calcination of Gypsum	0.164	0.3348	0.3722	0.129
346	Clay and Related Products Mfg.	0.4264	0.0979	0.0284	0.4473
348	Glass Melting Furnace	0.7893	0.1756	0.0143	0.0208
349	Fiberglass Forming Line	0.8059	0.1805	0.0074	0.0062
351	Steel Heat Treating-Salt Quench	0.6323	0.2298	0.0953	0.0426
352	Steel Sinter Plant	0.793	0.1781	0.0085	0.0204
353	Steel Abrasive Blasting	0.653	0.1436	0.0582	0.1452
354	Steel Open Hearth Furnace	0.7668	0.1667	0.0454	0.0211
355	Basic Oxygen Furnace-Steel	0.8111	0.181	0.0078	0.0001
356	Electric Arc Furnace	0.3892	0.2168	0.2145	0.1795
358	Aluminum Foundry	0.7445	0.1632	0.0401	0.0522
361	Wood Operation-Sanding	0.7284	0.1619	0.0272	0.0825
362	Wood Operation-Resawing	0.1717	0.1235	0.0893	0.6155
365	Pulp and Paper Mills	0.01	0.1394	0.3267	0.5239
371	Mineral Process Loss	0.01	0.1394	0.3267	0.5239
373	Rock Crushers	0.0062	0.024	0.0549	0.9149
374	Rock Screening and Handling	0.01	0.1394	0.3267	0.5239
381	Landfill Dust	0.2427	0.1453	0.146	0.466
391	Road and Bldg. Construction Dust	0.2002	0.1767	0.246	0.3771
393	Paved Road Dust	0.0222	0.0586	0.3524	0.5668
394	Unpaved Road Dust	0.0367	0.0917	0.4623	0.4093
396	Tire Wear	0.162	0.1714	0.0548	0.6118
411	Windblown Dust-Agricultural	0.0206	0.0802	0.3733	0.5259
412	Windblown Dust-Unpaved Areas	0.0479	0.0738	0.3529	0.5254
900	Unspecified	0.048	0.074	0.3528	0.5252

decay parameter was found to provide a good compromise between smooth shape and sufficient decay for cases where the adjacent bins had rapidly varying amounts of mass. In addition, after the estimated continuous distribution data are allocated to the UAM-AERO size bins, each distribution is renormalized such that the total integrated area equals the input data.

A number of changes in the source size/composition were made. For elemental carbon (EC), the observed ambient-size distribution data from SCAQS reported by Zhang (1990) was substituted for the original EC emission size data. All of the original organic carbon (OC) fractions were converted to organic material (OM) fractions by adding 40 percent to account for the oxygen and hydrogen associated with the OC; the mass fractions of the other PM species were reduced by the corresponding amount. The UAM-AERO model expects emissions and concentrations of organic material to include the total mass, rather than just the

Table 4-11. Summary of PM_{10} composition distribution data.

Profile Number	Profile Name	PM_{10}-SO_4 Fraction	PM_{10}-EC Fraction	PM_{10}-OM Fraction	PM_{10}-Other Fraction
110	Liquid Material Combustion	0.244	0.1465	0	0.5853
111	Fuel Combustion-Residual	0.4373	0.1727	0	0.2541
112	Fuel Combustion-Distillate	0.244	0.1465	0	0.5853
113	Utility Boilers-Residual	0.2879	0.1966	0	0.4846
114	Stat. I.C. Engine-Liquid Fuel	0.244	0.1465	0	0.5853
115	Stat. I.C. Engine-Gasoline	0.4472	0.1988	0	0.3479
116	Stat. I.C. Engine-Diesel	0.1439	0.0383	0	0.7766
117	Vehicular Sources-Gasoline	0.0228	0.134	0.4189	0.4181
118	Vehicular Sources-Diesel	0.0233	0.3155	0.5384	0.0817
119	Marine Vessels-Liquid Fuel	0.1439	0.0383	0	0.7766
120	Gaseous Material Combustion	0.2001	0.4999	0	0.3
121	Residential-Natural Gas	0.2001	0.4999	0	0.3
123	Stat. I.C.Engine-Gas	0.4472	0.1988	0	0.3479
125	Petroleum Heaters-Gas	0.4459	0.0662	0	0.4365
130	Solid Material Combustion	0.0263	0.2989	0	0.6711
131	Coal/Coke Combustion	0	0.0528	0	0.3242
132	Stat. I.C. Engine-Solid Fuel	0.0263	0.2989	0	0.6711
133	Wood Waste Combustion	0.0263	0.2989	0	0.6711
134	Other Waste Combustion	0.0263	0.2989	0	0.6711
135	Planned/Unplannd Forest Fires	0.0156	0.1011	0.4743	0.2863
136	Agricultural Burning	0.0156	0.1011	0.4743	0.2863
137	Unplanned Structural Fires	0.0003	0.2936	0	0.6847
138	Fireplaces	0.0094	0.2086	0.5659	0.1332
141	Aircraft-Jet Fuel	0.244	0.1465	0	0.5853
151	Orchard Heaters	0.244	0.1465	0	0.5853
161	Incineration-Liquid Fuel	0.244	0.1465	0	0.5853
162	Incineration-Gaseous Fuel	0.2001	0.4999	0	0.3
163	Incineration-Solid Fuel	0	0	0	0.2849
200	Evaporation	0.0192	0.5272	0	0.4121
220	Coating Material Evaporation	0.0192	0.5272	0	0.4121
222	Paint Application-Oil Based	0.0192	0.5272	0	0.4121
223	Paint Application-Water Based	0.0134	0.3363	0	0.3227
311	Chemical Manufacturing	0.018	0	0	0.881
312	Chemical Fertilizer-Urea	0.0387	0.3165	0	0.6042
321	Agricultural Tillage Dust	0.0041	0.0049	0.0892	0.335
322	Livestock Dust	0.0037	0.0066	0.143	0.3014
324	Feed And Grain Operations	0.0013	0.0791	0	0.183
325	Grain Drying	0	0	0	0.5264
327	Coffee Roasting	0.0032	0.147	0	0.4643
328	Cotton Ginning	0	0	0	0.6022
331	Petroleum Refining	0.2612	0.0202	0	0.3206
341	Asphalt Roofing Manufacture	0.2214	0.2349	0	0.5226

Table 4-11. Summary of PM_{10} composition distribution data.

Profile Number	Profile Name	PM_{10}-SO_4 Fraction	PM_{10}-EC Fraction	PM_{10}-OM Fraction	PM_{10}-Other Fraction
342	Asphaltic Concrete Batch Plant	0.002	0.0424	0	0.3446
343	Cement Prod./Concrete Batching	0.2185	0.1364	0	0.5589
344	Lime Manufacturing	0	0	0	0.2779
345	Calcination Of Gypsum	0.4718	0.0182	0	0.381
346	Clay and Related Products Mfg.	0.003	0	0	0.5497
348	Glass Melting Furnace	0.5415	0.1138	0	0.3239
349	Fiberglass Forming Line	0.0054	0.2976	0	0.6908
351	Steel Heat Treating-Salt Quench	0.238	0.0676	0	0.6518
352	Steel Sinter Plant	0.1935	0.1064	0	0.6797
353	Steel Abrasive Blasting	0.0003	0.0003	0	0.8542
354	Steel Open Hearth Furnace	0.388	0.1958	0	0.3951
355	Basic Oxygen Furnace-Steel	0.3999	0.2001	0	0.3999
356	Electric Arc Furnace	0.3282	0.1641	0	0.3282
358	Aluminum Foundry	0.1516	0.1232	0	0.673
361	Wood Operation-Sanding	0	0.3761	0	0.5414
362	Wood Operation-Resawing	0.002	0.1616	0	0.2209
365	Pulp and Paper Mills	0	0	0	0.4761
371	Mineral Process Loss	0.0025	0	0	0.4736
373	Rock Crushers	0.0004	0	0	0.0847
374	Rock Screening and Handling	0.0025	0	0	0.4736
381	Landfill Dust	0.0041	0.0049	0.0892	0.335
391	Road and Bldg. Construction Dust	0.0041	0.0049	0.0892	0.335
393	Paved Road Dust	0.0041	0.0049	0.0892	0.335
394	Unpaved Road Dust	0.0041	0.0049	0.0892	0.335
396	Tire Wear	0	0.3377	0	0.0505
411	Windblown Dust-Agricultural	0.0042	0.0021	0.0213	0.4465
412	Windblown Dust-Unpaved Areas	0.0041	0.0049	0.0892	0.335
900	Unspecified	0.0014	0.0002	0.021	0.452

mass of the carbon in OM. With regard to the OM data, there were significant gaps in the original database. The original PM_{10}-OM fractions were zero for numerous processes that have significant EC emissions and that were suspected of having OM emissions. The original EC fractions were reallocated between EC and OM for numerous categories. Even after these adjustments, the OM fractions may still be low for numerous emission categories. In addition, the motor vehicle exhaust profile and paved road dust profile that worked best in the CMB modeling of the SCAQS data (Watson et al., 1994b) were employed.

In the ARB's 1987 SCAQS emissions inventory that was used for this study, the total PM_{10} emissions in the SoCAB were estimated to be 1160 tons/day. The SCAQMD recently revised the PM emissions-related activity levels and emission factors for the emissions inventory used in their 1997 Air Quality Management Plan. The SCAQMD's revised estimate of total PM_{10} emissions in the SoCAB in 1987 is 502 tons/day (SCAQMD 1996). The SCAQMD's revised emissions inventory was not available in time for use in this study, however, based on their preliminary estimates, it was decided to reduce all PM_{10} emissions in the original ARB inventory by a factor of 2 for the current study. This brought the total PM_{10} emissions in the SoCAB to 580 tons/day which is comparable to the recent estimates.

SCAQMD, 1996. Final 1997 Air Quality Management Plan. South Coast Air Quality Management District, Diamond Bar, CA, December (see Table 3-1a).

5. SIMULATION OF A SUMMER EPISODE

5.1 EPISODE SELECTION

The UAM-AERO model is designed to simulate the relationships between emissions and ambient concentrations of ozone, acids, and aerosol species. Testing of the model during a summer period with high or relatively high concentrations of all of these species was considered essential. At the time this project was initiated, intensive ozone modeling had been performed for two summer SCAQS episodes: June 24-25, 1987 and August 26-28, 1987. These episodes were good candidates not only because of the extensive aerometric data that were available, but also because other modelers had developed refined wind fields and mixing heights for these episodes that could be used. Both episodes had high ozone concentrations (>240 ppb), and relatively high PM_{10} (>100 $\mu g/m^3$) and nitric acid (>15 ppb) concentrations. The June episode had some fog and had lower temperatures and higher relative humidities than the August episode. The June episode was selected because its moist conditions were thought to be a more stressful test of the aerosol portion of the model than the dry conditions associated with the August episode.

The model simulations were initiated 24 hours before the beginning of the SCAQS episode in order to allow sufficient time for the calculations to be driven by emissions rather than initial concentrations. On the urban scale, one day is a sufficient initialization period. The model inputs were set up for a 325 x 180 km region with 5 x 5 km grid resolution and 5 vertical layers. The far eastern portion of the original domain was not included in the simulated domain because sensitivity tests of this region did not significantly influence model predictions at SCAQS air monitoring stations. The UAM-AERO simulated domain was the 255 x 180 km region (51 x 36 grid squares) shown in **Figure 5-1**. The southwest corner of the domain is located at UTM coordinates of 275 km easting and 3670 km northing (in UTM zone 11).

5.2 METEOROLOGICAL AND AIR QUALITY CONDITIONS

Meteorological conditions for the June 23-25, 1987 period were fairly typical of summer ozone episodes. The wind flow patterns were similar on all three days. At night, the winds were light and most offshore. In the day, as shown in **Figures 5-2 through 5-4**, a southwesterly sea breeze developed, transporting pollution from the coastal and central areas to the inland area. The mixing heights were low at night and grew from several hundred meters in the morning to 2000 m in the inland desert areas in the afternoon. Fog was present in the coast area at night and in the early daylight morning hours.

Hourly 3-dimensional wind fields and mixing height fields were developed using diagnostic procedures for the episodes by the SCAQMD staff for use in the study. These were the same meteorological fields used for the 1994 ozone attainment demonstration for the SoCAB (SCAQMD 1994). Three-dimensional hourly temperature and water vapor concentration fields were also developed from the observed data using diagnostic procedures.

Two-dimensional fog fields, which classify conditions as clear, hazy, or foggy, were developed from the surface observations.

Air quality conditions were adverse during the episode. **Table 5-1** shows the maximum concentrations observed during the period. Peak 1-hr ozone levels reached 250 ppb at Claremont on June 24. The 4-hr average PM_{10} sulfate, PM_{10} nitrate, and PM_{10} mass reached 33, 81, and 165 $\mu g/m^3$, respectively, on June 24th with the highest sulfate occurring in the coastal area at Hawthorne and the highest nitrate and mass occurring in the inland area at the Riverside-Rubidoux station. The highest 4-hr average nitric acid was 20 ppb at Claremont and ammonia concentrations were 106 ppb at Riverside. The ambient concentration maxima were similar on both days.

Initial concentrations were developed from ambient concentration data. However, there were no observed PM_{10} or NMOC data for June 22 or 23. Initial concentrations for hour 0 on June 23 were obtained by spatial interpolation of observed NO, NO_2, ozone, SO_2, and CO data for that hour, monthly average PM_{10} values, 50 percent of the observed NMOC values at hour 6 on June 24. Dummy stations with background air quality conditions (see below) were used near the boundaries of the domain and in the less populated portions of the domain to establish plausible initial concentration fields. The PM size and chemical composition were estimated based on the annual average SoCAB PM data reported by Solomon et al. (1988). The fine and coarse size/composition fractions are given in **Table 5-2**. These PM split factors were used for initial and boundary conditions. The detailed size distributions were estimated by first calculating a continuous fractional-size distribution for each species using a bi-modal log-normal fit with mean diameters of 0.31 μm and 5.7 μm for the first and second modes, respectively (Hidy, 1984). The geometric standard deviations assumed for two modes were 0.25 and 0.1, respectively. These values were chosen by graphically fitting the PM size distributions and selecting the coefficients (C_{ij}) for each mode such that the integrated values (M_{ij}) of the distributions matched the split given in Table 5-2 using the following equations.

$$M_{ispec,fine} = \int_{0.039um}^{2.5um} C_{ispec,fine} \exp\left(-\frac{[\log_{10} d_p - \log_{10} 0.31]^2}{0.25}\right) + C_{ispec,coarse} \exp\left(-\frac{[\log_{10} d_p - \log_{10} 5.7]^2}{0.1}\right) \quad \textbf{(5-1)}$$

and

$$M_{ispec,coarse} = \int_{2.5um}^{10um} C_{ispec,fine} \exp\left(-\frac{[\log_{10} d_p - \log_{10} 0.31]^2}{0.25}\right) + C_{ispec,coarse} \exp\left(-\frac{[\log_{10} d_p - \log_{10} 5.7]^2}{0.1}\right) \quad \textbf{(5-2)}$$

These distributions were then split into the eight size bins used in the UAM-AERO simulations.

The boundary concentrations and initial concentrations above the mixing height are shown in **Table 5-3**. The NO, NO_2, ozone, CO, and NMOC concentrations were the values used by the SCAQMD in their ozone modeling studies. The NMOC level is 60 ppbC of which 52 ppbC is reactive, which is consistent with the NMOC data obtained from San Nicolas Island during the SCAQS (Lurmann and Main, 1992; Roberts et al., 1991). A background ambient PM_{10} level of 15 $\mu g/m^3$ was used for the simulations. This level is 30 percent lower than the annual average PM_{10} (21 $\mu g/m^3$) observed on San Nicolas Island (Solomon et al., 1988). The use of a value somewhat lower than the observed value is appropriate because while San Nicolas Island is remote, it is also dry and dusty, and this value is used from the surface up to 2000 m.

5.3 EMISSIONS

The UAM-AERO model requires hourly spatially resolved emissions of NO_x, ROG, CO, SO_2, NH_3, and PM_{10}. The NO_x emissions are partitioned into NO, NO_2, and HONO. The VOC emissions are partitioned into the appropriate classes for the chemical mechanism, which for this application were the chemical mechanism classes used by SAPRC90. The PM_{10} emissions are partitioned into six chemical classes and eight size bins, as described in Section 4. The modeling emission inventory was provided by the SCAQMD and included average summer day area-source emissions, day-specific on-road motor vehicle emissions, major point source emissions, and biogenic emissions. Two substantial adjustments were made to the inventory. First, because the SCAQS motor vehicle emissions were found to be underestimated (Ingalls et al., 1989; Fujita et al., 1992), which resulted in substantial unprediction of ozone concentration by the UAM and the CIT photochemical models, the on-road motor vehicle exhaust hydrocarbon (not carbonyls) were quadrupled. This approximately doubled the SoCAB ROG emissions. Second, based on model results showing consistent overprediction of primary PM, and recent studies that suggested that the road-dust and construction PM emission factors were high (SCAQMD, 1996), the PM emissions from all sources were reduced by 50 percent.

The adjusted summer emission inventory for the SoCAB is summarized in **Tables 5-4 through 5-6**. The total emissions of NO_x, ROG, CO, SO_2, and PM_{10} are 1244, 2528, 9100, 132, and 539 tons per day, respectively. These totals are for June 23. The estimated day-to-day variations in the regional emission totals are small during this period. The size distribution of the PM emissions are illustrated in **Figures 5-5 and 5-6**.

Ammonia and sea salt emissions are not included in the tables and figures. The ammonia emission estimates were based on the SCAQS inventory prepared by Dickson et al. (1991). The original sewage treatment plant ammonia emissions were reduced by 50 percent (and probably should have been reduced more) because the methodology overestimated these emissions (SCAQMD, 1996). The total ammonia emissions in the modeling inventory are 220 tons per day. Neither the SCAQMD nor ARB had an emissions inventory for sea salt, yet

it was important to include some sea salt contribution because nitric acid reacts with sea salt to form nonvolatile sodium nitrate and the nitrate predictions in coastal areas were likely to be poor without its inclusion. We explored modeling using exaggerated overwater NaCl boundary conditions to supply NaCl to the model and using normal NaCl boundary conditions with low uniform NaCl emissions in all ocean grid squares. The latter approach worked better. Simulations were made with 25, 75, and 150 tons per day of NaCl emissions included in the inventory, mostly as coarse PM, and the simulation with 75 tons per day produced the best aerosol Na predictions. Thus, the emission inventory includes an additional 29 and 46 tons per day of Na and Cl emissions. Like all primary PM emission estimates, these are quite uncertain.

5.4 MODEL RESULTS

5.4.1 Spatial Patterns

The spatial patterns of predicted 24-hr average pollutant concentrations on June 24 and 25 are shown in **Figures 5-7 through 5-34**. The predicted pattern of PM concentrations shown a band of high concentrations extending from the San Fernando Valley to the high desert region, covering the Burbank, central Los Angeles (CELA), Azusa, Claremont, and Riverside monitoring sites. The predicted spatial pattern was similar for both days for PM and most other species. The predicted concentrations were slightly higher on June 24 and concentrated in a narrower band than on June 25. The spatial pattern of $PM_{2.5}$ mass and chemical components was generally similar to PM_{10} mass and chemical components.

The nitrate and ammonium spatial patterns are similar to the PM mass pattern, with increased levels northeast of Riverside. Relatively high ammonium nitrate concentrations are predicted in and downwind of Riverside due to the reaction of photochemically formed nitric acid with high levels of ammonia which are emitted in and downwind of Chino. Nitric acid levels are low near the coast and highest in the central northern portion of the domain (in the mountainous region near Newhall and in a band 30 km north of Burbank and Claremont). Ammonia concentrations are low near the coast and in the central northern portion of the domain. Ammonia concentrations are high from 30 km upwind of Riverside to 50 km downwind of Riverside. The spatial patterns of nitric acid, ammonia, and ammonium nitrate suggest ammonium nitrate formation is ammonia-limited in the coastal areas and central northern portion of the domain and is nitric acid-limited (or NO_x limited) in the inland region near Riverside.

The spatial pattern of sulfate shows a major urban plume extending from the Long Beach area to Azusa and Claremont. This pattern is consistent with the southwesterly winds and the high SO_2 emission in the Long Beach area. SO_2 emitted in the coastal area reacts in the coastal fog to rapidly produce sulfate.

The spatial patterns of organic material, elemental carbon, and crustal PM are similar to the PM mass pattern, with the exception that the high concentrations are observed in the San

Fernando Valley rather than the San Gabrial Valley. The spatial patterns agree fairly well with the primary PM emissions pattern.

The spatial pattern of sodium shows high levels (up to 6 $\mu g/m^3$) over the ocean and lower levels onshore, which decline with increasing distance from the coastline. This is the expected pattern for the marine aerosol.

5.4.2 Predicted Aerosol-Size Distribution

The predicted aerosol-size distributions at the SCAQS stations are shown in **Figures 5-35 through 5-42**. The Long Beach size distributions show characteristics expected for a coast site with high SO_2 emissions and fog. Note that even though there are no particle emissions, initial concentrations, or boundary conditions for particles above 10 μm, about 15 percent of the 24-hr average mass is estimated to be in particles which grew to diameters above 10 μm. The predicted sulfate aerosol is mostly distributed between 0.08 and 1.2 μm. The predicted ammonium-size distribution tracts the sulfate quite closely. The nitrate is predicted to be mostly in the coarse mode in Long Beach, with a significant amount in particles larger than 10 μm. Most of the coarse nitrate is sodium nitrate at Long Beach.
The elemental carbon concentrations are low and almost all of the elemental carbon mass is predicted to occur in particles less than 2.5 μm in diameter. Organic material is predicted to occur in all of the particle size sections. The OM in small particles is largely secondary in orgin while the OM in larger particles (> 1 μm) is from primary emissions. The model predicts slightly more OM mass in particles above 2.5 μm in diameter than below 2.5 μm. Crustal material is predicted to comprise a large fraction of the PM and about 85 percent of the crustal material is in the coarse mode, as expected from the emissions distributions. The emissions inventory and model predictions may over-estimate the amount of crustal material in the fine mode because ambient data typically show only 5 or 10 percent of PM_{10} crustal material is in the fine mode (Watson et al 1994).

The Claremont aerosol-size distribution is typical of that at inland sites. The nitrate and ammonium aerosol is mostly concentrated in particles below 2.5 μm. The sulfate levels are low compared to the nitrate, and the sulfate size distribution extends fairly evenly across all of the size bins. The model does not predict a distinct bi-modal sulfate distribution at inland sites like Claremont, Azusa, and Riverside. The EC, organic, and crustal PM size distributions at Claremont correspond closely with the primary emission size distributions.
That is, most of the elemental carbon is in particles less than 2.5 μm in diameter and most of the crustal material is in particles larger than 2.5 μm in diameter. The OM is distributed across all of the size sections.

5.5 MODEL PERFORMANCE

The SCAQS provides the best currently available data on which to evaluate the performance of the UAM-AERO model. During SCAQS, both ambient gaseous and aerosol pollutant data were collected. The SCAQS HNO_3, NH_3, and PM data were collected on 4-hr to 6-hr samples from which 24-hr average concentration had been determined. In addition, 1-hr NMOC samples were collected 3 or 6 times per day and subsequently speciated. Continuous hourly data from the routine air monitoring network were collected for ozone, NO, NO_2, SO_2, and CO, although the SO_2 and CO are not particularly useful for model evaluation (because of rounding conventions). In this section, graphical and statistical comparisons of observed and predicted concentrations are made to assess model performance. The emphasis is place on the 24-hr average predictions for PM species because the relevant air quality standards use this averaging time. It is also important to note that, due to the inherent difficulties in aerosol sampling, the observed HNO_3, NH_3, and PM concentrations are less accurate than the observed ozone concentrations, which are normally used in model evaluations.

The predicted concentrations are compared to observed levels in **Figures 5-43 through 5-52**, and in **Tables 5-7 through 5-10**. The evaluation focuses on the mean bias and error at the stations with concentrations above minimum threshold values (1 $\mu g/m^3$ for PM components, 10 ppb for NO and NO_2, and 60 ppb for ozone) and the accuracy of the modeled concentrations at the monitoring stations with the highest observed concentration on each day. Tables 5-7 and 5-8 contain the model performance for 24-hr average concentrations. Tables 5-9 and 5-10 contain the model performance for short-term (1-hr to 6-hr) concentrations. Tables 5-8 and 5-10 show the maximum concentrations predicted anywhere in the domain as well as the maximum predicted at the highest station (paired in space). Note the predicted maxima in the domain often were significantly higher than observed at the highest SCAQS station. In addition, plots of the observed and predicted PM concentrations at each station are shown in Appendix A.

5.5.1 Ozone and Nitrogen Dioxide

The graphical display of the model's ozone performance in this simulation (Figure 5-43) shows there is a mixture of overprediction and underprediction, along with some stations with excellent predictions, such as Riverside, Crestline, and Newhall. On average for the hours with the observed ozone above 60 ppb, the model predicts 91 and 85 ppb when 108 and 105 ppb were observed. The mean error in the ozone predictions is ±35 percent. For the peak 1-hr values, the model predicted 152 ppb when 250 ppb was observed at Claremont on June 24, and 199 ppb when 240 ppb was observed at San Bernardino on June 25. Even with the adjusted ROG emissions, the model underpredicts the ozone levels in the central portion of the basin (see results for Pasadena, Glendora, Claremont, and Pico Rivera). In addition, ozone levels at numerous stations are overpredicted on the first day and underpredicted on the second and third days. These results mostly show that while the simulation is short on reactivity in the western and central areas, the simulation does have approximately correct photochemical reactivity by the time the smog cloud reaches the eastern portion of the domain where the highest secondary PM levels were observed.

The nitrogen dioxide predictions agree fairly well for the maximum 1-hr values, but show a tendency to underpredict on average (6 to 20 percent). The mean predicted NO_2 levels were 35 and 43 ppb when 45 and 50 ppb were observed. Figure 5-44 shows that the NO_2 predictions do not tract the dynamics well. The dynamic range of the observed and predicted values are similar; however, the peaks and valleys do not occur at the time of the observed peaks and valleys, and visually, the results do not show good correlation with the observations. This translates into significant model error for NO_2: ±20 ppb or ±45 percent. The poor NO_2 performance has been found in most UAM simulations, and is of particular concern here because, in theory, the ability of the model to predict nitric acid and aerosol nitrate depends on its ability to predict the precursor species, NO_2. Inaccurate simulated NO_2 diurnal profiles are believed to have significantly affected the short-term nitric acid and nitrate predictions and had less effect on the 24-hr nitric acid and nitrate.

5.5.2 Nitrate

The model predicted mean 24-hr average $PM_{2.5}$ nitrate of 16.8 $\mu g/m^3$ on both days, which was slightly higher than the 14.5 and 15.8 $\mu g/m^3$ observed on June 24 and 25, respectively. The predicted mean PM_{10} nitrate levels at the SCAQS stations were 20.4 and 21.2 $\mu g/m^3$, which compares well with the mean observed levels of 22.4 and 21.7 $\mu g/m^3$ on these days. On a percentage basis, the model overpredicted the mean 24-hr average $PM_{2.5}$ nitrate by 11 to 14 percent. It underpredicted the mean 24-hr average PM_{10} nitrate by 9 percent on June 24, and overpredicted the mean PM_{10} 24-hr average PM_{10} nitrate by 6 percent on June 25. The mean normalized errors are 37 and 18 percent for $PM_{2.5}$ nitrate, and 19 and 15 percent for PM_{10} nitrate on June 24 and 25, respectively. On average, the 24-hr nitrate performance statistics are good with the exception of the ±37 $PM_{2.5}$ nitrate error on June 24.

The maximum nitrate levels were observed at Riverside during both days of this episode. The model predicted 26.3 and 27.4 $\mu g/m^3$ of $PM_{2.5}$ nitrate at Riverside (24-hr average concentrations), which were slightly lower than the 34.6 and 30.3 $\mu g/m^3$ that were observed on June 24 and 25, respectively. For PM_{10} nitrate, the model predicted 32.5 $\mu g/m^3$ on both days at Riverside when 47.6 and 40.3 $\mu g/m^3$ were observed. Thus, the model underpredicted the maximum $PM_{2.5}$ nitrate by 10 to 21 percent and underpredicted the maximum PM_{10} nitrate by 19 to 32 percent. However, because of the inaccuracies 3-dimensional wind fields developed from sparse meteorological data, transport models may often displace the modeled peak from the correct location. On June 24, the maximum predicted $PM_{2.5}$ and PM_{10} nitrate concentrations (24-hr average) in the domain were 51 and 61 $\mu g/m^3$, which were 48 and 28 percent higher than the Riverside observations. Thus, while the model underpredicts the Riverside nitrate peaks, it predicts substantially higher levels just a few grid squares downwind of Riverside.

Comparison of the short-term nitrate predictions with observations show larger biases and error, especially for $PM_{2.5}$ nitrate, than those for the 24-hr average predictions. The mean error is ±7 $\mu g/m^3$ (and 30 to 68 percent). While this is a more difficult test than most aerosol models have been subjected to, it nevertheless indicates that the model does not tract the short-term dynamics affecting nitrate as well as one would like.

5.5.3 Ammonium

The model predictions of the mean 24-hr $PM_{2.5}$ ammonium are 7.7 and 7.8 $\mu g/m^3$ when 6.5 and 5.9 $\mu g/m^3$ were observed on June 24 and 25, respectively. The agreement for mean PM_{10} ammonium was better. On average, the model predicted 9.0 and 9.1 $\mu g/m^3$ when 9.3 and 8.9 $\mu g/m^3$ of PM_{10} ammonium were observed. The mean bias and error were 2 to 12 percent and 23 to 28 percent, respectively, in mean PM_{10} ammonium, which is reasonably good performance considering the uncertainties in ammonia emission. The good PM_{10} results are achieved with modest overprediction of $PM_{2.5}$ and underprediction of the coarse ammonium.

The bias and error for $PM_{2.5}$ ammonium are large on a percentage basis, but relatively small on an absolute basis (+1.8 $\mu g/m^3$ bias and ±2.2 $\mu g/m^3$ error).

The model's predictions for maximum 24-hr average ammonium are reasonably accurate. The model predicted 10.1 and 9.9 $\mu g/m^3$ for $PM_{2.5}$ ammonium at Riverside when 11.6 and 9.5 were observed, respectively. The model predicted a maximum 24-hr value of 12 $\mu g/m^3$ for $PM_{2.5}$ ammonium at Riverside on both days when 12 and 15 $\mu g/m^3$ were observed. Thus, the accuracy of the peak ammonium predictions range from -21 to +6 percent. The maximum ammonium predicted anywhere in the domain is typically 50 percent higher than that predicted for Riverside.

As with nitrate, statistical comparisons of short-term ammonium predictions with observations indicate they are less accurate than the 24-hr average predictions. These model simulations show a positive bias on short-term ammonium, with mean errors of 3 $\mu g/m^3$, or 56 to 80 percent for $PM_{2.5}$ ammonium and 34 to 45 percent for PM_{10} ammonium.

5.5.4 Nitric Acid

The model's predictions of the mean 24-hr nitric acid concentrations at SCAQS stations were 4.2 and 3.3 ppb when 6.3 and 5.5 ppb were observed on June 24 and 25, respectively. The mean bias and error were -32 to -37 percent and ±47 to ±40 percent, respectively. The maximum 24-hr average nitric acid concentrations were underpredicted by larger amounts: 9.7 ppb vs. 4.6 predicted on June 24 and 7.7 vs 1.9 predicted on June 25. The model's predictions for peak 4-hr average nitric acid were 14.9 ppb when 20.4 ppb was observed on June 24 and 9.4 ppb when 19.5 ppb was observed on June 25. The underprediction of nitric acid was most common at stations where ammonia was overpredicted. The nitric acid underprediction in the western and central portions of the basin is believed to be related to the underprediction of ozone and the rate of NO_2 oxidation in these areas (which is common in most UAM simulations of the SCAQS episodes). Predicted and observed nitric acid in Riverside where high ammonia occurs are quite low.

The errors in nitric acid are not just due to gas-aerosol partitioning errors. The predicted total inorganic nitrate (HNO_3 plus PM_{10} nitrate) is also under estimated by about 20 percent in these simulations, which suggests the gas-phase chemistry is not producing nitric acid fast enough or nitric acid is depositing too fast. The bias towards underprediction of nitric acid and nitrate deserves further investigation.

5.5.5 Ammonia

The ammonia concentrations were mostly underpredicted in the simulations. The mean 24-hr ammonia concentrations at the SCAQS stations (29 ppb) were underpredicted by 12 and 10 ppb on June 24 and 25. On a percentage basis, the model overpredicted ammonia on average (15 to 17 percent) but this is just because it overpredicted some low ammonia

concentrations by large amounts, making the percentage bias positive. The mean normalized error in the 24-hr ammonia predictions was 55 to 63 percent, which is large.

The maximum 4-hr and 24-hr ammonia were observed at Riverside, and the model underestimated the highest values by 50 to 57 percent. The model estimated 46 ppb for the highest 4-hr average ammonia when 106 ppb was observed.

The errors in the estimate ammonia is probably due to two factors. First, the ammonia emissions are quite uncertain and this is the first attempt to use the SCAQS ammonia emissions inventory simulations. The absolute amount of emissions, the spatial distribution, and the diurnal profiles are uncertain. Second, the coarse spatial resolution and vertical resolution in the UAM-AERO simulation is probably inadequate to accurately simulate the surface concentrations of primary emitted species like ammonia. The use of coarse resolution causes pseudo diffusion which biases the results towards underprediction.

5.5.6 Sulfate

The predicted sulfate levels are lower than the observed levels, especially on June 24. On average, the model predicted 8 $\mu g/m^3$ of $PM_{2.5}$ sulfate when 13.1 and 10.6 $\mu g/m^3$ were observed at the SCAQS stations. The bias in the PM_{10} sulfate was smaller than the $PM_{2.5}$ sulfate. On average, the model predicted 11 $\mu g/m^3$ of PM10 sulfate when 15.4 and 12.3 $\mu g/m^3$ were observed on June 24 and 25. The mean normalized error in the 24-hr average sulfate was ±40 percent.

The highest 4-hr average PM_{10} sulfate was observed at Hawthorne on both days. The model estimated 12 and 21 $\mu g/m^3$ when 33 and 25 $\mu g/m^3$ were observed. The significant underprediction in the peak sulfate levels could be a result of underestimating the spatial and temporal extent of the fog, and/or the rate of SO_2 oxidation in the fog, which is treated empirically in the model.

5.5.7 Organic Material

The organic PM estimated by the model is a combination of primary and secondary organic material. The mean predicted $PM_{2.5}$ OM is 6.5 $\mu g/m^3$ which is below the mean observed level of 10.7 $\mu g/m^3$. The mean predicted PM_{10} OM is 13 $\mu g/m3$ which is below the mean observed levels of 16.7 and 17.6 $\mu g/m^3$ on June 24 and 25. The mean bias in PM_{10} OM is -16 percent and the mean error is ±24 and ±32 on June 24 and 25. The model underestimates the fine OM and produces accurate estimates of the coarse OM, which results in a modest underprediction of the PM_{10} OM on average.

The highest 4-hr and 24-hr PM_{10} OM concentrations were underestimated by the model. The highest 24-hr values, which occurred at Riverside, were underestimated by 35 percent. The highest 4-hr PM_{10} OM concentrations were 41 $\mu g/m^3$ at Azusa on June 24 and 71 $\mu g/m^3$ at

Claremont on June 25; the corresponding modeled 4-hr concentrations were 23 and 16 $\mu g/m^3$. The highest 4-hr $PM_{2.5}$ OM concentrations were 30 and 27 $\mu g/m^3$ at Azusa on June 24 and 25, where the corresponding modeled 4-hr concentrations were 16 and 13 $\mu g/m^3$.

Most of the modeled OM is primary PM, rather than secondary PM. The underprediction may be due to coarse spatial and vertical resolution used in the simulation, and uncertainties in the emissions (primary OM and VOCs) and the organic aerosol yields from the gas-phase reactions. Without ambient data to separate the primary and secondary OM, it is difficult to judge the accuracy of the secondary OM predictions. However, the largest errors tend to occur when the observed coarse OM is large compared to the fine OM, which suggest uncertainties in the local emissions and dispersion could mostly be responsible for the lack of agreement. The model predictions for OM were better without the 50 percent reduction in PM emissions, however, our approach did not include adjusting PM emissions by chemical component.

5.5.8 Elemental Carbon

The elemental carbon content of the aerosol is small on a mass basis but it is important for visibility because of its high efficiency for light absorption. On average, the model predicted 1.5 and 1.3 $\mu g/m^3$ of $PM_{2.5}$ EC when 1.4 and 1.5 $\mu g/m^3$ were observed at the SCAQS stations. The bias in the PM_{10} EC was larger than that in the $PM_{2.5}$ EC. On average, the model predicted 2.1 and 2 $\mu g/m^3$ of PM_{10} EC when 2 and 2.7 $\mu g/m^3$ were observed on June 24 and 25. The mean normalized error in the 24-hr average EC ranged from ±15 to ±40 percent. The maximum 4-hr and 24-hr EC concentrations were underestimated by the model 1 to 79 percent. Overall, the model performance for the mean EC was better than expected for a primary component of PM. The performance on the peak EC concentrations was similar to that for other primary PM species.

5.5.9 Sodium and Chloride

The mass of sodium and chloride in PM_{10} is small, but it is reported here because it is a component of the model predictions. As indicated above, the emissions of sodium and chloride are not known and model performance statistics show that the approximate emissions used in the simulations produce PM_{10} sodium and chloride that are within ±40 percent of the observed data on average. The mean sodium predictions were 1.7 and 2 $\mu g/m^3$ when 2.1 and 1.5 $\mu g/m^3$ were observed. The mean chloride predictions were 0.9 and 1.3 $\mu g/m^3$ when 1.3 and 1 $\mu g/m^3$ were observed. The maximum 4-hr and 24-hr sodium levels in the coastal area were overestimated by modest amounts.

5.5.10 PM Mass

The estimated mean $PM_{2.5}$ mass concentrations were 54 and 52 $\mu g/m^3$ which agrees reasonably well with the observed levels of 55 and 47 $\mu g/m^3$ on June 24 and 25. The mean bias in $PM_{2.5}$ mass was +2 and +20 percent, and the mean error was ±21 and ±32 percent on June 24 and 25. The maximum 24-hr $PM_{2.5}$ mass estimates were 69 and 67 $\mu g/m^3$ when 82 and 66 $\mu g/m^3$ were observed at Riverside and Azusa. Recall numerous measured components of $PM_{2.5}$ were underestimated in the simulations, however, the crustal $PM_{2.5}$ was overestimated which produced reasonably accurate $PM_{2.5}$ mass estimates. Even after the 50 percent downward adjustment in the PM emissions, the $PM_{2.5}$ crustal emissions are still probably overestimated.

The estimated PM_{10} mass concentrations are higher than the observed data. On average, the model predicted 90 $\mu g/m^3$ of PM_{10} mass when 63 to 57 $\mu g/m^3$ were observed. The mean bias in the PM_{10} mass concentrations was 47 and 72 percent on June 24 and 25, and the mean error was ±52 to ±72 percent. The model predicted 24-hr maximum PM_{10} concentrations of 122 and 120 $\mu g/m^3$ at Riverside when 106 and 94 $\mu g/m^3$ were observed. For 4-hr maxima, the model predicted 187 and 191 $\mu g/m^3$ when 166 and 146 were observed. Examination of the biases in the modeled components of PM_{10} shows that PM_{10} is overestimated because the crustal component is overestimated. The extent of the PM_{10} overestimation is offset by underprediction of ammonium, sulfate, and OM. Overall, the most accurately simulation component of PM_{10} in these simulations was PM_{10} nitrate.

5.6 DEPOSITION

The UAM-AERO model predicts the amount material deposited by each species each hour in each grid square. Unfortunately, data are not available for direct comparison with the model estimates. **Figures 5-53 through 5-63** shown the predicted spatial pattern of deposition on the third day of this summer simulation for ozone, NO_2, nitric acid, ammonia, PM_{10} nitrate, PM_{10} ammonium, PM_{10} sulfate, PM_{10} OM, crustal PM_{10}, PM_{10} mass. The spatial deposition patterns are quite similar to the 24-hr ambient concentration spatial patterns. This similarity is expected because the dry deposition loss rate is a linear function of surface layer concentrations in the model.

The estimated total amount of material deposited within the domain on June 25 is shown in **Table 5-11**. For gaseous species, the results indicate the ozone has the highest deposition rate, followed by nitric acid, hydrogen peroxide (H_2O_2), NO_2, formaldehyde, and ammonia on a mole basis. The predicted formic and acetic acid deposition is low. For PM, the results indicate $PM_{2.5}$ species deposit substantially less than PM_{10} species as expected. The PM components with high predicted deposition were water, crustal material, organic material, nitrate, sulfate, sodium, and ammonium on a mass basis.

Table 5-1. Observed maximum air quality concentrations on June 24-25, 1987.

Species	Day	Station with the Highest Short-Term Observed Concentration	
		Location	Maximum Observed
PM_{10} NO3	June 24	Riverside	81
PM_{10} NO3	June 25	Riverside	77
PM_{10} NH4	June 24	Riverside	26
PM_{10} NH4	June 25	Riverside	24
PM_{10} SO4	June 24	Hawthorne	33
PM_{10} SO4	June 25	Hawthorne	25
PM_{10} EC	June 24	Burbank	4.8
PM_{10} EC	June 25	Claremont	11.6
PM_{10} OM	June 24	Azusa	41
PM_{10} OM	June 25	Claremont	71
$PM_{2.5}$ Mass	June 24	Riverside	136
$PM_{2.5}$ Mass	June 25	Riverside	128
PM_{10} Mass	June 24	Riverside	165
PM_{10} Mass	June 25	Riverside	146
HNO3 (ppb)	June 24	Claremont	20
HNO3 (ppb)	June 25	Burbank	19
NH3 (ppb)	June 24	Riverside	106
NH3 (ppb)	June 25	Riverside	98
Ozone (ppb)[a]	June 24	Claremont	250
Ozone (ppb)[a]	June 25	San Bernardino	240
NO2 (ppb)[a]	June 24	Pasadena	90
NO2 (ppb)[a]	June 25	Burbank	110
NO (ppb)[a]	June 24	Upland	90
NO (ppb)[a]	June 25	Pomona	100

[a] Ozone, NO_2, and NO concentrations are 1-hr maxima. All other species concentrations are 4- to 6-hr averages.

Table 5-2. PM size/composition fractions of PM_{10} used for initial and boundary conditions.

Component	0-2.5-μm Mass Fraction of PM_{10}	2.5-10-μm Mass Fraction of PM_{10}
NA	0.01495	0.01218
NH_4	0.05984	0.01774
NO_3	0.11250	0.03750
Cl	0.01750	0.01750
SO_4	0.08000	0.02000
EC	0.04611	0.00689
OM	0.20250	0.06750
OTR	0.20795	0.06932
H2O[a]	0.00800	0.00200
Total	0.75000	0.25000

[a] Estimated for a fairly dry aerosol.

Table 5-3. Boundary concentrations for the June 23-25, 1987 episode simulation.

Species	Concentration (ppm)	Species	Concentration ($\mu g/m^3$)
NO	0.001	PM_{10} Mass	15.00
NO2	0.002	$PM_{2.5-10}$ Mass	3.75
O3	0.04	$PM_{2.5}$ Mass	11.25
HONO	0.00001	$PM_{2.5}$ NO_3	1.688
HNO3	0.00001	$PM_{2.5-10}$ NO_3	0.5623
HNO4	0.00001	$PM_{2.5}$ NH_4	0.8977
H2O2	0.003	$PM_{2.5-10}$ NH_4	0.266
CO	0.2	$PM_{2.5}$ SO_4	1.2
ALK1	3.68E-03	$PM_{2.5-10}$ SO_4	0.2999
ALK2	2.14E-03	$PM_{2.5}$ EC	0.1383
OLE1	8.28E-04	$PM_{2.5-10}$ EC	2.07E-02
OLE2	3.23E-04	$PM_{2.5}$ OM	3.038
OLE3	1.00E-04	$PM_{2.5-10}$ OM	1.012
ARO1	4.92E-04	$PM_{2.5}$ NA	0.2243
ARO2	2.70E-04	$PM_{2.5-10}$ NA	0.1826
ETHE	1.40E-03	$PM_{2.5}$ CL	0.2626
HCHO	5.78E-03	$PM_{2.5-10}$ CL	0.2624
CCHO	4.57E-04	$PM_{2.5}$ OTR	3.673
RCHO	2.02692-05	$PM_{2.5-10}$ OTR	1.122
MEK	5.47E-04	$PM_{2.5}$ H^+	1.50E-04
MGLY	1.00E-05	$PM_{2.5-10}$ H^+	7.83E-07
PAN	1.00E-04	$PM_{2.5-10}$ H_2O	3.00E-02
PPN	1.00E-05	$PM_{2.5}$ H2O	0.12
AFG2	1.00E-05		
CRES	1.00E-05		
SO2	1.00E-04		
Formic Acid	1.00E-04		
Acetic Acid	1.00E-04		
HCL	1.00E-05		
NH3	1.00E-04		

Table 5-4. 1987 Summer emissions (tons/day) for South Coast Air Basin.

	SOURCE CATEGORY	TBC	ROG	CO	NOx	SO2	PART
100	RESOURCE DEVELOPMENT & AGRICULTURE	.8252	.3067	4.668	.0000E+00	.0000E+00	.4126
110	AGRICULTURAL PRODUCTION	.6994	.5407	6.746	1.961	.1632	.5327E-01
111	AGRICULTURAL CROPS	2.343	1.879	.2515	.0000E+00	.0000E+00	2.637
112	AGRICULTURAL LIVESTOCK	124.5	20.68	.0000E+00	.0000E+00	.0000E+00	33.90
113	AGRICULTURAL SERVICES	.2205	.1488	.3131	.2606	.0000E+00	.7843
120	FORESTRY	.0000E+00	.0000E+00	.0000E+00	.0000E+00	.0000E+00	.0000E+00
130	MINING	.0000E+00	.0000E+00	.0000E+00	.0000E+00	.0000E+00	.0000E+00
131	METAL MINING	.0000E+00	.0000E+00	.0000E+00	.0000E+00	.0000E+00	.0000E+00
132	COAL MINING	.0000E+00	.0000E+00	.0000E+00	.0000E+00	.0000E+00	.0000E+00
133	STONE & CLAY (MINING)	.6575E-01	.4920E-01	.4730E-01	.2454	.1858E-01	.2681
134	CHEMICALS & FERTILIZER MINERAL	.0000E+00	.0000E+00	.0000E+00	.0000E+00	.0000E+00	.0000E+00
140	OIL & GAS EXTRACTION	63.20	29.62	4.620	25.18	2.134	.2532
141	LIQUID GAS PRODUCTION	4.566	1.360	.0000E+00	.0000E+00	.0000E+00	.0000E+00
200	MANUFACTURING & INDUSTRIAL	49.57	42.27	3.180	18.80	3.946	.3997
210	FOOD & KINDRED	20.19	12.90	.1015	.6935	.1888	12.21
211	FRUIT/VEG PRESERVATION	2.686	2.315	26.94	4.204	1.456	1.686
212	GRAIN MILL PRODUCTS	.2156	.1824	.3363E-01	.9274E-01	.4784E-01	.1167
213	BAKERY PRODUCTS	6.717	8.915	.1166E-01	.8709E-01	.2745E-02	.4824E-01
214	VEGETABLE OIL	.5512E-03	.1943E-03	.2756E-03	.6581E-02	.0000E+00	.4134E-03
215	SUGAR MFG/REFINING	.0000E+00	.0000E+00	.0000E+00	.0000E+00	.0000E+00	.0000E+00
216	MALT BEVERAGES	.7763E-01	.5092E-01	.7025E-01	.4962	.1262	.1558E-01
217	WINES & BRANDY	.1140	.1523	.0000E+00	.0000E+00	.0000E+00	.0000E-00
220	LUMBER & WOOD PRODUCTS	4.848	4.439	.2459E-01	.3543E-01	.1816E-01	7.623
230	PAPER & ALLIED	19.67	17.67	.1947	.9368	.3107E-01	.3852E-01
231	PULP & PAPER MILLS	.4005	.1097	.7231	2.466	.4112E-02	.9907E-01
240	CHEMICAL & ALLIED	1.158	.6840	.6312	1.456	2.905	.2679
241	RUBBER & PLASTICS MFG	.9762	.6600	.1493E-01	.2479	.2116E-01	.8594E-01
242	DRUGS	1.113	.7031	.5743E-01	.1630	.1323E-02	.7538E-01
243	CLEANING/TOILET PREP	.7149	.4624	.5933	1.171	.6691E-01	.1999
244	PAINT MFG	5.314	4.727	.6512E-02	.2548E-01	.7716E-03	.9068E-01
245	AGRI CHEMICALS	.4803	.3801	.0000E+00	.1049E-01	.0000E+00	.2428E-01
260	PETROLEUM REFINING/RELATED	.3409	.2596	.9273E-02	.2598	.9534E-01	.2479E-01
261	PETROLEUM REFINING	32.48	20.34	9.007	34.10	14.20	3.152
262	PAVING & ROOFING MATERIALS	.2988	.2296	1.472	.4398	.1487	.4857
263	PET COKE/BRIQUETTE	.0000E+00	.0000E+00	.0000E+00	.0000E+00	.0000E+00	.6835E-01
270	MINERAL PRODUCTS	1.085	.8122	1.849	1.280	.3420E-01	1.318
271	GLASS/GLASS PRODUCTS	.3641	.1818	.5618E-01	4.260	1.455	.1837
280	METALLURGICAL	1.013	.1311	.1085	.7074	.7716E-03	.3339
281	IRON/STEEL PRODUCTION	1.215	.9724	.6378	.3007	.4157E-01	.1649
282	IRON/STEEL FOUNDRY	1.081	.6586	.1184E-01	.1512	.3858E-03	.5662E-01
283	NONFERROUS METALS	1.169	.7109	.5436	1.088	.5923	.5638
290	MISC. MANUFACTURING	3.487	2.058	.4282E-02	.3009E-01	.1701E-01	.2483E-01
291	TEXTILES & APPAREL	2.334	1.730	.2287E-01	.2974	.1717E-01	.9115E-01
292	FURNITURE & FIXTURES	25.57	24.52	.1365	.1906	.1188E-02	.2012
293	FABRICATED METAL	39.64	23.29	.3398	1.950	.1306	.5057
294	MACHINERY	17.67	6.846	.8202E-01	.5717	.2302E-02	.9424E-01
295	TRANSPORTATION EQUIPMENT	37.00	17.77	2.836	1.762	.1775	.3233
296	RUBBER & PLASTICS FAB.	5.399	3.920	.1612E-01	.2540	.1549E-02	.1793
297	TOBACCO MANUFACTURING	.0000E+00	.0000E+00	.0000E+00	.0000E+00	.0000E+00	.0000E+00
298	INSTRUMENTS	4.533	.5615	.3659E-01	.3774E-01	.1343E-01	.1008E-02
300	SERVICES & COMMERCE	54.81	47.97	62.48	33.19	9.457	1.014
310	ELECTRIC UTILITIES	1.056	.3934	2.068	7.781	.9265	.2121
320	PETROLEUM & GAS MARKETING	6.215	3.132	1.066	4.156	.8360E-01	.2514E-01
321	BULK PLANTS	7.208	6.258	.6596	.1488	.7871E-03	.3510E-01
322	SERVICE STATIONS	14.91	13.63	.0000E+00	.0000E+00	.0000E+00	.0000E+00
323	PIPE LINES	218.4	4.278	.2191E-01	.1444	.6980E-01	.1696E-01
330	MISC. SERVICES	15.57	13.92	1.106	1.371	.3221	.4588
331	STEAM SUPPLY	1.004	.9756E-01	.3860	2.720	.6856E-02	.8659E-02
332	PRINTING & PUBLISHING	4.877	4.068	.2449E-01	.1496	.8697E-02	.4272E-01
333	LAUNDRY & DRYCLEANERS	19.71	1.215	.5329E-02	.1678	.9641E-01	.1289E-01
334	SANITARY & WATER	379.9	5.010	4.459	5.116	.9679	.3616
335	HEALTH SERVICES	1.172	.4785	.8573	2.684	.4591	.1271
336	EDUCATIONAL SERVICES	1.117	.9005	3.484	1.196	.2774	.1531
400	TRANSPORTATION	.2750	.2077	.1102E-02	.4652E-02	.0000E+00	.1378E-03
410	ON-ROAD TRAVEL	2040.	1787.	8464.	719.8	33.93	740.4
420	RAIL TRANSPORT	1.458	1.095	4.120	27.49	1.931	.3096
430	WATER BORNE	2.981	2.278	5.599	39.34	35.07	1.701
440	AIR TRANSPORTATION	20.49	13.77	85.93	16.96	1.405	1.829
500	DOMESTIC	96.25	100.7	.0000E+00	.0000E+00	.0000E+00	.0000E+00
510	RESIDENTIAL	9.305	6.147	58.46	46.07	1.695	2.238
520	RECREATIONAL	13.32	12.16	58.25	2.849	.2327	.5664E-01
600	MISC. ACTIVITIES	32.12	26.81	188.7	192.2	13.64	3.380
610	CONSTRUCTION	.9565E-01	.9649E-01	.0000E+00	.0000E+00	.0000E+00	.0000E+00
611	BUILDING CONSTRUCTION	9.000	6.115	.0000E+00	.0000E+00	.0000E+00	200.4
612	ROAD CONSTRUCTION	3.133	2.220	.0000E+00	.0000E+00	.0000E+00	34.78
620	NATURAL SOURCES	.0000E+00	.0000E+00	.0000E+00	.0000E+00	.0000E+00	51.64
630	GOVERNMENT	.3616	.3283	4.934	.1796	.2290E-01	15.03
631	NATIONAL SECURITY	1.104	.8006	.1011	.5265	.9086E-01	.5148E-01
801	SEEPS/BIOGENIC	71.79	71.79	.0000E+00	.0000E+00	.0000E+00	.0000E+00
802	CHANNEL SHIPPING	.0000E+00	.0000E+00	.0000E+00	.0000E+00	.0000E+00	.0000E+00
803	OCS AND RELATED SOURCES	.0000E+00	.0000E+00	.0000E+00	.0000E+00	.0000E+00	.0000E+00
804	TIDELAND PLATFORMS	.0000E+00	.0000E+00	.0000E+00	.0000E+00	.0000E+00	.0000E+00
900	UNSPECIFIED ACTIVITIES	180.7	138.4	85.15	33.48	3.390	9.934
	TOTAL	3694.	2528.	9099.	1244.	132.1	1133.

Table 5-4. 1987 Summer emissions (tons/day) for South Coast Air Basin.

	SOURCE CATEGORY	THC	ROG	CO	NOx	SO2	PART
THC =	Total organic gases, including methane and other less reactive compounds.						
ROG =	Reactive organic gases.						
PART =	Total PM (including particles with D_p > 10 μm.						
100	RESOURCE DEVELOPMENT & AGRICULTURE	.0000E+00	.0000E+00	.0000E+00	.4826E-01	.6322E-01	.1443
110	AGRICULTURAL PRODUCTION	1.828	.1236	.9807E-02	.9301E-01	.1721	.7991E-01
111	AGRICULTURAL CROPS	.0000E+00	.0000E+00	.0000E+00	.5729	.6521	.6910E-02
112	AGRICULTURAL LIVESTOCK	.0000E+00	.0000E+00	.0000E+00	14.03	5.417	.0000E+00
113	AGRICULTURAL SERVICES	.2429	.1642E-01	.1303E-02	.1012	.2076E-01	.7510E-02
120	FORESTRY	.0000E+00	.0000E+00	.0000E+00	.0000E+00	.0000E+00	.0000E+00
130	MINING	.0000E+00	.0000E+00	.0000E+00	.0000E+00	.0000E+00	.0000E+00
131	METAL MINING	.0000E+00	.0000E+00	.0000E+00	.0000E+00	.0000E+00	.0000E+00
132	COAL MINING	.0000E+00	.0000E+00	.0000E+00	.0000E+00	.0000E+00	.0000E+00
133	STONE & CLAY (MINING)	.2287	.1546E-01	.1227E-02	.2493E-01	.7590E-02	.4955E-02
134	CHEMICALS & FERTILIZER MINERAL	.0000E+00	.0000E+00	.0000E+00	.0000E+00	.0000E+00	.0000E+00
140	OIL & GAS EXTRACTION	23.47	1.586	.1259	22.36	5.770	.3441
141	LIQUID GAS PRODUCTION	.0000E+00	.0000E+00	.0000E+00	.7845	.5739	.0000E+00
200	MANUFACTURING & INDUSTRIAL	17.52	1.185	.9401E-01	7.075	14.44	.8233E-01
210	FOOD & KINDRED	.6463	.4369E-01	.3467E-02	8.900	1.787	.6260
211	FRUIT/VEG PRESERVATION	3.918	.2648	.2102E-01	.4542	.5416	.3129
212	GRAIN MILL PRODUCTS	.8643E-01	.5842E-02	.4637E-03	.4279E-01	.5803E-01	.4170E-03
213	BAKERY PRODUCTS	.8117E-01	.5486E-02	.4354E-03	8.805	.7910E-02	.1383E-03
214	VEGETABLE OIL	.6133E-02	.4146E-03	.3290E-04	.1299E-03	.6337E-05	.0000E+00
215	SUGAR MFG/REFINING	.0000E+00	.0000E+00	.0000E+00	.0000E+00	.0000E+00	.0000E+00
216	MALT BEVERAGES	.4624	.3126E-01	.2481E-02	.2940E-01	.1061E-01	.2322E-02
217	WINES & BRANDY	.0000E+00	.0000E+00	.0000E+00	.1523	.0000E+00	.0000E+00
220	LUMBER & WOOD PRODUCTS	.3302E-01	.2232E-02	.1772E-03	1.164	1.539	.7339E-02
230	PAPER & ALLIED	.8731	.5902E-01	.4684E-02	2.489	5.855	.1325E-01
231	PULP & PAPER MILLS	2.299	.1554	.1233E-01	.6479E-01	.2233E-01	.4104E-02
240	CHEMICAL & ALLIED	1.357	.9171E-01	.7279E-02	.4307	.1240	.2523E-01
241	RUBBER & PLASTICS MFG	.2310	.1562E-01	.1240E-02	.3867	.1173	.2281E-01
242	DRUGS	.1519	.1027E-01	.8149E-03	.4317	.1266	.2615E-01
243	CLEANING/TOILET PREP	1.091	.7375E-01	.5853E-02	.3125	.6809E-01	.1925E-01
244	PAINT MFG	.2375E-01	.1605E-02	.1274E-03	.6412	1.642	.4921E-02
245	AGRI CHEMICALS	.9780E-02	.6611E-03	.5247E-04	.1324	.1236	.2034E-02
260	PETROLEUM REFINING/RELATED	.2422	.1637E-01	.1299E-02	.1799	.4747E-01	.5976E-02
261	PETROLEUM REFINING	31.79	2.149	.1705	16.14	2.937	.6193E-01
262	PAVING & ROOFING MATERIALS	.4099	.2771E-01	.2199E-02	.1301	.7507E-01	.2263E-02
263	PET COKE/BRIQUETTE	.0000E+00	.0000E+00	.0000E+00	.0000E+00	.0000E+00	.0000E+00
270	MINERAL PRODUCTS	1.193	.8065E-01	.6401E-02	.3371	.2390	.1222E-01
271	GLASS/GLASS PRODUCTS	3.970	.2684	.2130E-01	.9605E-01	.2334E-01	.4774E-02
280	METALLURGICAL	.6593	.4456E-01	.3537E-02	.6669E-01	.5355E-01	.2066E-02
281	IRON/STEEL PRODUCTION	.2803	.1894E-01	.1504E-02	.2674	.3293	.9863E-02
282	IRON/STEEL FOUNDRY	.1409	.9523E-02	.7558E-03	.3066	.2259	.7627E-02
283	NONFERROUS METALS	1.014	.6854E-01	.5440E-02	.2894	.2285	.1020E-01
290	MISC. MANUFACTURING	.2804E-01	.1895E-02	.1504E-03	.9364	.5027	.2619E-01
291	TEXTILES & APPAREL	.2772	.1874E-01	.1487E-02	.3304	.4208	.1012E-01
292	FURNITURE & FIXTURES	.1776	.1201E-01	.9530E-03	5.979	8.109	.2175E-01
293	FABRICATED METAL	1.818	.1229	.9752E-02	7.715	7.113	.9524E-01
294	MACHINERY	.5328	.3602E-01	.2858E-02	2.645	2.240	.3787E-01
295	TRANSPORTATION EQUIPMENT	1.642	.1110	.8811E-02	4.607	5.667	.1371
296	RUBBER & PLASTICS FAB.	.2367	.1600E-01	.1270E-02	2.032	.9526	.7712E-01
297	TOBACCO MANUFACTURING	.0000E+00	.0000E+00	.0000E+00	.0000E+00	.0000E+00	.0000E+00
298	INSTRUMENTS	.3517E-01	.2378E-02	.1887E-03	.2297	.1781	.3048E-02
300	SERVICES & COMMERCE	30.94	2.091	.1660	3.853	24.04	.7028
310	ELECTRIC UTILITIES	7.252	.4902	.3891E-01	.2050	.4144E-01	.3680E-01
320	PETROLEUM & GAS MARKETING	3.874	.2618	.2078E-01	2.292	.5514	.1747E-01
321	BULK PLANTS	.1387	.9376E-02	.7442E-03	4.799	.5945	.4811E-01
322	SERVICE STATIONS	.0000E+00	.0000E+00	.0000E+00	11.00	.9040	.0000E+00
323	PIPE LINES	.1346	.9098E-02	.7221E-03	4.230	.2804E-01	.2965E-02
330	MISC. SERVICES	1.278	.8636E-01	.6854E-02	7.011	4.108	.4602E-01
331	STEAM SUPPLY	2.535	.1714	.1360E-01	.5914E-01	.3959E-03	.6990E-02
332	PRINTING & PUBLISHING	.1394	.9423E-02	.7479E-03	2.037	1.498	.7855E-02
333	LAUNDRY & DRYCLEANERS	.1564	.1057E-01	.8389E-03	.5848	.5935	.6354E-02
334	SANITARY & WATER	4.768	.3223	.2558E-01	2.945	.5412E-01	.2709
335	HEALTH SERVICES	2.502	.1691	.1342E-01	.2130	.1189	.1145E-01
336	EDUCATIONAL SERVICES	1.115	.7534E-01	.5979E-02	.3754	.2331	.3302E-01
400	TRANSPORTATION	.4335E-02	.2931E-03	.2326E-04	.1476	.5069E-01	.0000E+00
410	ON-ROAD TRAVEL	670.8	45.34	3.599	498.7	366.7	185.2
420	RAIL TRANSPORT	25.62	1.732	.1375	.1607	.4541	.1470
430	WATER BORNE	36.66	2.478	.1967	.5383	.8335	.2683
440	AIR TRANSPORTATION	15.81	1.069	.8481E-01	.3352	3.913	.1291
500	DOMESTIC	.0000E+00	.0000E+00	.0000E+00	86.27	11.98	.0000E+00
510	RESIDENTIAL	42.94	2.902	.2303	1.668	1.172	.6053
520	RECREATIONAL	2.655	.1795	.1425E-01	2.536	2.239	1.637
600	MISC. ACTIVITIES	179.1	12.11	.9608	4.684	7.399	3.744
610	CONSTRUCTION	.0000E+00	.0000E+00	.0000E+00	.4069E-01	.2874E-01	.2624E-04
611	BUILDING CONSTRUCTION	.0000E+00	.0000E+00	.0000E+00	3.321	1.535	.2700E-01
612	ROAD CONSTRUCTION	.0000E+00	.0000E+00	.0000E+00	.0000E+00	1.138	.0000E+00
620	NATURAL SOURCES	.0000E+00	.0000E+00	.0000E+00	.0000E+00	.0000E+00	.0000E+00
630	GOVERNMENT	.1674	.1132E-01	.8980E-03	.8670E-01	.7347E-01	.3173E-01

Table 5-4. 1987 Summer emissions (tons/day) for South Coast Air Basin.

	SOURCE CATEGORY	TEC	ROG	CO	NOX	SO2	PART
631	NATIONAL SECURITY	.4907	.3317E-01	.2633E-02	.2229	.3991	.1321E-02
801	SEEPS/BIOGENIC	.0000E-00	.0000E+00	.0000E+00	.0000E+00	.0000E+00	.0000E+00
802	CHANNEL SHIPPING	.0000E-00	.0000E+00	.0000E+00	.0000E+00	.0000E+00	.0000E+00
803	OCS AND RELATED SOURCES	.0000E+00	.0000E+00	.0000E+00	.0000E+00	.0000E+00	.0000E+00
804	TIDELAND PLATFORMS	.0000E-00	.0000E+00	.0000E+00	.0000E+00	.0000E-00	.0000E+00
900	UNSPECIFIED ACTIVITIES	31.21	2.109	.1674	62.70	39.66	3.020
	TOTAL	1159.	78.36	6.219	812.9	538.8	198.2
100	RESOURCE DEVELOPMENT & AGRICULTURE	.3895E-01	.1199E-01	.0000E+00	.0000E+00	.0000E+00	.0000E+00
110	AGRICULTURAL PRODUCTION	.6431E-01	.1241E-01	.0000E+00	.7986E-04	.5419E-01	.2561E-01
111	AGRICULTURAL CROPS	.4590E-02	.5932E-02	.0000E+00	.2303E-03	.2310	.4036
112	AGRICULTURAL LIVESTOCK	.0000E+00	.0000E+00	.0000E+00	.0000E+00	.0000E+00	.0000E+00
113	AGRICULTURAL SERVICES	.4897E-03	.1244E-03	.0000E+00	.0000E+00	.1842E-01	.1972E-03
120	FORESTRY	.0000E+00	.0000E+00	.0000E+00	.0000E+00	.0000E+00	.0000E+00
130	MINING	.0000E+00	.0000E+00	.0000E+00	.0000E+00	.0000E+00	.0000E+00
131	METAL MINING	.0000E+00	.0000E+00	.0000E+00	.0000E+00	.0000E+00	.0000E+00
132	COAL MINING	.0000E+00	.0000E-00	.0000E+00	.0000E+00	.0000E+00	.0000E+00
133	STONE & CLAY (MINING)	.4413E-02	.1109E-02	.0000E+00	.0000E+00	.4514E-02	.3733E-03
134	CHEMICALS & FERTILIZER MINERAL	.0000E+00	.0000E+00	.0000E+00	.0000E+00	.0000E+00	.0000E+00
140	OIL & GAS EXTRACTION	.2754	.1257	.0000E+00	.3223E-04	.4484	.4624E-01
141	LIQUID GAS PRODUCTION	.0000E+00	.0000E+00	.0000E+00	.0000E+00	.1665E-02	.0000E+00
200	MANUFACTURING & INDUSTRIAL	.1033	.5621E-02	.0000E+00	.9732E-04	14.61	3.360
210	FOOD & KINDRED	.1464E-02	.2033E-03	.0000E+00	.1151E-05	1.582	.6769E-03
211	FRUIT/VEG PRESERVATION	.3190	.7407E-01	.0000E+00	.1409E-03	.2961	.1287
212	GRAIN MILL PRODUCTS	.5028E-03	.9335E-04	.0000E+00	.1151E-05	.5590E-01	.1373E-01
213	BAKERY PRODUCTS	.1588E-03	.3991E-04	.0000E+00	.0000E+00	.5545E-03	.8648E-04
214	VEGETABLE OIL	.0000E+00	.0000E+00	.0000E+00	.0000E+00	.1570E-04	.0000E+00
215	SUGAR MFG/REFINING	.0000E+00	.0000E+00	.0000E+00	.0000E+00	.0000E+00	.0000E+00
216	MALT BEVERAGES	.4646E-03	.3932E-04	.0000E+00	.1532E-05	.5200E-02	.5670E-03
217	WINES & BRANDY	.0000E+00	.0000E+00	.0000E+00	.0000E+00	.0000E+00	.0000E+00
220	LUMBER & WOOD PRODUCTS	.4648E-02	.6778E-04	.0000E+00	.0000E+00	1.182	.2409
230	PAPER & ALLIED	.8368E-02	.5491E-03	.0000E+00	.3288E-04	6.866	1.600
231	PULP & PAPER MILLS	.4719E-02	.5541E-03	.0000E+00	.0000E+00	.8681E-02	.4501E-03
240	CHEMICAL & ALLIED	.3598E-02	.2609E-02	.0000E+00	.8757E-06	.6670E-01	.1760E-02
241	RUBBER & PLASTICS MFG	.6095E-03	.1507E-02	.0000E+00	.1534E-05	.8880E-01	.8732E-02
242	DRUGS	.1826E-03	.2144E-04	.0000E+00	.0000E+00	.7505E-01	.6165E-02
243	CLEANING/TOILET PREP	.1727E-02	.2137E-03	.0000E+00	.9414E-06	.4856E-01	.1842E-02
244	PAINT MFG	.2148E-02	.4301E-03	.0000E+00	.3164E-04	1.664	.4118
245	AGRI CHEMICALS	.4947E-03	.9726E-03	.0000E+00	.4181E-04	.4707E-01	.7325E-01
260	PETROLEUM REFINING/RELATED	.8325E-03	.4707E-04	.0000E+00	.3369E-05	.1852E-01	.1547E-02
261	PETROLEUM REFINING	.2897	.2144	.0000E+00	.1847E-04	.3741	.1235
262	PAVING & ROOFING MATERIALS	.1817E-02	.1048E-02	.0000E+00	.1102E-05	.4636E-02	.1155E-01
263	PET COKE/BRIQUETTE	.0000E+00	.0000E+00	.0000E+00	.0000E+00	.0000E+00	.0000E+00
270	MINERAL PRODUCTS	.9044E-02	.2424E-02	.0000E+00	.7716E-07	.1072	.2790E-01
271	GLASS/GLASS PRODUCTS	.5973E-03	.3459E-04	.0000E+00	.0000E+00	.1580E-01	.6805E-03
280	METALLURGICAL	.1360E-03	.3271E-04	.0000E+00	.0000E+00	.6289E-02	.2484E-03
281	IRON/STEEL PRODUCTION	.6919E-02	.1708E-02	.0000E+00	.1929E-06	.2621	.4624E-01
282	IRON/STEEL FOUNDRY	.1732E-03	.3522E-04	.0000E+00	.0000E+00	.4876E-01	.1485E-01
283	NONFERROUS METALS	.4273E-02	.8508E-03	.0000E+00	.0000E+00	.7994E-01	.2403E-01
290	MISC. MANUFACTURING	.3910E-03	.0000E+00	.0000E+00	.0000E+00	.3146	.9335E-01
291	TEXTILES & APPAREL	.4699E-03	.0000E+00	.0000E+00	.0000E+00	.4449	.9900E-01
292	FURNITURE & FIXTURES	.1223E-01	.5080E-03	.0000E+00	.1918E-04	7.261	1.694
293	FABRICATED METAL	.1137E-01	.9188E-03	.0000E+00	.2378E-04	4.391	1.492
294	MACHINERY	.1882E-02	.6193E-03	.0000E+00	.3419E-04	.9880	.2859
295	TRANSPORTATION EQUIPMENT	.2731E-01	.7481E-02	.0000E+00	.7745E-04	4.893	1.117
296	RUBBER & PLASTICS FAB.	.4471E-02	.3007E-01	.0000E+00	.4606E-03	.3591	.1004
297	TOBACCO MANUFACTURING	.0000E+00	.0000E+00	.0000E+00	.0000E+00	.0000E+00	.0000E+00
298	INSTRUMENTS	.6656E-03	.8395E-03	.0000E+00	.4932E-04	.2513E-01	.2006E-01
300	SERVICES & COMMERCE	.8140	.1945	.0000E+00	.1344E-03	13.40	3.266
310	ELECTRIC UTILITIES	.4271E-01	.1086E-01	.0000E+00	.1118E-04	.1867E-01	.1094E-02
320	PETROLEUM & GAS MARKETING	.6809E-01	.1046	.0000E+00	.0000E+00	.5680E-01	.5216E-02
321	BULK PLANTS	.1356	.4880	.0000E+00	.0000E+00	.1399	.2839E-01
322	SERVICE STATIONS	.2429	1.336	.0000E+00	.0000E+00	.1288	.1615E-01
323	PIPE LINES	.8097E-03	.3715E-02	.0000E+00	.5490E-06	.1154E-01	.1088E-03
330	MISC. SERVICES	.1354E-01	.3099E-02	.0000E+00	.2009E-05	1.317	.3762
331	STEAM SUPPLY	.1949E-01	.2550E-02	.0000E+00	.2183E-06	.6237E-03	.2125E-04
332	PRINTING & PUBLISHING	.2098E-01	.3243E-01	.0000E+00	.1967E-02	.1486	.2165
333	LAUNDRY & DRYCLEANERS	.0000E+00	.0000E+00	.0000E+00	.0000E+00	.2155E-01	.1102E-02
334	SANITARY & WATER	.3127	.7720E-01	.0000E+00	.3774	.4309	.4138
335	HEALTH SERVICES	.1342E-01	.2763E-02	.0000E+00	.1863E-05	.4205E-01	.2144E-01
336	EDUCATIONAL SERVICES	.3059E-01	.6405E-02	.0000E+00	.5583E-05	.1131	.3716E-01
400	TRANSPORTATION	.1332E-03	.4909E-03	.0000E+00	.0000E+00	.4601E-02	.4352E-03
410	ON-ROAD TRAVEL	166.3	78.33	1.627	.2448	213.1	204.5
420	RAIL TRANSPORT	.6809E-01	.3789E-02	.0000E+00	.2713E-03	.5022E-01	.2991E-01
430	WATER BORNE	.1298	.1080E-01	.0000E+00	.4458E-03	.1379	.5821E-01
440	AIR TRANSPORTATION	.9126	1.032	.0000E+00	.0000E+00	.7296	5.788
500	DOMESTIC	.2324E-01	.4677E-01	.0000E+00	.5341E-03	.6010	1.119
510	RESIDENTIAL	.7424	.1760	.0000E+00	.2326E-05	.7553	.2924
520	RECREATIONAL	1.937	.4889	.0000E+00	.7014E-04	1.851	.7798

Table 5-4. 1987 Summer emissions (tons/day) for South Coast Air Basin.

	SOURCE CATEGORY	THC	ROG	CO	NOx	SO2	PART
100	RESOURCE DEVELOPMENT & AGRICULTURE	.8252	.3067	4.668	.0000E+00	.0000E+00	.4126
110	AGRICULTURAL PRODUCTION	.6994	.5407	6.746	1.961	.1632	.5327E-01
111	AGRICULTURAL CROPS	2.343	1.879	.2515	.0000E+00	.0000E+00	2.637
112	AGRICULTURAL LIVESTOCK	124.5	20.68	.0000E+00	.0000E+00	.0000E+00	33.90
113	AGRICULTURAL SERVICES	.2205	.1488	.3131	.2606	.0000E+00	.7843
120	FORESTRY	.0000E+00	.0000E+00	.0000E+00	.0000E+00	.0000E+00	.0000E+00
130	MINING	.0000E+00	.0000E+00	.0000E+00	.0000E+00	.0000E+00	.0000E+00
131	METAL MINING	.0000E+00	.0000E+00	.0000E+00	.0000E+00	.0000E+00	.0000E+00
132	COAL MINING	.0000E+00	.0000E+00	.0000E+00	.0000E+00	.0000E+00	.0000E+00
133	STONE & CLAY (MINING)	.6575E-01	.4920E-01	.4730E-01	.2454	.1858E-01	.2681
134	CHEMICALS & FERTILIZER MINERAL	.0000E+00	.0000E+00	.0000E+00	.0000E+00	.0000E+00	.0000E+00
140	OIL & GAS EXTRACTION	63.20	29.62	4.620	25.18	2.134	.2532
141	LIQUID GAS PRODUCTION	4.566	1.360	.0000E+00	.0000E+00	.0000E+00	.0000E+00
200	MANUFACTURING & INDUSTRIAL	49.57	42.27	3.180	18.80	3.946	.3997
210	FOOD & KINDRED	20.19	12.90	.1015	.6935	.1888	12.21
211	FRUIT/VEG PRESERVATION	2.686	2.315	26.94	4.204	1.456	1.686
212	GRAIN MILL PRODUCTS	.2156	.1824	.3363E-01	.9274E-01	.4784E-01	.1167
213	BAKERY PRODUCTS	6.717	8.915	.1166E-01	.8709E-01	.2745E-02	.4824E-01
214	VEGETABLE OIL	.5512E-03	.1943E-03	.2756E-03	.6581E-02	.0000E+00	.4134E-03
215	SUGAR MFG/REFINING	.0000E+00	.0000E+00	.0000E+00	.0000E+00	.0000E+00	.0000E+00
216	MALT BEVERAGES	.7763E-01	.5092E-01	.7025E-01	.4962	.1262	.1558E-01
217	WINES & BRANDY	.1140	.1523	.0000E+00	.0000E+00	.0000E+00	.0000E+00
220	LUMBER & WOOD PRODUCTS	4.848	4.439	.2459E-01	.3543E-01	.1816E-01	7.623
230	PAPER & ALLIED	19.67	17.67	.1947	.9368	.3107E-01	.3852E-01
231	PULP & PAPER MILLS	.4005	.1097	.7231	2.466	.4112E-02	.9907E-01
240	CHEMICAL & ALLIED	1.158	.6840	.6312	1.456	2.905	.2679
241	RUBBER & PLASTICS MFG	.9762	.6600	.1493E-01	.2479	.2116E-01	.8594E-01
242	DRUGS	1.113	.7031	.5743E-01	.1630	.1323E-02	.7538E-01
243	CLEANING/TOILET PREP	.7149	.4624	.5933	1.171	.6691E-01	.1999
244	PAINT MFG	5.314	4.727	.6512E-02	.2548E-01	.7716E-03	.9068E-01
245	AGRI CHEMICALS	.4803	.3801	.0000E+00	.1049E-01	.0000E+00	.2428E-01
260	PETROLEUM REFINING/RELATED	.3409	.2596	.9273E-02	.2598	.9534E-01	.2479E-01
261	PETROLEUM REFINING	32.48	20.34	9.007	34.10	14.20	3.152
262	PAVING & ROOFING MATERIALS	.2988	.2296	1.472	.4398	.1487	.4857
263	PET COKE/BRIQUETTE	.0000E+00	.0000E+00	.0000E+00	.0000E+00	.0000E+00	.6835E-01
270	MINERAL PRODUCTS	1.085	.8122	1.849	1.280	.3420E-01	1.318
271	GLASS/GLASS PRODUCTS	.3641	.1818	.5618E-01	4.260	1.455	.1837
280	METALLURGICAL	1.013	.1311	.1085	.7074	.7716E-03	.3339
281	IRON/STEEL PRODUCTION	1.215	.9724	.6378	.3007	.4157E-01	.1649
282	IRON/STEEL FOUNDRY	1.081	.6586	.1184E-01	.1512	.3858E-03	.5662E-01
283	NONFERROUS METALS	1.169	.7109	.5436	1.088	.5923	.5638
290	MISC. MANUFACTURING	3.487	2.058	.4282E-02	.3009E-01	.1701E-01	.2483E-01
291	TEXTILES & APPAREL	2.334	1.730	.2287E-01	.2974	.1717E-01	.9115E-01
292	FURNITURE & FIXTURES	25.57	24.52	.1365	.1906	.1188E-02	.2012
293	FABRICATED METAL	39.64	23.29	.3398	1.950	.1306	.5057
294	MACHINERY	17.67	6.846	.8202E-01	.5717	.2302E-02	.9424E-01
295	TRANSPORTATION EQUIPMENT	37.00	17.77	2.836	1.762	.1775	.3233
296	RUBBER & PLASTICS FAB.	5.399	3.920	.1612E-01	.2540	.1549E-02	.1793
297	TOBACCO MANUFACTURING	.0000E+00	.0000E+00	.0000E+00	.0000E+00	.0000E+00	.0000E+00
298	INSTRUMENTS	4.533	.5615	.3659E-01	.3774E-01	.1343E-01	.1008E-02
300	SERVICES & COMMERCE	54.81	47.97	62.48	33.19	9.457	1.014
310	ELECTRIC UTILITIES	1.056	.3934	2.068	7.781	.9265	.2121
320	PETROLEUM & GAS MARKETING	6.215	3.132	1.066	4.156	.8360E-01	.2514E-01
321	BULK PLANTS	7.208	6.258	.6596	.1488	.7871E-03	.3510E-01
322	SERVICE STATIONS	14.91	13.63	.0000E+00	.0000E+00	.0000E+00	.0000E+00
323	PIPE LINES	218.4	4.278	.2191E-01	.1444	.6980E-01	.1696E-01
330	MISC. SERVICES	15.57	13.92	1.106	1.371	.3221	.4588
331	STEAM SUPPLY	1.004	.9756E-01	.3860	2.720	.6856E-02	.8659E-02
332	PRINTING & PUBLISHING	4.877	4.068	.2449E-01	.1496	.8697E-02	.4272E-01
333	LAUNDRY & DRYCLEANERS	19.71	1.215	.5329E-02	.1678	.9641E-01	.1289E-01
334	SANITARY & WATER	379.9	5.010	4.459	5.116	.9679	.3616
335	HEALTH SERVICES	1.172	.4785	.8573	2.684	.4591	.1271
336	EDUCATIONAL SERVICES	1.117	.9005	3.484	1.196	.2774	.1531
400	TRANSPORTATION	.2750	.2077	.1102E-02	.4652E-02	.0000E+00	.1378E-03
410	ON-ROAD TRAVEL	2040.	1787.	8464.	719.8	33.93	740.4
420	RAIL TRANSPORT	1.458	1.095	4.120	27.49	1.931	.3096
430	WATER BORNE	2.981	2.278	5.599	39.34	35.07	1.701
440	AIR TRANSPORTATION	20.49	13.77	85.93	16.96	1.405	1.829
500	DOMESTIC	96.25	100.7	.0000E+00	.0000E+00	.0000E+00	.0000E+00
510	RESIDENTIAL	9.305	6.147	58.46	46.07	1.695	2.238
520	RECREATIONAL	13.32	12.16	58.25	2.849	.2327	.5664E-01
600	MISC. ACTIVITIES	32.12	26.81	188.7	192.2	13.64	3.380
610	CONSTRUCTION	.9565E-01	.9649E-01	.0000E+00	.0000E+00	.0000E+00	.0000E+00
611	BUILDING CONSTRUCTION	9.000	6.115	.0000E+00	.0000E+00	.0000E+00	200.4
612	ROAD CONSTRUCTION	3.133	2.220	.0000E+00	.0000E+00	.0000E+00	34.78
620	NATURAL SOURCES	.0000E+00	.0000E+00	.0000E+00	.0000E+00	.0000E+00	51.64
630	GOVERNMENT	.3616	.3283	4.934	.1796	.2290E-01	15.03
631	NATIONAL SECURITY	1.104	.8006	.1011	.5265	.9086E-01	.5148E-01
801	SEEPS/BIOGENIC	71.79	71.79	.0000E+00	.0000E+00	.0000E+00	.0000E+00
802	CHANNEL SHIPPING	.0000E+00	.0000E+00	.0000E+00	.0000E+00	.0000E+00	.0000E+00
803	OCS AND RELATED SOURCES	.0000E+00	.0000E+00	.0000E+00	.0000E+00	.0000E+00	.0000E+00
804	TIDELAND PLATFORMS	.0000E+00	.0000E+00	.0000E+00	.0000E+00	.0000E+00	.0000E+00
900	UNSPECIFIED ACTIVITIES	180.7	138.4	85.15	33.48	3.390	9.934
	TOTAL	**3694.**	**2528.**	**9099.**	**1244.**	**132.1**	**1133.**

Table 5-4. 1987 Summer emissions (tons/day) for South Coast Air Basin.

	SOURCE CATEGORY	NO	NO2	HONO	ALK1	ALK2	ETHE
100	RESOURCE DEVELOPMENT & AGRICULTURE	.0000E+00	.0000E+00	.0000E+00	.4826E-01	.6322E-01	.1443
110	AGRICULTURAL PRODUCTION	1.828	.1236	.9807E-02	.9301E-01	.1721	.7991E-01
111	AGRICULTURAL CROPS	.0000E+00	.0000E+00	.0000E+00	.5729	.6521	.6910E-02
112	AGRICULTURAL LIVESTOCK	.0000E+00	.0000E+00	.0000E+00	14.03	5.417	.0000E+00
113	AGRICULTURAL SERVICES	.2429	.1642E-01	.1303E-02	.1012	.2076E-01	.7510E-02
120	FORESTRY	.0000E+00	.0000E+00	.0000E+00	.0000E+00	.0000E+00	.0000E+00
130	MINING	.0000E+00	.0000E+00	.0000E+00	.0000E+00	.0000E+00	.0000E+00
131	METAL MINING	.0000E+00	.0000E+00	.0000E+00	.0000E+00	.0000E+00	.0000E+00
132	COAL MINING	.0000E+00	.0000E+00	.0000E+00	.0000E+00	.0000E+00	.0000E+00
133	STONE & CLAY (MINING)	.2287	.1546E-01	.1227E-02	.2493E-01	.7590E-02	.4955E-02
134	CHEMICALS & FERTILIZER MINERAL	.0000E+00	.0000E+00	.0000E+00	.0000E+00	.0000E+00	.0000E+00
140	OIL & GAS EXTRACTION	23.47	1.586	.1259	22.36	5.770	.3441
141	LIQUID GAS PRODUCTION	.0000E+00	.0000E+00	.0000E+00	.7845	.5739	.0000E+00
200	MANUFACTURING & INDUSTRIAL	17.52	1.185	.9401E-01	7.075	14.44	.8233E-01
210	FOOD & KINDRED	.6463	.4369E-01	.3467E-02	8.900	1.787	.6260
211	FRUIT/VEG PRESERVATION	3.918	.2648	.2102E-01	.4542	.5416	.3129
212	GRAIN MILL PRODUCTS	.8643E-01	.5842E-02	.4637E-03	.4279E-01	.5803E-01	.4170E-03
213	BAKERY PRODUCTS	.8117E-01	.5486E-02	.4354E-03	8.905	.7910E-02	.1383E-03
214	VEGETABLE OIL	.6133E-02	.4146E-03	.3290E-04	.1299E-03	.6337E-05	.0000E+00
215	SUGAR MFG/REFINING	.0000E+00	.0000E+00	.0000E+00	.0000E+00	.0000E+00	.0000E+00
216	MALT BEVERAGES	.4624	.3126E-01	.2481E-02	.2940E-01	.1061E-01	.2322E-02
217	WINES & BRANDY	.0000E+00	.0000E+00	.0000E+00	.1523	.0000E+00	.0000E+00
220	LUMBER & WOOD PRODUCTS	.3302E-01	.2232E-02	.1772E-03	1.164	1.539	.7339E-02
230	PAPER & ALLIED	.8731	.5902E-01	.4684E-02	2.489	5.855	.1325E-01
231	PULP & PAPER MILLS	2.299	.1554	.1233E-01	.6479E-01	.2233E-01	.4104E-02
240	CHEMICAL & ALLIED	1.357	.9171E-01	.7279E-02	.4307	.1240	.2523E-01
241	RUBBER & PLASTICS MFG	.2310	.1562E-01	.1240E-02	.3867	.1173	.2281E-01
242	DRUGS	.1519	.1027E-01	.8149E-03	.4317	.1266	.2615E-01
243	CLEANING/TOILET PREP	1.091	.7375E-01	.5853E-02	.3125	.6809E-01	.1925E-01
244	PAINT MFG	.2375E-01	.1605E-02	.1274E-03	.6412	1.642	.4921E-02
245	AGRI CHEMICALS	.9780E-02	.6611E-03	.5247E-04	.1324	.1236	.2034E-02
260	PETROLEUM REFINING/RELATED	.2422	.1637E-01	.1299E-02	.1799	.4747E-01	.5976E-02
261	PETROLEUM REFINING	31.79	2.149	.1705	16.14	2.937	.6193E-01
262	PAVING & ROOFING MATERIALS	.4099	.2771E-01	.2199E-02	.1301	.7507E-01	.2263E-02
263	PET COKE/BRIQUETTE	.0000E+00	.0000E+00	.0000E+00	.0000E+00	.0000E+00	.0000E+00
270	MINERAL PRODUCTS	1.193	.8065E-01	.6401E-02	.3371	.2390	.1222E-01
271	GLASS/GLASS PRODUCTS	3.970	.2684	.2130E-01	.9605E-01	.2334E-01	.4774E-02
280	METALLURGICAL	.6593	.4456E-01	.3537E-02	.6669E-01	.5355E-01	.2066E-02
281	IRON/STEEL PRODUCTION	.2803	.1894E-01	.1504E-02	.2674	.3293	.9863E-02
282	IRON/STEEL FOUNDRY	.1409	.9523E-02	.7558E-03	.3066	.2259	.7627E-02
283	NONFERROUS METALS	1.014	.6854E-01	.5440E-02	.2894	.2285	.1020E-01
290	MISC. MANUFACTURING	.2804E-01	.1895E-02	.1504E-03	.9364	.5027	.2619E-01
291	TEXTILES & APPAREL	.2772	.1874E-01	.1487E-02	.3304	.4208	.1012E-01
292	FURNITURE & FIXTURES	.1776	.1201E-01	.9530E-03	5.979	8.109	.2175E-01
293	FABRICATED METAL	1.818	.1229	.9752E-02	7.715	7.113	.9524E-01
294	MACHINERY	.5328	.3602E-01	.2858E-02	2.645	2.240	.3787E-01
295	TRANSPORTATION EQUIPMENT	1.642	.1110	.8811E-02	4.607	5.667	.1371
296	RUBBER & PLASTICS FAB.	.2367	.1600E-01	.1270E-02	2.032	.9526	.7712E-01
297	TOBACCO MANUFACTURING	.0000E+00	.0000E+00	.0000E+00	.0000E+00	.0000E+00	.0000E+00
298	INSTRUMENTS	.3517E-01	.2378E-02	.1887E-03	.2297	.1781	.3048E-02
300	SERVICES & COMMERCE	30.94	2.091	.1660	3.853	24.04	.7028
310	ELECTRIC UTILITIES	7.252	.4902	.3891E-01	.2050	.4144E-01	.3680E-01
320	PETROLEUM & GAS MARKETING	3.874	.2618	.2078E-01	2.292	.5514	.1747E-01
321	BULK PLANTS	.1387	.9376E-02	.7442E-03	4.799	.5945	.4811E-01
322	SERVICE STATIONS	.0000E+00	.0000E+00	.0000E+00	11.00	.9040	.0000E+00
323	PIPE LINES	.1346	.9098E-02	.7221E-03	4.230	.2804E-01	.2965E-02
330	MISC. SERVICES	1.278	.8636E-01	.6854E-02	7.011	4.108	.4602E-01
331	STEAM SUPPLY	2.535	.1714	.1360E-01	.5914E-01	.3959E-03	.6990E-02
332	PRINTING & PUBLISHING	.1394	.9423E-02	.7479E-03	2.037	1.498	.7855E-02
333	LAUNDRY & DRYCLEANERS	.1564	.1057E-01	.8389E-03	.5848	.5935	.6354E-02
334	SANITARY & WATER	4.768	.3223	.2558E-01	2.945	.5412E-01	.2709
335	HEALTH SERVICES	2.502	.1691	.1342E-01	.2130	.1189	.1145E-01
336	EDUCATIONAL SERVICES	1.115	.7534E-01	.5979E-02	.3754	.2331	.3302E-01
400	TRANSPORTATION	.4335E-02	.2931E-03	.2326E-04	.1476	.5069E-01	.0000E+00
410	ON-ROAD TRAVEL	670.8	45.34	3.599	498.7	366.7	185.2
420	RAIL TRANSPORT	25.62	1.732	.1375	.1607	.4541	.1470
430	WATER BORNE	36.66	2.478	.1967	.5383	.8335	.2683
440	AIR TRANSPORTATION	15.81	1.069	.8481E-01	.3352	3.913	.1291
500	DOMESTIC	.0000E+00	.0000E+00	.0000E+00	86.27	11.98	.0000E+00
510	RESIDENTIAL	42.94	2.902	.2303	1.668	1.172	.6053
520	RECREATIONAL	2.655	.1795	.1425E-01	2.536	2.239	1.637
600	MISC. ACTIVITIES	179.1	12.11	.9608	4.684	7.399	3.744
610	CONSTRUCTION	.0000E+00	.0000E+00	.0000E+00	.4069E-01	.2874E-01	.2624E-04
611	BUILDING CONSTRUCTION	.0000E+00	.0000E+00	.0000E+00	3.321	1.535	.2700E-01
612	ROAD CONSTRUCTION	.0000E+00	.0000E+00	.0000E+00	.0000E+00	1.138	.0000E+00
620	NATURAL SOURCES	.0000E+00	.0000E+00	.0000E+00	.0000E+00	.0000E+00	.0000E+00
630	GOVERNMENT	.1674	.1132E-01	.8980E-03	.8670E-01	.7347E-01	.3173E-01
631	NATIONAL SECURITY	.4907	.3317E-01	.2633E-02	.2229	.3991	.1321E-02
801	SEEPS/BIOGENIC	.0000E+00	.0000E+00	.0000E+00	.0000E+00	.0000E+00	.0000E+00
802	CHANNEL SHIPPING	.0000E+00	.0000E+00	.0000E+00	.0000E+00	.0000E+00	.0000E+00
803	OCS AND RELATED SOURCES	.0000E+00	.0000E+00	.0000E+00	.0000E+00	.0000E+00	.0000E+00
804	TIDELAND PLATFORMS	.0000E+00	.0000E+00	.0000E+00	.0000E+00	.0000E+00	.0000E+00
900	UNSPECIFIED ACTIVITIES	31.21	2.109	.1674	62.70	39.66	3.020
	TOTAL	**1159.**	**78.36**	**6.219**	**812.9**	**538.8**	**198.2**

Table 5-4. 1987 Summer emissions (tons/day) for South Coast Air Basin.

	SOURCE CATEGORY	OLE1	OLE2	OLE3	OLE4	ARO1	ARO2
100	RESOURCE DEVELOPMENT & AGRICULTURE	.3895E-01	.1199E-01	.0000E+00	.0000E+00	.0000E+00	.0000E+00
110	AGRICULTURAL PRODUCTION	.6431E-01	.1241E-01	.0000E+00	.7986E-04	.5419E-01	.2561E-01
111	AGRICULTURAL CROPS	.4590E-02	.5932E-02	.0000E+00	.2303E-03	.2310	.4036
112	AGRICULTURAL LIVESTOCK	.0000E+00	.0000E+00	.0000E+00	.0000E+00	.0000E+00	.0000E+00
113	AGRICULTURAL SERVICES	.4897E-03	.1244E-03	.0000E+00	.0000E+00	.1842E-01	.1972E-03
120	FORESTRY	.0000E+00	.0000E+00	.0000E+00	.0000E+00	.0000E+00	.0000E+00
130	MINING	.0000E+00	.0000E+00	.0000E+00	.0000E+00	.0000E+00	.0000E+00
131	METAL MINING	.0000E+00	.0000E+00	.0000E+00	.0000E+00	.0000E+00	.0000E+00
132	COAL MINING	.0000E+00	.0000E+00	.0000E+00	.0000E+00	.0000E+00	.0000E+00
133	STONE & CLAY (MINING)	.4413E-02	.1109E-02	.0000E+00	.0000E+00	.4514E-02	.3733E-03
134	CHEMICALS & FERTILIZER MINERAL	.0000E+00	.0000E+00	.0000E+00	.0000E+00	.0000E+00	.0000E+00
140	OIL & GAS EXTRACTION	.2754	.1257	.0000E+00	.3223E-04	.4484	.4624E-01
141	LIQUID GAS PRODUCTION	.0000E+00	.0000E+00	.0000E+00	.0000E+00	.1665E-02	.0000E+00
200	MANUFACTURING & INDUSTRIAL	.1033	.5621E-02	.0000E+00	.9732E-04	14.61	3.360
210	FOOD & KINDRED	.1464E-02	.2033E-03	.0000E+00	.1151E-05	1.582	.6769E-03
211	FRUIT/VEG PRESERVATION	.3190	.7407E-01	.0000E+00	.1409E-03	.2961	.1287
212	GRAIN MILL PRODUCTS	.5028E-03	.9335E-04	.0000E+00	.1151E-05	.5590E-01	.1373E-01
213	BAKERY PRODUCTS	.1588E-03	.3991E-04	.0000E+00	.0000E+00	.5545E-03	.8648E-04
214	VEGETABLE OIL	.0000E+00	.0000E+00	.0000E+00	.0000E+00	.1570E-04	.0000E+00
215	SUGAR MFG/REFINING	.0000E+00	.0000E+00	.0000E+00	.0000E+00	.0000E+00	.0000E+00
216	MALT BEVERAGES	.4646E-03	.3932E-04	.0000E+00	.1532E-05	.5200E-02	.5670E-03
217	WINES & BRANDY	.0000E+00	.0000E+00	.0000E+00	.0000E+00	.0000E+00	.0000E+00
220	LUMBER & WOOD PRODUCTS	.4648E-02	.6778E-04	.0000E+00	.0000E+00	1.182	.2409
230	PAPER & ALLIED	.8368E-02	.5491E-03	.0000E+00	.3288E-04	6.866	1.600
231	PULP & PAPER MILLS	.4719E-02	.5541E-03	.0000E+00	.0000E+00	.8681E-02	.4501E-03
240	CHEMICAL & ALLIED	.3598E-02	.2609E-02	.0000E+00	.8757E-06	.6670E-01	.1760E-02
241	RUBBER & PLASTICS MFG	.6095E-03	.1507E-02	.0000E+00	.1534E-05	.8880E-01	.8732E-02
242	DRUGS	.1826E-03	.2144E-04	.0000E+00	.0000E+00	.7505E-01	.6165E-02
243	CLEANING/TOILET PREP	.1727E-02	.2137E-03	.0000E+00	.9414E-06	.4856E-01	.1842E-02
244	PAINT MFG	.2148E-02	.4301E-03	.0000E+00	.3164E-04	1.664	.4118
245	AGRI CHEMICALS	.4947E-03	.9726E-03	.0000E+00	.4181E-04	.4707E-01	.7325E-01
260	PETROLEUM REFINING/RELATED	.8325E-03	.4707E-04	.0000E+00	.3369E-05	.1852E-01	.1547E-02
261	PETROLEUM REFINING	.2897	.2144	.0000E+00	.1847E-04	.3741	.1235
262	PAVING & ROOFING MATERIALS	.1817E-02	.1048E-02	.0000E+00	.1102E-05	.4636E-02	.1155E-01
263	PET COKE/BRIQUETTE	.0000E+00	.0000E+00	.0000E+00	.0000E+00	.0000E+00	.0000E+00
270	MINERAL PRODUCTS	.9044E-02	.2424E-02	.0000E+00	.7716E-07	.1072	.2790E-01
271	GLASS/GLASS PRODUCTS	.5973E-03	.3459E-04	.0000E+00	.0000E+00	.1580E-01	.6805E-03
280	METALLURGICAL	.1360E-03	.3271E-04	.0000E+00	.0000E+00	.6289E-02	.2484E-03
281	IRON/STEEL PRODUCTION	.6919E-02	.1708E-02	.0000E+00	.1929E-06	.2621	.4624E-01
282	IRON/STEEL FOUNDRY	.1732E-03	.3522E-04	.0000E+00	.0000E+00	.4876E-01	.1485E-01
283	NONFERROUS METALS	.4273E-02	.8508E-03	.0000E+00	.0000E+00	.7994E-01	.2403E-01
290	MISC. MANUFACTURING	.3910E-03	.0000E+00	.0000E+00	.0000E+00	.3146	.9335E-01
291	TEXTILES & APPAREL	.4699E-03	.0000E+00	.0000E+00	.0000E+00	.4449	.9900E-01
292	FURNITURE & FIXTURES	.1223E-01	.5080E-03	.0000E+00	.1918E-04	7.261	1.694
293	FABRICATED METAL	.1137E-01	.9188E-03	.0000E+00	.2378E-04	4.391	1.492
294	MACHINERY	.1882E-02	.6193E-03	.0000E+00	.3419E-04	.9880	.2859
295	TRANSPORTATION EQUIPMENT	.2731E-01	.7481E-02	.0000E+00	.7745E-04	4.893	1.117
296	RUBBER & PLASTICS FAB.	.4471E-02	.3007E-01	.0000E+00	.4606E-03	.3591	.1004
297	TOBACCO MANUFACTURING	.0000E+00	.0000E+00	.0000E+00	.0000E+00	.0000E+00	.0000E+00
298	INSTRUMENTS	.6656E-03	.8395E-03	.0000E+00	.4932E-04	.2513E-01	.2006E-01
300	SERVICES & COMMERCE	.8140	.1945	.0000E+00	.1344E-03	13.40	3.266
310	ELECTRIC UTILITIES	.4271E-01	.1086E-01	.0000E+00	.1118E-04	.1867E-01	.1094E-02
320	PETROLEUM & GAS MARKETING	.6809E-01	.1046	.0000E+00	.0000E+00	.5680E-01	.5216E-02
321	BULK PLANTS	.1356	.4880	.0000E+00	.0000E+00	.1399	.2839E-01
322	SERVICE STATIONS	.2429	1.336	.0000E+00	.0000E+00	.1288	.1615E-01
323	PIPE LINES	.8097E-03	.3715E-02	.0000E+00	.5490E-06	.1154E-01	.1088E-03
330	MISC. SERVICES	.1354E-01	.3099E-02	.0000E+00	.2009E-05	1.317	.3762
331	STEAM SUPPLY	.1949E-01	.2550E-02	.0000E+00	.2183E-06	.6237E-03	.2125E-04
332	PRINTING & PUBLISHING	.2098E-01	.3243E-01	.0000E+00	.1967E-02	.1486	.2165
333	LAUNDRY & DRYCLEANERS	.0000E+00	.0000E+00	.0000E+00	.0000E+00	.2155E-01	.1102E-02
334	SANITARY & WATER	.3127	.7720E-01	.0000E+00	.3774	.4309	.4138
335	HEALTH SERVICES	.1342E-01	.2763E-02	.0000E+00	.1863E-05	.4205E-01	.2144E-01
336	EDUCATIONAL SERVICES	.3059E-01	.6405E-02	.0000E+00	.5583E-05	.1131	.3716E-01
400	TRANSPORTATION	.1332E-03	.4909E-03	.0000E+00	.0000E+00	.4601E-02	.4352E-03
410	ON-ROAD TRAVEL	166.3	78.33	1.627	.2448	213.1	204.5
420	RAIL TRANSPORT	.6809E-01	.3789E-02	.0000E+00	.2713E-03	.5022E-01	.2991E-01
430	WATER BORNE	.1298	.1080E-01	.0000E+00	.4458E-03	.1379	.5821E-01
440	AIR TRANSPORTATION	.9126	1.032	.0000E+00	.0000E+00	.7296	5.788
500	DOMESTIC	.2324E-01	.4677E-01	.0000E+00	.5341E-03	.6010	1.119
510	RESIDENTIAL	.7424	.1760	.0000E+00	.2326E-05	.7553	.2924
520	RECREATIONAL	1.937	.4889	.0000E+00	.7014E-04	1.851	.7798
600	MISC. ACTIVITIES	3.332	.7019	.0000E+00	.2910E-02	2.921	1.331
610	CONSTRUCTION	.0000E+00	.0000E+00	.0000E+00	.0000E+00	.7077E-02	.2804E-02
611	BUILDING CONSTRUCTION	1.010	.2129E-01	.0000E+00	.0000E+00	.1996	.0000E+00
612	ROAD CONSTRUCTION	.0000E+00	.6386E-01	.0000E+00	.0000E+00	.0000E+00	.9836
620	NATURAL SOURCES	.0000E+00	.0000E+00	.0000E+00	.0000E+00	.0000E+00	.0000E+00
630	GOVERNMENT	.3811E-01	.9684E-02	.0000E+00	.0000E+00	.4301E-01	.1903E-01
631	NATIONAL SECURITY	.2111E-02	.1574E-02	.0000E+00	.1537E-04	.4259E-01	.3022E-01
801	SEEPS/BIOGENIC	.0000E+00	.0000E+00	20.42	51.37	.0000E+00	.0000E+00
802	CHANNEL SHIPPING	.0000E+00	.0000E+00	.0000E+00	.0000E+00	.0000E+00	.0000E+00
803	OCS AND RELATED SOURCES	.0000E+00	.0000E+00	.0000E+00	.0000E+00	.0000E+00	.0000E+00
804	TIDELAND PLATFORMS	.0000E+00	.0000E+00	.0000E+00	.0000E+00	.0000E+00	.0000E+00
900	UNSPECIFIED ACTIVITIES	.9428	.9079	.0000E+00	.1701E-02	18.56	4.485
	TOTAL	**178.4**	**84.57**	**22.04**	**52.00**	**301.8**	**235.3**

Table 5-4. 1987 Summer emissions (tons/day) for South Coast Air Basin.

	SOURCE CATEGORY	HCHO	CCHO	RCHO	MEK
100	RESOURCE DEVELOPMENT & AGRICULTURE	.0000E+00	.0000E+00	.0000E+00	.0000E+00
110	AGRICULTURAL PRODUCTION	.1507E-01	.2369E-01	.0000E+00	.3518E-03
111	AGRICULTURAL CROPS	.0000E+00	.0000E+00	.0000E+00	.1431E-02
112	AGRICULTURAL LIVESTOCK	.0000E+00	.0000E+00	.0000E+00	1.237
113	AGRICULTURAL SERVICES	.9888E-04	.6580E-04	.0000E+00	.0000E+00
120	FORESTRY	.0000E+00	.0000E+00	.0000E+00	.0000E+00
130	MINING	.0000E+00	.0000E+00	.0000E+00	.0000E+00
131	METAL MINING	.0000E+00	.0000E+00	.0000E+00	.0000E+00
132	COAL MINING	.0000E+00	.0000E+00	.0000E+00	.0000E+00
133	STONE & CLAY (MINING)	.2430E-03	.0000E+00	.0000E+00	.1077E-02
134	CHEMICALS & FERTILIZER MINERAL	.0000E+00	.0000E+00	.0000E+00	.0000E+00
140	OIL & GAS EXTRACTION	.2315	.8480E-02	.0000E+00	.1029E-01
141	LIQUID GAS PRODUCTION	.0000E+00	.0000E+00	.0000E+00	.0000E+00
200	MANUFACTURING & INDUSTRIAL	.3683E-01	.2239E-01	.0000E+00	2.539
210	FOOD & KINDRED	.2121E-02	.1645E-04	.0000E+00	.1497E-02
211	FRUIT/VEG PRESERVATION	.8180E-01	.1038	.0000E+00	.3279E-02
212	GRAIN MILL PRODUCTS	.2892E-03	.1535E-04	.0000E+00	.1058E-01
213	BAKERY PRODUCTS	.6761E-03	.0000E+00	.0000E+00	.2496E-03
214	VEGETABLE OIL	.4233E-04	.0000E+00	.0000E+00	.0000E+00
215	SUGAR MFG/REFINING	.0000E+00	.0000E+00	.0000E+00	.0000E+00
216	MALT BEVERAGES	.9210E-03	.7677E-05	.0000E+00	.1385E-02
217	WINES & BRANDY	.0000E+00	.0000E+00	.0000E+00	.0000E+00
220	LUMBER & WOOD PRODUCTS	.2290E-02	.0000E+00	.0000E+00	.2985
230	PAPER & ALLIED	.7053E-02	.0000E+00	.0000E+00	.8296
231	PULP & PAPER MILLS	.2749E-02	.0000E+00	.0000E+00	.1299E-02
240	CHEMICAL & ALLIED	.6516E-02	.1331E-03	.0000E+00	.2277E-01
241	RUBBER & PLASTICS MFG	.9870E-03	.0000E+00	.0000E+00	.3264E-01
242	DRUGS	.3359E-02	.0000E+00	.0000E+00	.3374E-01
243	CLEANING/TOILET PREP	.2406E-02	.1208E-02	.1787E-02	.4814E-02
244	PAINT MFG	.3399E-02	.0000E+00	.0000E+00	.3576
245	AGRI CHEMICALS	.0000E+00	.0000E+00	.0000E+00	.2597E-03
260	PETROLEUM REFINING/RELATED	.6541E-03	.0000E+00	.0000E+00	.4671E-02
261	PETROLEUM REFINING	.1160	.2590E-02	.0000E+00	.8559E-01
262	PAVING & ROOFING MATERIALS	.2555E-02	.0000E+00	.0000E+00	.5639E-03
263	PET COKE/BRIQUETTE	.0000E+00	.0000E+00	.0000E+00	.0000E+00
270	MINERAL PRODUCTS	.6604E-02	.4443E-03	.0000E+00	.7028E-01
271	GLASS/GLASS PRODUCTS	.4739E-02	.0000E+00	.0000E+00	.3575E-01
280	METALLURGICAL	.1507E-02	.1645E-04	.0000E+00	.5747E-03
281	IRON/STEEL PRODUCTION	.1611E-02	.5846E-03	.0000E+00	.4667E-01
282	IRON/STEEL FOUNDRY	.5861E-04	.0000E+00	.0000E+00	.5461E-01
283	NONFERROUS METALS	.6326E-02	.2620E-03	.0000E+00	.6707E-01
290	MISC. MANUFACTURING	.1125E-01	.0000E+00	.0000E+00	.1730
291	TEXTILES & APPAREL	.9424E-02	.0000E+00	.0000E+00	.4149
292	FURNITURE & FIXTURES	.7096E-02	.5343E-04	.0000E+00	1.433
293	FABRICATED METAL	.6405E-01	.1680E-03	.0000E+00	2.403
294	MACHINERY	.2848E-01	.1597E-04	.0000E+00	.6184
295	TRANSPORTATION EQUIPMENT	.1182E-01	.2229E-02	.1039E-02	1.295
296	RUBBER & PLASTICS FAB.	.5955E-02	.0000E+00	.0000E+00	.3580
297	TOBACCO MANUFACTURING	.0000E+00	.0000E+00	.0000E+00	.0000E+00
298	INSTRUMENTS	.1408E-03	.3040E-04	.0000E+00	.1037
300	SERVICES & COMMERCE	.2367	.1019	.0000E+00	1.352
310	ELECTRIC UTILITIES	.3676E-01	.0000E+00	.0000E+00	.4926E-04
320	PETROLEUM & GAS MARKETING	.2267E-01	.0000E+00	.0000E+00	.1364E-01
321	BULK PLANTS	.1160E-01	.6762E-02	.0000E+00	.5909E-02
322	SERVICE STATIONS	.0000E+00	.0000E+00	.0000E+00	.0000E+00
323	PIPE LINES	.1410E-02	.0000E+00	.0000E+00	.3502E-04
330	MISC. SERVICES	.2077E-01	.9204E-03	.0000E+00	1.023
331	STEAM SUPPLY	.8244E-02	.1017E-03	.0000E+00	.9615E-06
332	PRINTING & PUBLISHING	.3790E-01	.0000E+00	.0000E+00	.6729E-01
333	LAUNDRY & DRYCLEANERS	.4826E-02	.0000E+00	.0000E+00	.3179E-02
334	SANITARY & WATER	.1158	.5223E-03	.0000E+00	.1224E-01
335	HEALTH SERVICES	.2806E-01	.5635E-03	.0000E+00	.2684E-01
336	EDUCATIONAL SERVICES	.1073E-01	.3255E-02	.0000E+00	.5779E-01
400	TRANSPORTATION	.2116E-04	.0000E+00	.0000E+00	.3806E-02
410	ON-ROAD TRAVEL	10.39	6.688	.5808	1.995
420	RAIL TRANSPORT	.4218E-01	.1264	.0000E+00	.1240E-01
430	WATER BORNE	.7138E-01	.2052	.0000E+00	.2381E-01
440	AIR TRANSPORTATION	.3115E-01	.2073E-01	.8697	.1102E-01
500	DOMESTIC	.2820	.0000E+00	.0000E+00	.3399
510	RESIDENTIAL	.4218	.1685	.1189	.2770E-01
520	RECREATIONAL	.3986	.2907	.0000E+00	.3090E-03
600	MISC. ACTIVITIES	.9780	1.706	.0000E+00	.1282E-01
610	CONSTRUCTION	.0000E+00	.0000E+00	.0000E+00	.1716E-01
611	BUILDING CONSTRUCTION	.0000E+00	.0000E+00	.0000E+00	.0000E+00
612	ROAD CONSTRUCTION	.0000E+00	.0000E+00	.0000E+00	.3369E-01
620	NATURAL SOURCES	.0000E+00	.0000E+00	.0000E+00	.0000E+00
630	GOVERNMENT	.7911E-02	.5121E-02	.0000E+00	.1355E-01
631	NATIONAL SECURITY	.1413E-02	.0000E+00	.2125E-03	.9918E-01
801	SEEPS/BIOGENIC	.0000E+00	.0000E+00	.0000E+00	.0000E+00
802	CHANNEL SHIPPING	.0000E+00	.0000E+00	.0000E+00	.0000E+00
803	OCS AND RELATED SOURCES	.0000E+00	.0000E+00	.0000E+00	.0000E+00
804	TIDELAND PLATFORMS	.0000E+00	.0000E+00	.0000E+00	.0000E+00
900	UNSPECIFIED ACTIVITIES	.2085	.1395E-01	.0000E+00	7.879
	TOTAL	**14.05**	**9.504**	**1.572**	**25.58**

THC = Total organic gases, including methane and other less reactive compounds.
ROG = Reactive organic gases.
PART = Total PM (including particles with D_p > 10 μm.

Table 5-5. Estimated emissions of $PM_{2.5}$ sulfate, elemental carbon, organic material, and other (crustal) material on June 24, 1987 in the SoCAB in tons per day.

	SOURCE CATEGORY	$PM_{2.5}$ SO4	$PM_{2.5}$ EC	$PM_{2.5}$ OM	$PM_{2.5}$ OTHER
100	RESOURCE DEVELOPMENT & AGRICULTURE	.6231E-02	.4081E-01	.1901	.1155
110	AGRICULTURAL PRODUCTION	.5323E-02	.1430E-01	.2328E-01	.9985E-02
111	AGRICULTURAL CROPS	.2087E-02	.4015E-02	.5147E-01	.1684
112	AGRICULTURAL LIVESTOCK	.9492E-01	.1356	1.203	1.536
113	AGRICULTURAL SERVICES	.5568E-03	.1407E-02	.1189E-01	.4609E-01
120	FORESTRY	.0000E+00	.0000E+00	.0000E+00	.0000E+00
130	MINING	.0000E+00	.0000E+00	.0000E+00	.0000E+00
131	METAL MINING	.0000E+00	.0000E+00	.0000E+00	.0000E+00
132	COAL MINING	.0000E+00	.0000E+00	.0000E+00	.0000E+00
133	STONE & CLAY (MINING)	.5152E-01	.1867E-01	.2275E-04	.8434E-01
134	CHEMICALS & FERTILIZER MINERAL	.0000E+00	.0000E+00	.0000E+00	.0000E+00
140	OIL & GAS EXTRACTION	.5827E-01	.3866E-01	.2301E-05	.1468
141	LIQUID GAS PRODUCTION	.0000E+00	.0000E+00	.0000E+00	.0000E+00
200	MANUFACTURING & INDUSTRIAL	.1439	.5591E-01	.2408E-03	.2301
210	FOOD & KINDRED	.1635E-01	.2183E-01	.2022	.7739
211	FRUIT/VEG PRESERVATION	.6001E-01	.4286	.8086	.2883
212	GRAIN MILL PRODUCTS	.7746E-03	.2368E-02	.0000E+00	.3793E-02
213	BAKERY PRODUCTS	.6022E-03	.1424E-02	.6565E-03	.3385E-02
214	VEGETABLE OIL	.8205E-04	.2051E-03	.0000E+00	.1231E-03
215	SUGAR MFG/REFINING	.0000E+00	.0000E+00	.0000E+00	.0000E+00
216	MALT BEVERAGES	.5250E-02	.4943E-02	.0000E+00	.6908E-02
217	WINES & BRANDY	.0000E+00	.0000E+00	.0000E+00	.0000E+00
220	LUMBER & WOOD PRODUCTS	.6204E-02	.2026E-01	.1268	.4863
230	PAPER & ALLIED	.5084E-02	.1252E-01	.2215E-03	.8610E-02
231	PULP & PAPER MILLS	.2090E-01	.1204E-01	.6364E-03	.2871E-01
240	CHEMICAL & ALLIED	.5398E-01	.1699E-01	.5615E-05	.1984
241	RUBBER & PLASTICS MFG	.2717E-02	.1293E-01	.0000E+00	.6263E-01
242	DRUGS	.3062E-02	.8146E-02	.3222E-05	.5531E-01
243	CLEANING/TOILET PREP	.9402E-02	.1913E-01	.0000E+00	.1537
244	PAINT MFG	.1798E-02	.5441E-02	.4162E-04	.7214E-01
245	AGRI CHEMICALS	.6541E-04	.1592E-03	.0000E+00	.3339E-02
260	PETROLEUM REFINING/RELATED	.7830E-02	.1830E-02	.2154E-04	.1224E-01
261	PETROLEUM REFINING	1.078	.2919	.3500E-03	1.045
262	PAVING & ROOFING MATERIALS	.4665E-01	.3483E-01	.0000E+00	.1514
263	PET COKE/BRIQUETTE	.1770E-01	.1374E-02	.0000E+00	.1950E-01
270	MINERAL PRODUCTS	.6956E-01	.4875E-01	.2414E-03	.2947
271	GLASS/GLASS PRODUCTS	.9733E-01	.2304E-01	.0000E+00	.5326E-01
280	METALLURGICAL	.1301E-02	.5113E-02	.5394E-02	.2459E-01
281	IRON/STEEL PRODUCTION	.4191E-02	.1934E-02	.2295E-02	.2694E-01
282	IRON/STEEL FOUNDRY	.2143E-03	.4754E-03	.9290E-03	.3845E-02
283	NONFERROUS METALS	.5269E-01	.7300E-01	.3335E-02	.2229
290	MISC. MANUFACTURING	.5458E-03	.4110E-02	.0000E+00	.1649E-01
291	TEXTILES & APPAREL	.3233E-02	.1180E-01	.4884E-03	.2890E-01
292	FURNITURE & FIXTURES	.6300E-02	.1021	.0000E+00	.7915E-01
293	FABRICATED METAL	.2603E-01	.1334	.9587E-03	.2444
294	MACHINERY	.4227E-02	.2289E-01	.6701E-03	.2159E-01
295	TRANSPORTATION EQUIPMENT	.3024E-01	.9184E-01	.4017E-03	.1552
296	RUBBER & PLASTICS FAB.	.4835E-02	.3203E-01	.3544E-03	.1080
297	TOBACCO MANUFACTURING	.0000E+00	.0000E+00	.0000E+00	.0000E+00
298	INSTRUMENTS	.3986E-03	.4998E-03	.0000E+00	.2999E-03
300	SERVICES & COMMERCE	.3857	.2656	.0000E+00	.4599
310	ELECTRIC UTILITIES	.7531E-01	.5823E-01	.0000E+00	.8720E-01
320	PETROLEUM & GAS MARKETING	.6350E-02	.6206E-02	.0000E+00	.1210E-01
321	BULK PLANTS	.1787E-02	.3072E-02	.4530E-03	.4556E-02
322	SERVICE STATIONS	.0000E+00	.0000E+00	.0000E+00	.0000E+00
323	PIPE LINES	.3713E-02	.5976E-02	.0000E+00	.7081E-02
330	MISC. SERVICES	.2093E-01	.9897E-01	.9971E-03	.2240
331	STEAM SUPPLY	.2545E-02	.2308E-02	.0000E+00	.3731E-02
332	PRINTING & PUBLISHING	.5581E-02	.5260E-02	.3640E-03	.1038E-01
333	LAUNDRY & DRYCLEANERS	.3436E-02	.6345E-02	.0000E+00	.4219E-02
334	SANITARY & WATER	.7630E-01	.1124	.1030E-02	.1060
335	HEALTH SERVICES	.2930E-01	.5222E-01	.2301E-05	.3927E-01
336	EDUCATIONAL SERVICES	.1975E-01	.5346E-01	.7087E-04	.5183E-01
400	TRANSPORTATION	.2735E-04	.6836E-04	.0000E+00	.4102E-04
410	ON-ROAD TRAVEL	2.182	7.640	33.43	64.88
420	RAIL TRANSPORT	.3435E-01	.9585E-01	.1636	.2483E-01
430	WATER BORNE	.5756	.4270	.6994	.3911
440	AIR TRANSPORTATION	.4634	.2665	.3222E-05	1.063
500	DOMESTIC	.0000E+00	.0000E+00	.0000E+00	.0000E+00
510	RESIDENTIAL	.3094	.8253	.4898	.5141
520	RECREATIONAL	.4681E-02	.1253E-01	.2673E-01	.1404E-01
600	MISC. ACTIVITIES	.2717	.9691	1.736	.4179
610	CONSTRUCTION	.0000E+00	.0000E+00	.0000E+00	.0000E+00
611	BUILDING CONSTRUCTION	.1406	.1901	3.346	12.53
612	ROAD CONSTRUCTION	.2435E-01	.3131E-01	.5809	2.174
620	NATURAL SOURCES	.4594E-01	.3180E-01	.3095	4.764
630	GOVERNMENT	.1268E-01	.1530E-01	.2509	.9410
631	NATIONAL SECURITY	.5299E-02	.7746E-02	.5451E-04	.3051E-01
801	SEEPS/BIOGENIC	.0000E+00	.0000E+00	.0000E+00	.0000E+00
802	CHANNEL SHIPPING	.0000E+00	.0000E+00	.0000E+00	.0000E+00
803	OCS AND RELATED SOURCES	.0000E+00	.0000E+00	.0000E+00	.0000E+00
804	TIDELAND PLATFORMS	.0000E+00	.0000E+00	.0000E+00	.0000E+00
900	UNSPECIFIED ACTIVITIES	.4355	.8395	1.995	2.739
	TOTAL	7.136	13.78	45.66	98.48

Table 5-6. Estimated emissions of $PM_{2.5-10}$ (coarse) sulfate, elemental carbon, organic material, and other (crustal) material on June 24, 1987 in the SoCAB in tons per day.

	SOURCE CATEGORY	SO4	EC	OM	OTHER
100	RESOURCE DEVELOPMENT & AGRICULTURE	.2063E-03	.9078E-03	.5570E-02	.2682E-02
110	AGRICULTURAL PRODUCTION	.7244E-04	.2506E-03	.4221E-03	.1086E-03
111	AGRICULTURAL CROPS	.8916E-02	.1052E-01	.2902	.7141
112	AGRICULTURAL LIVESTOCK	.3051E-01	.8814E-01	3.644	8.682
113	AGRICULTURAL SERVICES	.2508E-02	.7887E-02	.5162E-01	.2058
120	FORESTRY	.0000E+00	.0000E+00	.0000E+00	.0000E+00
130	MINING	.0000E+00	.0000E+00	.0000E+00	.0000E+00
131	METAL MINING	.0000E+00	.0000E+00	.0000E+00	.0000E+00
132	COAL MINING	.0000E+00	.0000E+00	.0000E+00	.0000E+00
133	STONE & CLAY (MINING)	.1756E-02	.1156E-01	.9878E-04	.5532E-01
134	CHEMICALS & FERTILIZER MINERAL	.0000E+00	.0000E+00	.0000E+00	.0000E+00
140	OIL & GAS EXTRACTION	.1670E-02	.6400E-03	.9990E-05	.5205E-02
141	LIQUID GAS PRODUCTION	.0000E+00	.0000E+00	.0000E+00	.0000E+00
200	MANUFACTURING & INDUSTRIAL	.1289E-02	.5036E-03	.1045E-02	.6517E-02
210	FOOD & KINDRED	.4131E-01	.5314E-01	.8777	3.312
211	FRUIT/VEG PRESERVATION	.9348E-03	.1073E-01	.1328E-01	.1095E-01
212	GRAIN MILL PRODUCTS	.2895E-03	.7950E-02	.0000E+00	.1838E-01
213	BAKERY PRODUCTS	.1458E-03	.6057E-03	.2850E-02	.1173E-01
214	VEGETABLE OIL	.6614E-06	.1571E-05	.0000E+00	.9507E-06
215	SUGAR MFG/REFINING	.0000E+00	.0000E+00	.0000E+00	.0000E+00
216	MALT BEVERAGES	.3828E-04	.3867E-04	.0000E+00	.5080E-04
217	WINES & BRANDY	.0000E+00	.0000E+00	.0000E+00	.0000E+00
220	LUMBER & WOOD PRODUCTS	.2583E-01	.3078E-01	.5504	2.069
230	PAPER & ALLIED	.8693E-04	.1787E-03	.9616E-03	.3698E-02
231	PULP & PAPER MILLS	.2856E-03	.2550E-03	.2763E-02	.1058E-01
240	CHEMICAL & ALLIED	.7163E-03	.8013E-03	.2437E-04	.4336E-02
241	RUBBER & PLASTICS MFG	.3020E-04	.3577E-03	.0000E+00	.5858E-03
242	DRUGS	.2859E-04	.2871E-03	.1399E-04	.8152E-03
243	CLEANING/TOILET PREP	.9735E-04	.8892E-03	.0000E+00	.2798E-02
244	PAINT MFG	.2395E-04	.1705E-03	.1807E-03	.1202E-02
245	AGRI CHEMICALS	.3794E-04	.5019E-03	.0000E+00	.6395E-02
260	PETROLEUM REFINING/RELATED	.1062E-03	.3290E-04	.9350E-04	.7027E-03
261	PETROLEUM REFINING	.1845E-01	.2665E-02	.1520E-02	.7678E-01
262	PAVING & ROOFING MATERIALS	.1032E-02	.3186E-02	.0000E+00	.4560E-01
263	PET COKE/BRIQUETTE	.1572E-03	.6835E-05	.0000E+00	.2413E-02
270	MINERAL PRODUCTS	.8552E-02	.1419E-01	.1048E-02	.3451
271	GLASS/GLASS PRODUCTS	.1602E-02	.1855E-03	.0000E+00	.1066E-01
280	METALLURGICAL	.1110E-02	.1392E-02	.2342E-01	.8816E-01
281	IRON/STEEL PRODUCTION	.5133E-03	.5674E-03	.9965E-02	.3847E-01
282	IRON/STEEL FOUNDRY	.1906E-03	.2281E-03	.4033E-02	.1516E-01
283	NONFERROUS METALS	.5627E-02	.2961E-02	.1448E-01	.6315E-01
290	MISC. MANUFACTURING	.8557E-05	.1185E-03	.0000E+00	.1068E-02
291	TEXTILES & APPAREL	.1574E-03	.1585E-02	.2120E-02	.1108E-01
292	FURNITURE & FIXTURES	.1352E-03	.3040E-02	.0000E+00	.2396E-02
293	FABRICATED METAL	.4836E-03	.3371E-02	.4162E-02	.2835E-01
294	MACHINERY	.2354E-03	.6871E-03	.2909E-02	.1340E-01
295	TRANSPORTATION EQUIPMENT	.8122E-03	.2519E-02	.1744E-02	.1313E-01
296	RUBBER & PLASTICS FAB.	.1344E-03	.9835E-03	.1539E-02	.7106E-02
297	TOBACCO MANUFACTURING	.0000E+00	.0000E+00	.0000E+00	.0000E+00
298	INSTRUMENTS	.3122E-05	.3829E-05	.0000E+00	.2317E-05
300	SERVICES & COMMERCE	.4936E-02	.5972E-02	.0000E+00	.5501E-02
310	ELECTRIC UTILITIES	.6552E-03	.5363E-03	.0000E+00	.7655E-03
320	PETROLEUM & GAS MARKETING	.4959E-04	.8650E-04	.0000E+00	.4135E-03
321	BULK PLANTS	.1167E-03	.1570E-03	.1967E-02	.7440E-02
322	SERVICE STATIONS	.0000E+00	.0000E+00	.0000E+00	.0000E+00
323	PIPE LINES	.6377E-04	.1799E-03	.0000E+00	.1768E-03
330	MISC. SERVICES	.7119E-03	.2826E-02	.4329E-02	.2933E-01
331	STEAM SUPPLY	.1999E-04	.1756E-04	.0000E+00	.3232E-04
332	PRINTING & PUBLISHING	.1479E-03	.1921E-03	.1580E-02	.6210E-02
333	LAUNDRY & DRYCLEANERS	.2965E-04	.8976E-04	.0000E+00	.6534E-04
334	SANITARY & WATER	.2682E-02	.1141E-02	.4471E-02	.2277E-01
335	HEALTH SERVICES	.2610E-03	.4104E-03	.9990E-05	.1376E-02
336	EDUCATIONAL SERVICES	.2059E-03	.8843E-03	.3077E-03	.4426E-02
400	TRANSPORTATION	.2205E-06	.5236E-06	.0000E+00	.3169E-06
410	ON-ROAD TRAVEL	2.347	2.803	50.[illegible]	187.5
420	RAIL TRANSPORT	.6423E-03	.1827E-02	.3227E-02	.4644E-03
430	WATER BORNE	.1093E-01	.8166E-02	.1337E-01	.8050E-02
440	AIR TRANSPORTATION	.3252E-02	.1844E-02	.1399E-04	.7377E-02
500	DOMESTIC	.0000E+00	.0000E+00	.0000E+00	.0000E+00
510	RESIDENTIAL	.3231E-02	.1457E-01	.1489E-01	.1255E-01
520	RECREATIONAL	.5250E-04	.1952E-03	.3763E-03	.1332E-03
600	MISC. ACTIVITIES	.4455E-02	.1779E-01	.3111E-01	.5816E-02
610	CONSTRUCTION	.0000E+00	.0000E+00	.0000E+00	.0000E+00
611	BUILDING CONSTRUCTION	.6813	.8018	14.53	54.60
612	ROAD CONSTRUCTION	.1183	.1391	2.522	9.479
620	NATURAL SOURCES	.1707	.8424E-01	.9744	17.99
630	GOVERNMENT	.5109E-01	.6011E-01	1.089	4.094
631	NATIONAL SECURITY	.5230E-04	.7504E-04	.2366E-03	.2641E-02
801	SEEPS/BIOGENIC	.0000E+00	.0000E+00	.0000E+00	.0000E+00
802	CHANNEL SHIPPING	.0000E+00	.0000E+00	.0000E+00	.0000E+00
803	OCS AND RELATED SOURCES	.0000E+00	.0000E+00	.0000E+00	.0000E+00
804	TIDELAND PLATFORMS	.0000E+00	.0000E+00	.0000E+00	.0000E+00
900	UNSPECIFIED ACTIVITIES	.2708E-01	.5503E-01	.1354	1.194
	TOTAL	3.584	4.265	74.76	290.9

Table 5-7. UAM-AERO model performance on mean 24-hr average concentrations ($\mu g/m^3$) on June 24-25, 1987.

Species	Day	Mean Observed	Mean Predicted	Mean Normalized Bias (%)	Mean Bias	Mean Normalized Error (%)	Mean Error
$PM_{2.5}$ NO_3	175	14.5	16.7	14	2.2	37	4.9
$PM_{2.5}$ NO_3	176	15.8	16.8	11	1	18	2.3
PM_{10} NO_3	175	22.4	20.4	-9	-2	19	4.4
PM_{10} NO_3	176	21.7	21.2	6	-0.5	15	2.6
$PM_{2.5}$ NH_4	175	6.5	7.8	28	1.3	41	2.2
$PM_{2.5}$ NH_4	176	5.9	7.7	56	1.8	57	1.9
PM_{10} NH_4	175	9.3	9	2	-0.3	28	2.4
PM_{10} NH_4	176	8.9	9.1	12	0.2	23	1.3
$PM_{2.5}$ SO_4	175	13.1	8	-30	-5.1	50	6.9
$PM_{2.5}$ SO_4	176	10.6	8.2	-10	-2.5	48	5.3
PM_{10} SO_4	175	15.4	10.7	-20	-4.7	41	6.9
PM_{10} SO_4	176	12.3	11	2	-1.3	40	4.9
$PM_{2.5}$ EC	175	1.4	1.5	9	0.1	31	0.4
$PM_{2.5}$ EC	176	1.5	1.3	-10	-0.1	15	0.2
PM_{10} EC	175	2.1	2	10	-0.1	40	0.8
PM_{10} EC	176	2.7	2.1	-15	-0.6	34	0.9
$PM_{2.5}$ OM	175	10.7	6.5	-39	-4.1	39	4.1
$PM_{2.5}$ OM	176	10.8	6.4	-38	-4.4	38	4.4
PM_{10} OM	175	16.3	12.9	-15	-3.4	24	3.9
PM_{10} OM	176	17.6	12.9	-16	-4.7	32	5.8
PM_{10} Na	175	2.1	1.7	-21	-0.4	32	0.6
PM_{10} Na	176	1.5	2	38	0.6	47	0.7
PM_{10} Cl	175	1.3	0.9	-34	-0.4	34	0.4
PM_{10} Cl	176	1	1.3	24	0.2	24	0.2
$PM_{2.5}$ Mass	175	54.8	54.5	2	-0.3	21	11.2
$PM_{2.5}$ Mass	176	46.5	51.6	24	5.1	32	8.7
PM_{10} Mass	175	62.6	89.4	47	26.8	52	29.5
PM_{10} Mass	176	57	90.3	72	33.2	72	33.2
HNO_3 (ppb)	175	6.3	4.2	-32	-2.1	47	3.2
HNO_3 (ppb)	176	5.5	3.3	-37	-2.3	40	2.4
NH_3 (ppb)	175	28.9	17	17	-11.9	63	13.6
NH_3 (ppb)	176	28.9	19	15	-10	55	12.3
Coarse NO_3	175	7.9	3.7	-51	-4.2	51	4.2
Coarse NO_3	176	5.9	4.4	-12	-1.5	41	2.3
Coarse NH_4	175	2.8	1.2	-55	-1.6	55	1.6
Coarse NH_4	176	3	1.4	-50	-1.5	50	1.5
Coarse SO_4	175	2.3	2.7	37	0.4	63	1.2
Coarse SO_4	176	1.9	2.9	65	0.9	72	1.2
Coarse EC	175	1.4	0.6	-58	-0.8	58	0.8
Coarse EC	176	2	0.6	-68	-1.4	68	1.4
Coarse OM	175	5.7	6.4	33	0.6	41	1.8
Coarse OM	176	6.8	6.6	28	-0.3	50	2.6
Coarse Mass	175	9.2	37.3	430	28.1	430	28.1
Coarse Mass	176	7.3	36.4	518	29.1	518	29.1

Table 5-8. UAM-AERO model performance for maximum concentrations ($\mu g/m^3$) on June 24-25, 1987.

Species	Day	Location	Maximum Observed	Maximum Predicted	Accuracy (%)	Maximum In Domain
$PM_{2.5}$ NO_3	175	Riverside	34.6	27.4	-21	51.3
$PM_{2.5}$ NO_3	176	Riverside	30.3	26.3	-10	44.9
$PM_{2.5}$ NO_3	175	Riverside	47.6	32.5	-32	60.8
$PM_{2.5}$ NO_3	176	Riverside	40.3	32.5	-19	57.3
$PM_{2.5}$ NH_4	175	Riverside	11.6	10.1	-12	17
$PM_{2.5}$ NH_4	176	Riverside	9.5	9.9	6	14.8
$PM_{2.5}$ NH_4	175	Riverside	15.1	12	-21	20.3
$PM_{2.5}$ NH_4	176	Riverside	12.1	12	-1	19.1
$PM_{2.5}$ SO_4	175	Los Angeles	18.5	7.9	-57	33
$PM_{2.5}$ SO_4	176	Hawthorne	15	6.9	-54	32.4
$PM_{2.5}$ SO_4	175	Hawthorne	21.7	7.7	-64	40.6
$PM_{2.5}$ SO_4	176	Los Angeles	17.3	9.6	-42	38.1
$PM_{2.5}$ EC	175	Riverside	1.6	0.8	-53	3.2
$PM_{2.5}$ EC	176	Azusa	1.8	1.8	1	2.5
PM_{10} EC	175	Riverside	3	1.4	-55	4.2
PM_{10} EC	176	Claremont	3.5	1.9	-45	3.6
$PM_{2.5}$ OM	175	Los Angeles	15.2	8.4	-45	21
$PM_{2.5}$ OM	176	Azusa	17	9	-43	17.2
PM_{10} OM	175	Riverside	27.5	17.4	-37	32.2
PM_{10} OM	176	Riverside	26.9	16.7	-35	23.3
PM_{10} Na	175	Hawthorne	2.7	3.3	22	5
PM_{10} Na	176	Long Beach	1.6	2.7	69	5.5
PM_{10} Cl	175	Riverside	1.4	1	-25	3.5
PM_{10} Cl	176	Riverside	1	1.3	24	3.6
$PM_{2.5}$ Mass	175	Riverside	82.3	68.8	-16	109.7
$PM_{2.5}$ Mass	176	Azusa	65.7	67.1	11	91.9
PM_{10} Mass	175	Riverside	105.6	121.6	15	175.9
PM_{10} Mass	176	Riverside	94.3	119.7	29	143.6
HNO_3 (ppb)	175	Burbank	9.7	4.6	-53	42.7
HNO_3 (ppb)	176	Los Angeles	7.7	1.9	-76	25.9
NH_3 (ppb)	175	Riverside	55.8	30.3	-46	59.8
NH_3 (ppb)	176	Riverside	54.5	32.3	-41	76.6
Coarse NO_3	175	Riverside	13	5.2	-60	12.9
Coarse NO_3	176	Riverside	10.1	6.2	-39	14.9
Coarse NH_4	175	Burbank	4.1	1.1	-74	4.5
Coarse NH_4	176	Claremont	4.5	2	-56	5
Coarse SO_4	175	Hawthorne	3.9	2.1	-45	9.1
Coarse SO_4	176	Burbank	3.3	2.5	-27	5.8
Coarse EC	175	Riverside	1.4	0.6	-58	1.6
Coarse EC	176	Riverside	2.2	0.6	-72	1.9
Coarse OM	175	Riverside	13.7	9.3	-33	12.2
Coarse OM	176	Riverside	14.5	9.4	-35	10.9
Coarse Mass	175	Riverside	23.4	52.8	126	66.2
Coarse Mass	176	Claremont	11.5	37.5	226	56.9

Table 5-9. UAM-AERO model performance for mean short-term (1 to 6-hr) average concentrations ($\mu g/m^3$) on June 24-25, 1987.

Species	Day	Mean Observed	Mean Predicted	Mean Normalized Bias (%)	Mean Bias	Mean Normalized Error (%)	Mean Error
$PM_{2.5}$ NO_3	175	14.5	16.7	22	2.2	52	6.8
$PM_{2.5}$ NO_3	176	14.8	16.2	34	1.4	68	7.1
PM_{10} NO_3	175	22.4	20.4	-2	-2	30	6.9
PM_{10} NO_3	176	20.8	20.5	15	-0.3	41	7.2
$PM_{2.5}$ NH_4	175	6.5	7.8	37	1.3	56	3.1
$PM_{2.5}$ NH_4	176	6	7.7	60	1.7	80	3.1
PM_{10} NH_4	175	9.3	9	7	-0.3	34	2.9
PM_{10} NH_4	176	8.6	9	19	0.4	45	2.7
$PM_{2.5}$ SO_4	175	13.1	8	-26	-5.1	54	7.4
$PM_{2.5}$ SO_4	176	10.8	8.2	-14	-2.7	52	5.6
PM_{10} SO_4	175	15.4	10.7	-16	-4.7	52	8.1
PM_{10} SO_4	176	12.6	11	-1	-1.5	48	5.7
$PM_{2.5}$ EC	175	1.9	1.6	-11	-0.3	33	0.7
$PM_{2.5}$ EC	176	1.9	1.7	0	-0.2	47	0.9
PM_{10} EC	175	2.4	2	-3	-0.4	38	0.9
PM_{10} EC	176	2.9	2.1	-8	-0.8	37	1.3
$PM_{2.5}$ OM	175	11.2	6.8	-28	-4.3	48	4.9
$PM_{2.5}$ OM	176	11	6.4	-38	-4.6	46	4.9
PM_{10} OM	175	17	13.2	-13	-3.8	28	5.1
PM_{10} OM	176	18	12.9	-16	-5.2	31	6.3
PM_{10} Na	175	2.1	1.7	-15	-0.4	47	0.9
PM_{10} Na	176	1.6	1.9	24	0.3	42	0.6
PM_{10} Cl	175	1.6	1	-38	-0.6	47	0.7
PM_{10} Cl	176	1.3	1.1	-12	-0.2	57	0.7
$PM_{2.5}$ Mass	175	54.8	54.5	7	-0.3	35	18
$PM_{2.5}$ Mass	176	49.9	53	19	3.1	41	15.8
PM_{10} Mass	175	62.6	89.4	51	26.8	57	31.8
PM_{10} Mass	176	58.2	89.9	67	31.7	69	33.8
HNO3 (ppb)	175	8	4.1	-55	-3.9	58	4.1
HNO3 (ppb)	176	6.8	4.4	-34	-2.3	52	3.2
NH3 (ppb)	175	27.8	15.2	-39	-12.6	42	12.7
NH3 (ppb)	176	15.8	11	10	-4.9	67	7.1
Ozone (ppb)	175	108.5	90.6	-11	-17.9	32	34.3
Ozone (ppb)	176	105.3	85.5	-15	-19.9	34	36.5
NO2 (ppb)	175	45.4	35.1	-20	-10.3	43	18.5
NO2 (ppb)	176	50.4	42.9	-6	-7.5	45	20.2
NO (ppb)	175	32.4	15.2	-39	-17.2	85	27.7
NO (ppb)	176	29.9	19.6	-23	-10.3	73	21.9

Table 5-10. UAM-AERO model performance for maximum short-term (1 to 6-hr) average concentrations (mg/m^3) on June 24-25, 1987.

Species	Day	Station with the Highest Short-Term Observed Concentration				Maximum On Grid
		Location	Maximum Observed	Maximum Predicted	Accuracy (%)	
$PM_{2.5}$ NO3	175	Riverside	62.7	61.2	-2	76.9
$PM_{2.5}$ NO3	176	Riverside	61.9	63.9	3	70.3
PM_{10} NO3	175	Riverside	81	64.8	-20	95.3
PM_{10} NO3	176	Riverside	77	69.3	-10	87.7
$PM_{2.5}$ NH4	175	Riverside	20.6	19.7	-4	24.5
$PM_{2.5}$ NH4	176	Riverside	16.8	20.2	20	21.9
PM_{10} NH4	175	Riverside	25.9	21	-19	30.4
PM_{10} NH4	176	Riverside	23.7	22.2	-6	27.7
$PM_{2.5}$ SO4	175	Los Angeles	27.7	14.1	-49	54.6
$PM_{2.5}$ SO4	176	Hawthorne	21.1	16.3	-23	67.4
PM_{10} SO4	175	Hawthorne	32.8	11.9	-64	70.1
PM_{10} SO4	176	Hawthorne	24.7	20.8	-16	70.4
$PM_{2.5}$ EC	175	Burbank	3.3	2.7	-20	5.2
$PM_{2.5}$ EC	176	Claremont	3.4	1.6	-52	4.7
PM_{10} EC	175	Burbank	4.8	3.4	-29	7.6
PM_{10} EC	176	Claremont	11.6	2.4	-79	9
$PM_{2.5}$ OM	175	Azusa	29.6	15.6	-47	40.2
$PM_{2.5}$ OM	176	Azusa	27.3	13	-43	20.6
PM_{10} OM	175	Azusa	41.5	22.6	-46	50.6
PM_{10} OM	176	Claremont	71.2	16.1	-75	34.8
PM_{10} Na	175	Hawthorne	4.2	4.2	-1	5.9
PM_{10} Na	176	Long Beach	3.1	3.8	23	8.2
PM_{10} Cl	175	Riverside	2.2	2.1	29	5.1
PM_{10} Cl	176	Long Beach	1.8	1.3	31	6.5
$PM_{2.5}$ Mass	175	Riverside	136.3	129.5	-5	189.1
$PM_{2.5}$ Mass	176	Riverside	127.9	128.4	1	135.4
PM_{10} Mass	175	Riverside	165.5	187	13	265.1
PM_{10} Mass	176	Riverside	146.3	190.6	30	230.2
HNO3 (ppb)	175	Claremont	20.4	14.9	-23	76.9
HNO3(ppb)	176	Burbank	19.5	9.4	-37	44.7
NH3(ppb)	175	Riverside	105.9	45.8	-57	78
NH3 (ppb)	176	Riverside	98.5	46.8	-53	113.9
Ozone (ppb)[a]	175	Claremont	250	152.2	-34	404.8
Ozone (ppb)[a]	176	San Bernardino	240	199.1	-7	353.5
NO2 (ppb)[a]	175	Pasadena	90	92.5	3	230.3
NO2 (ppb)[a]	176	Burbank	110	99.4	-10	279.9
NO (ppb)[a]	175	Upland	90	16.5	-81	633.9
NO (ppb)[a]	176	Pomona	100	19.3	-81	867.9

[a] Ozone, NO_2, and NO concentrations are 1-hr maxima. All other species concentrations are 4 to 6-hr averages.

Table 5-11. Predicted domain-wide pollutant deposition for June 24-25, 1987.

Species	Deposition Moles/hectare-day	Species	Deposition Grams/hectare-day
O3	2.86	HNO3	38.5
NO2	.226	NH3	2.48
HNO3	.611	NO3 $PM_{2.5}$	.857
NH3	.146	NO3 PM_{10}	6.07
H2O2	.250	NH4 $PM_{2.5}$	.345
HCHO	.197	NH4 PM_{10}	1.82
CCHO	.513E-01	SO4 $PM_{2.5}$	.311
RCHO	.169E-01	SO4 PM_{10}	3.66
PAN	.483E-01	EC $PM_{2.5}$	.408E-01
PPN	.180E-01	EC PM_{10}	.552
SO2	.591E-01	OM $PM_{2.5}$	.427
FACD	.322E-01	OM PM_{10}	7.36
AACD	.215E-01	OTR $PM_{2.5}$	.569
HCL	.803E-01	OTR PM_{10}	19.1
NO	.110E-03	NA $PM_{2.5}$	.330E-01
HONO	.191E-02	NA PM_{10}	1.83
HNO4	.277E-03	CL $PM_{2.5}$	.195E-01
XOOH	.464E-01	CL PM_{10}	.236
RNO3	.257E-01	H2O $PM_{2.5}$	1.93
MGLY	.268E-02	H2O PM_{10}	27.4
CRES	.114E-02		

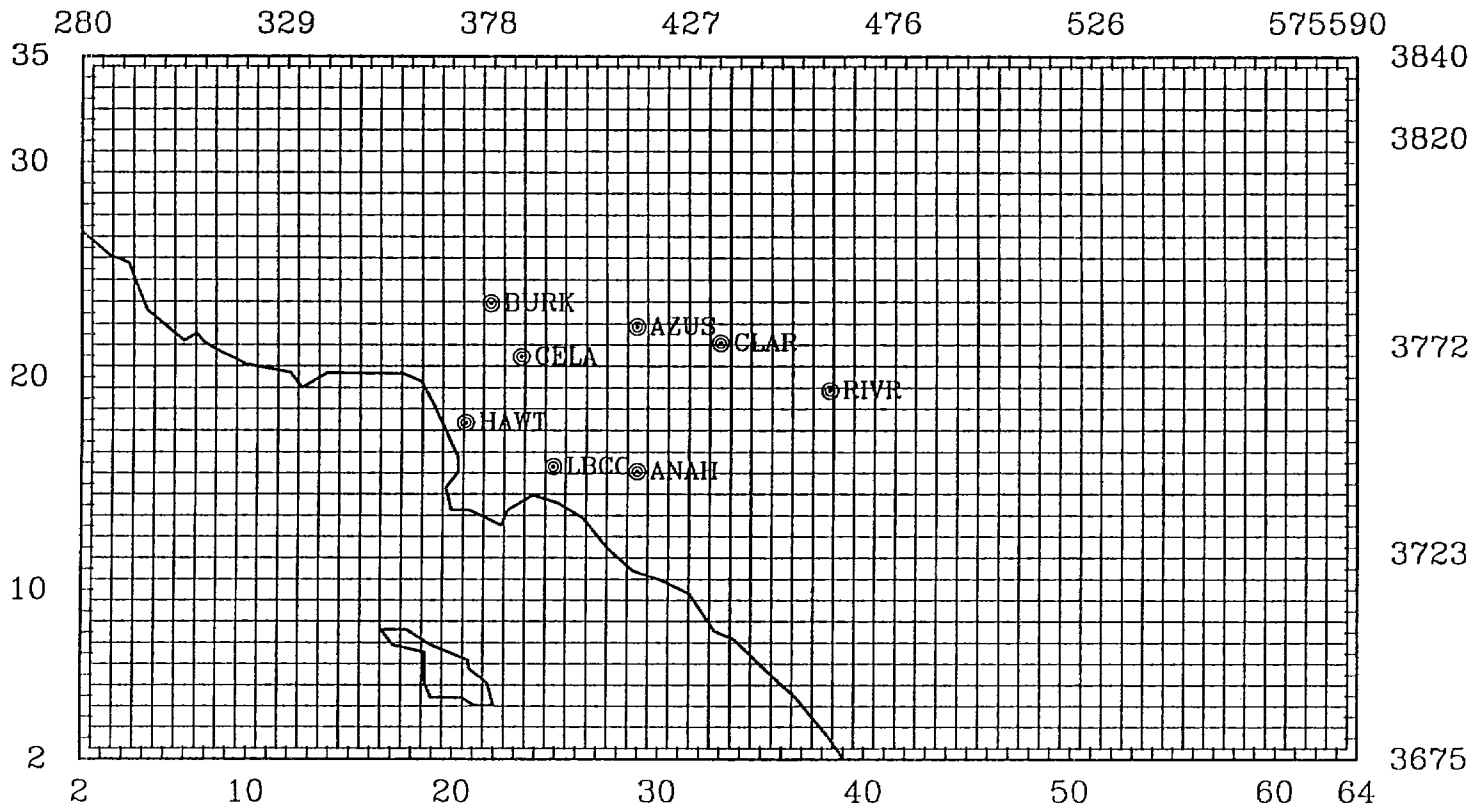

Figure 5-1. The SoCAB Modeling domain and location of SCAQS monitoring stations.

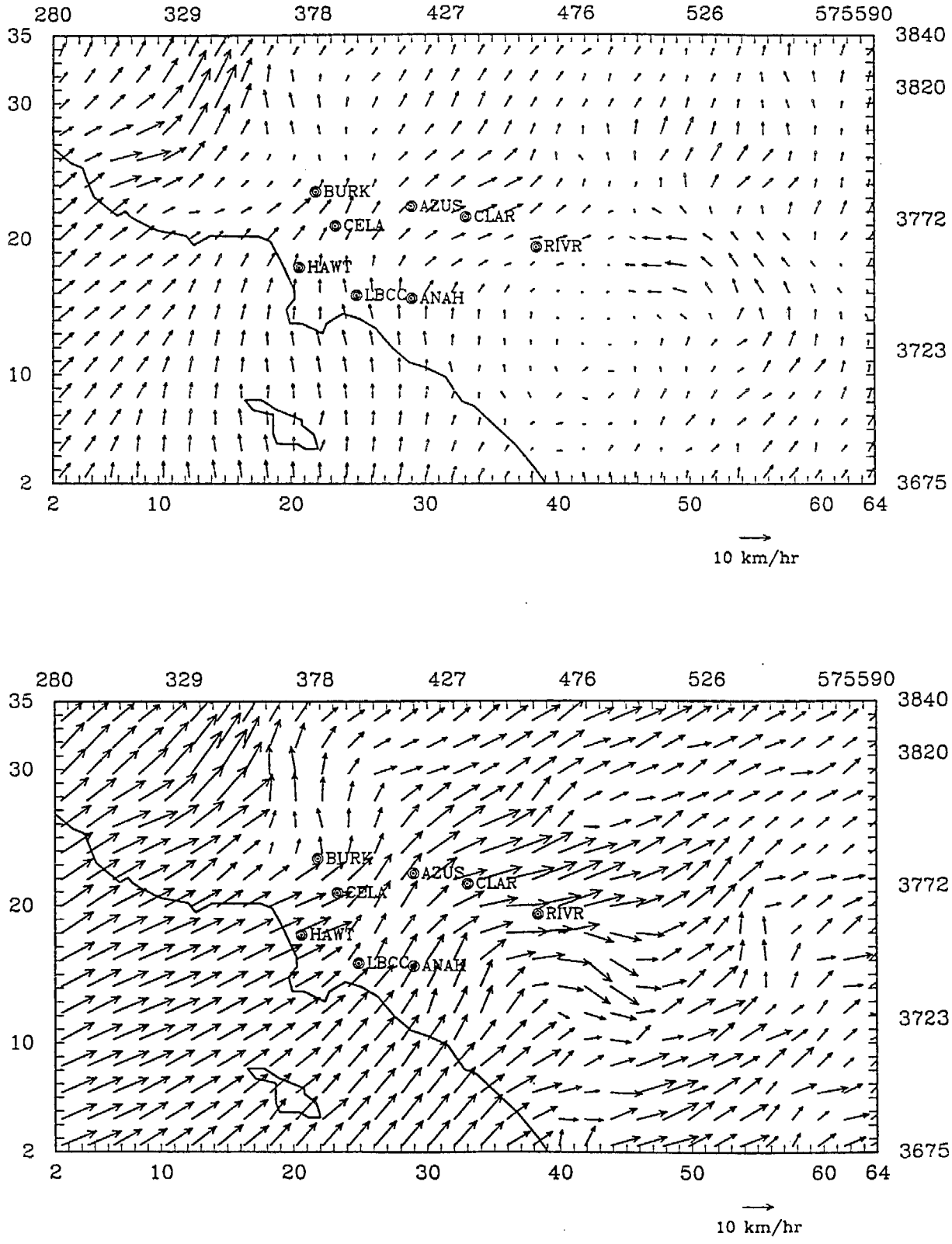

Figure 5-2. Surface layer windfield for hours 09 (top) and 15 (bottom) on June 23, 1987.

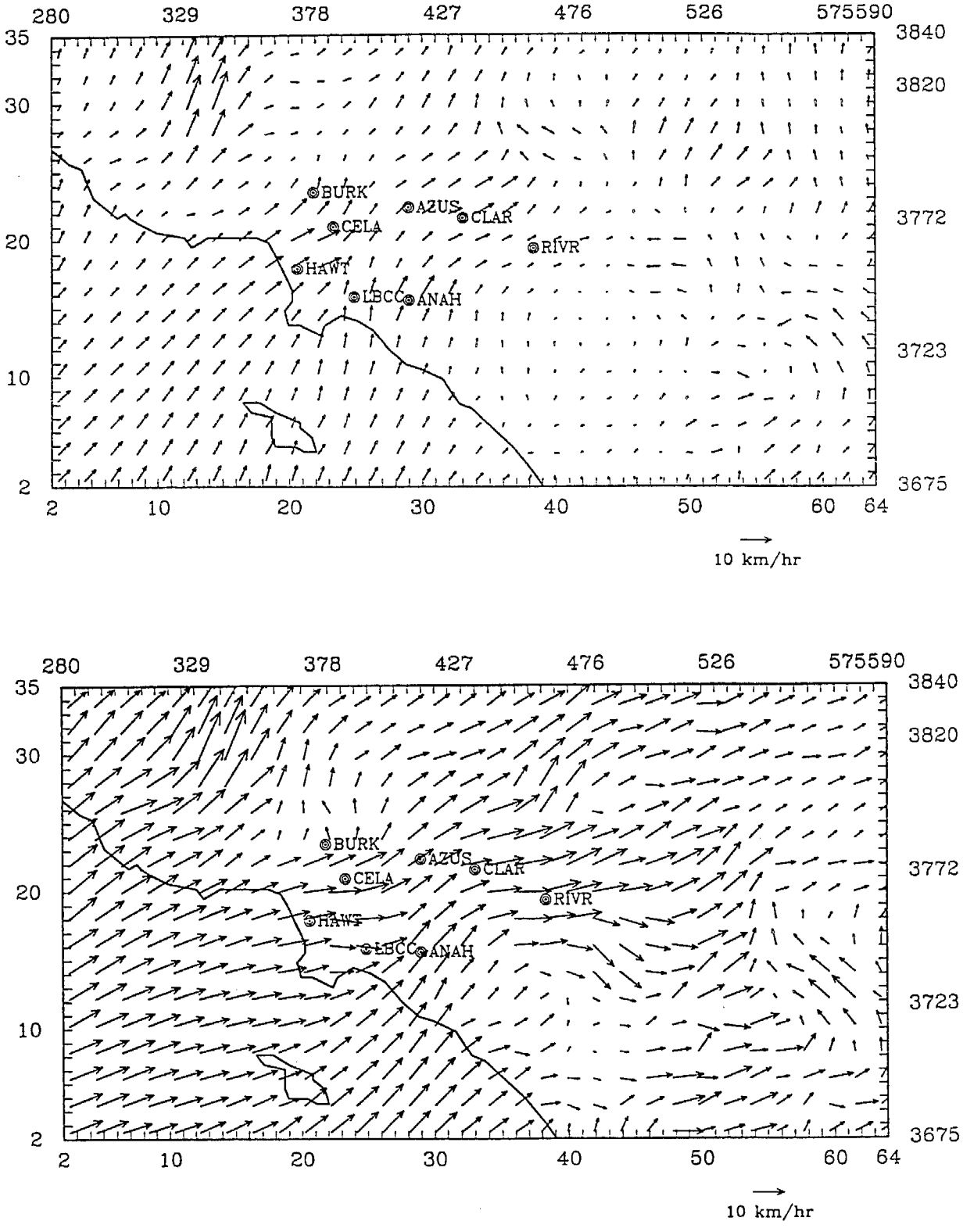

Figure 5-3. Surface layer windfield for hours 09 (top) and 15 (bottom) on June 24, 1987.

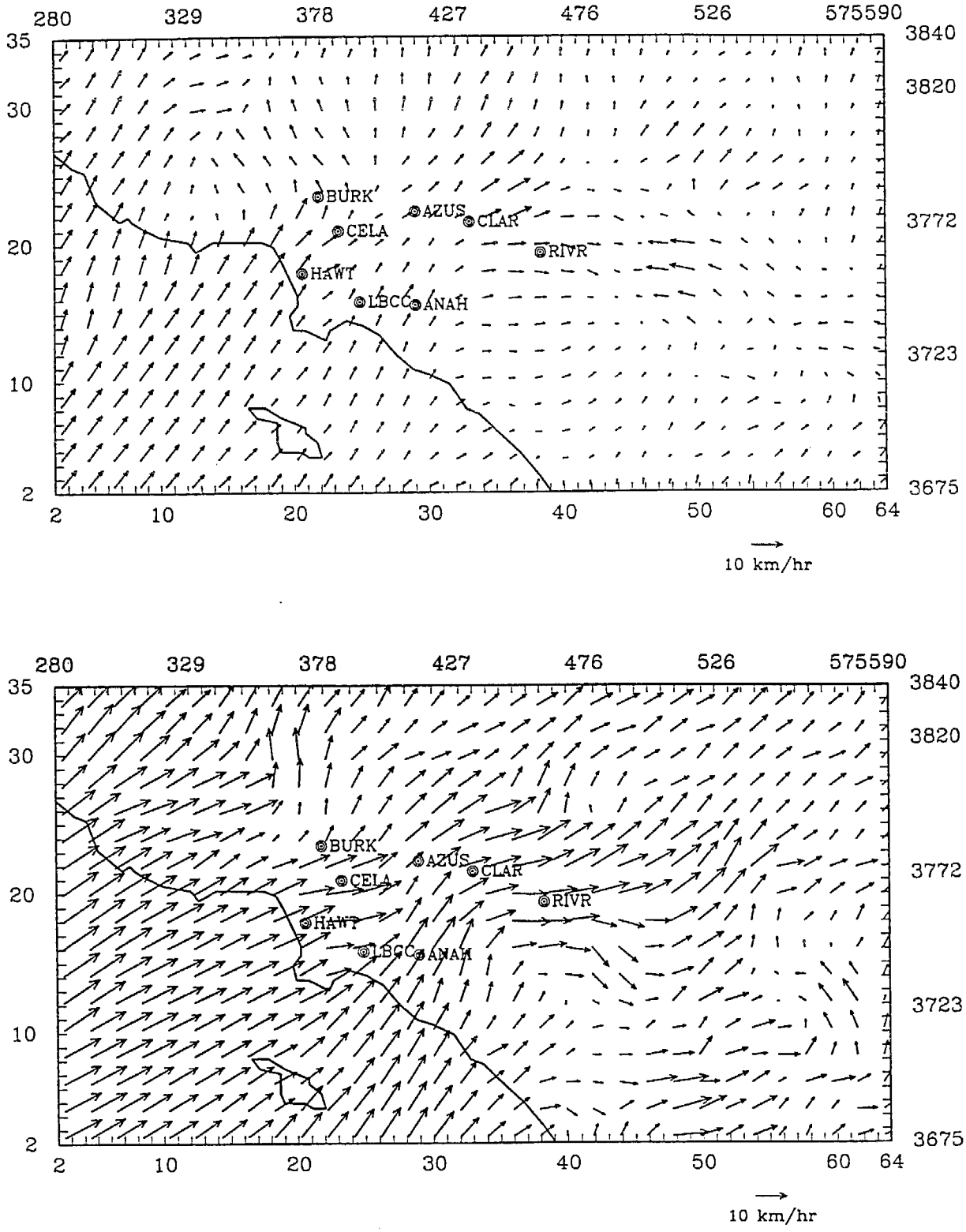

Figure 5-4. Surface layer windfield for hours 09 (top) and 15 (bottom) on June 25, 1987.

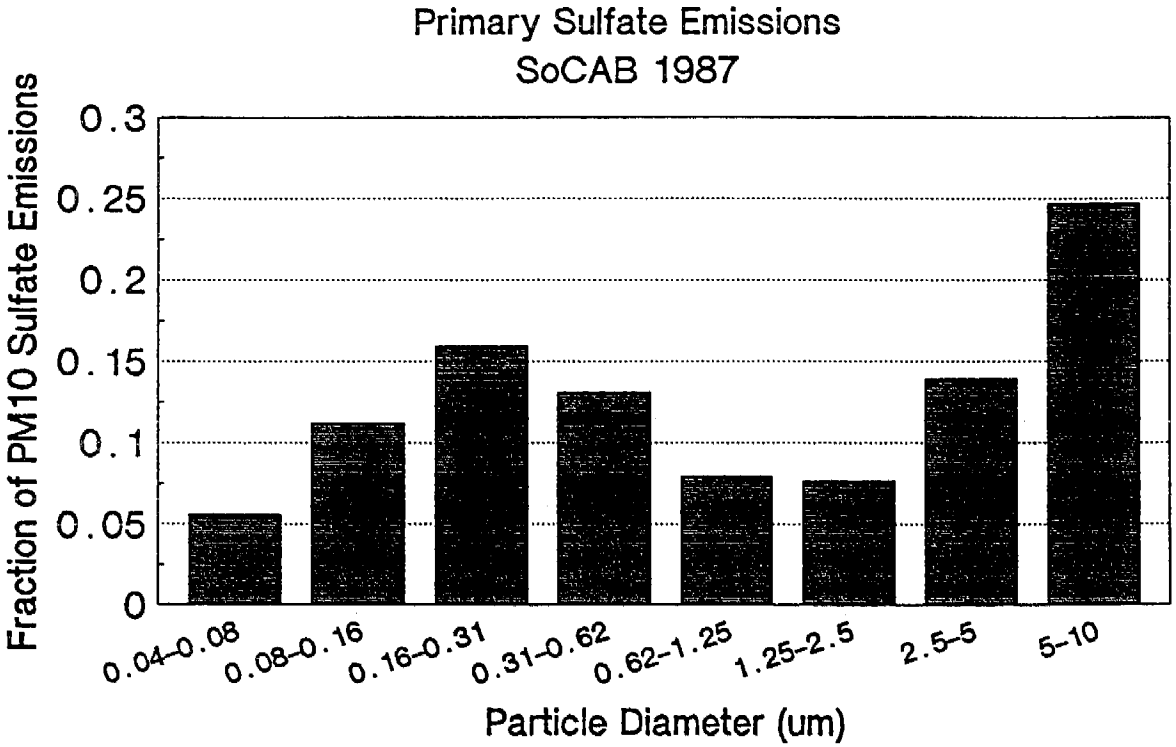

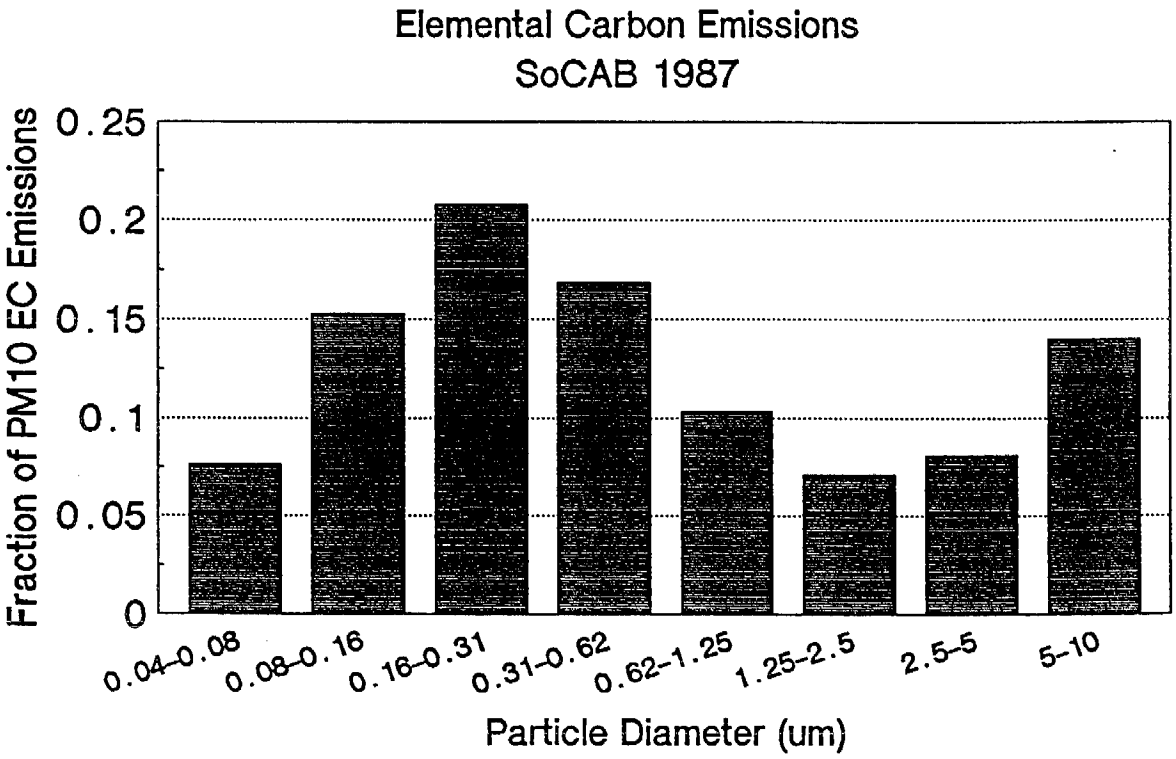

Figure 5-5. Estimated overall sulfate and elemental carbon emissions size distribution.

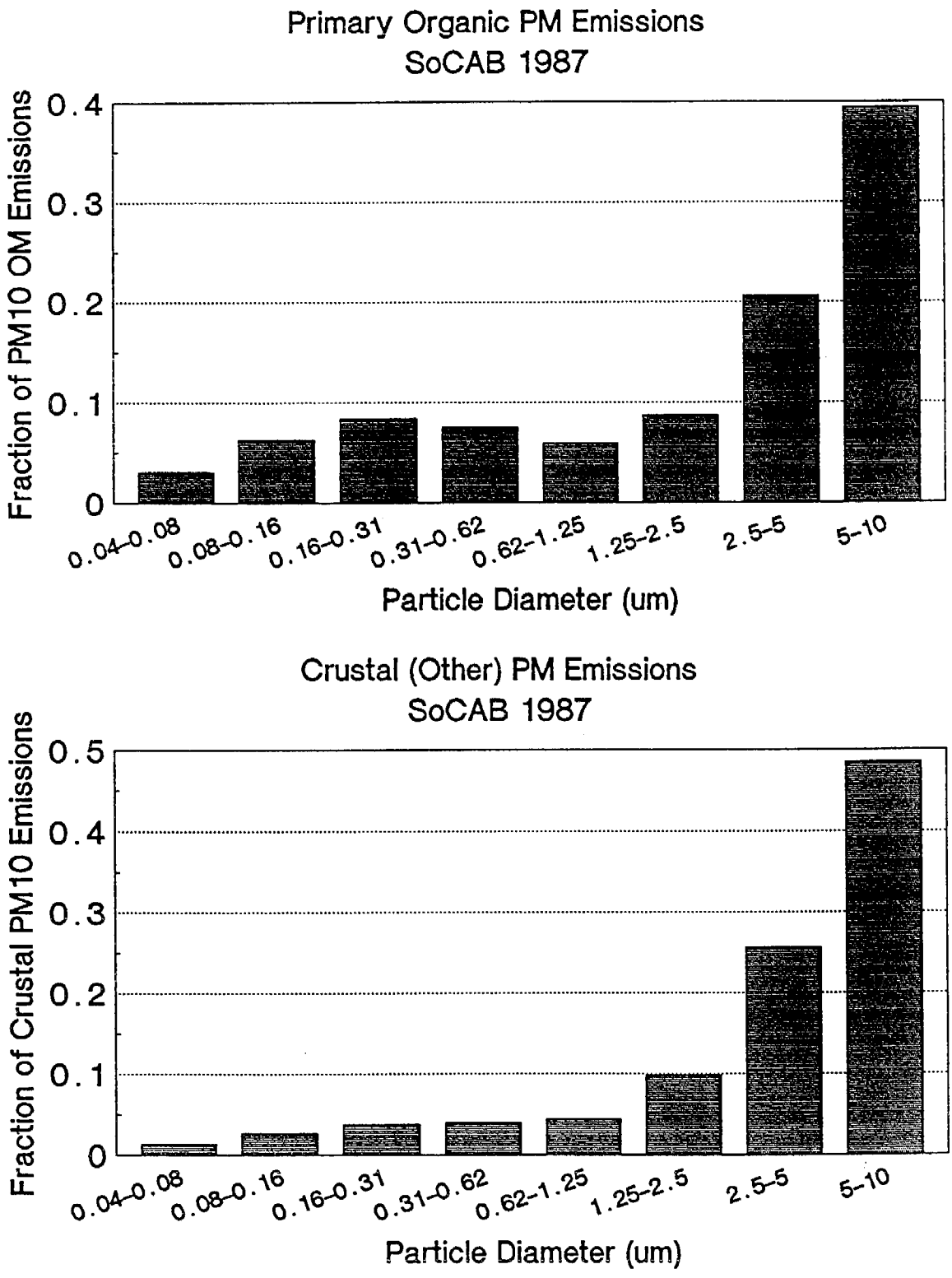

Figure 5-6. Estimated overall organic PM and crustal (other) PM emissions size distribution.

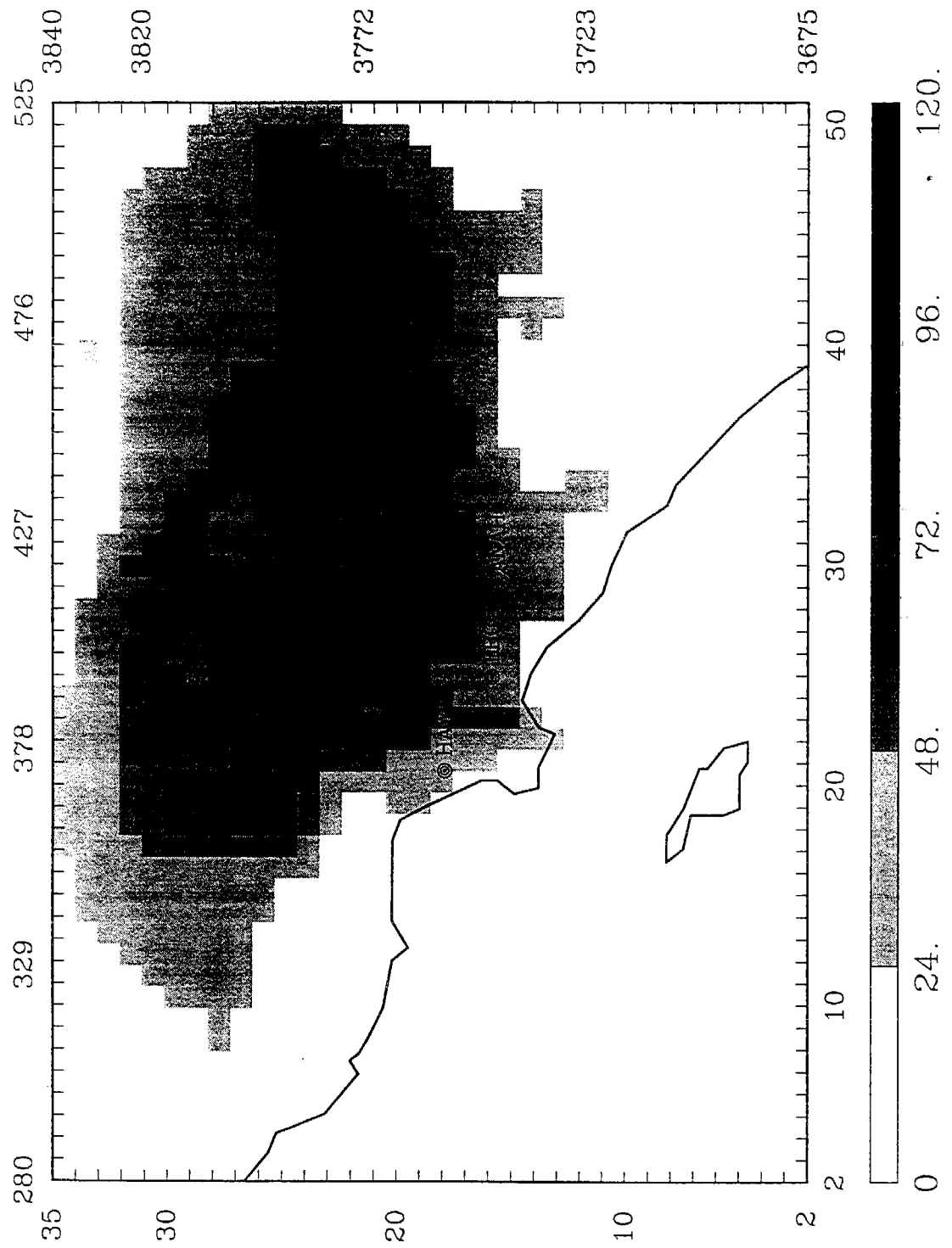

Figure 5-7. Predicted 24-hr average $PM_{2.5}$ mass concentration ($\mu g/m^3$) on June 24, 1987 for baseline case.

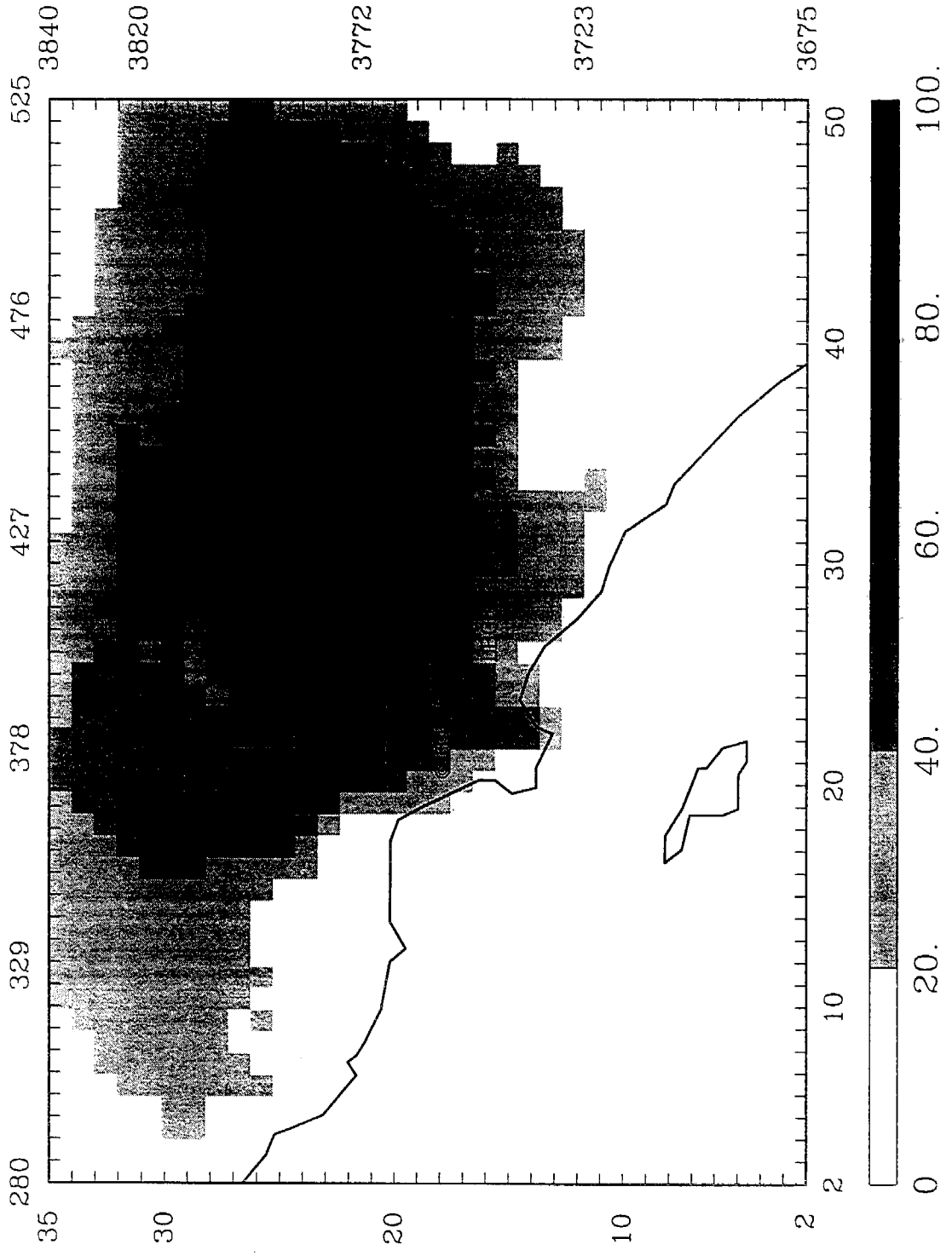

Figure 5-8. Predicted 24-hr average $PM_{2.5}$ mass concentration ($\mu g/m^3$) on June 25, 1987 for baseline case.

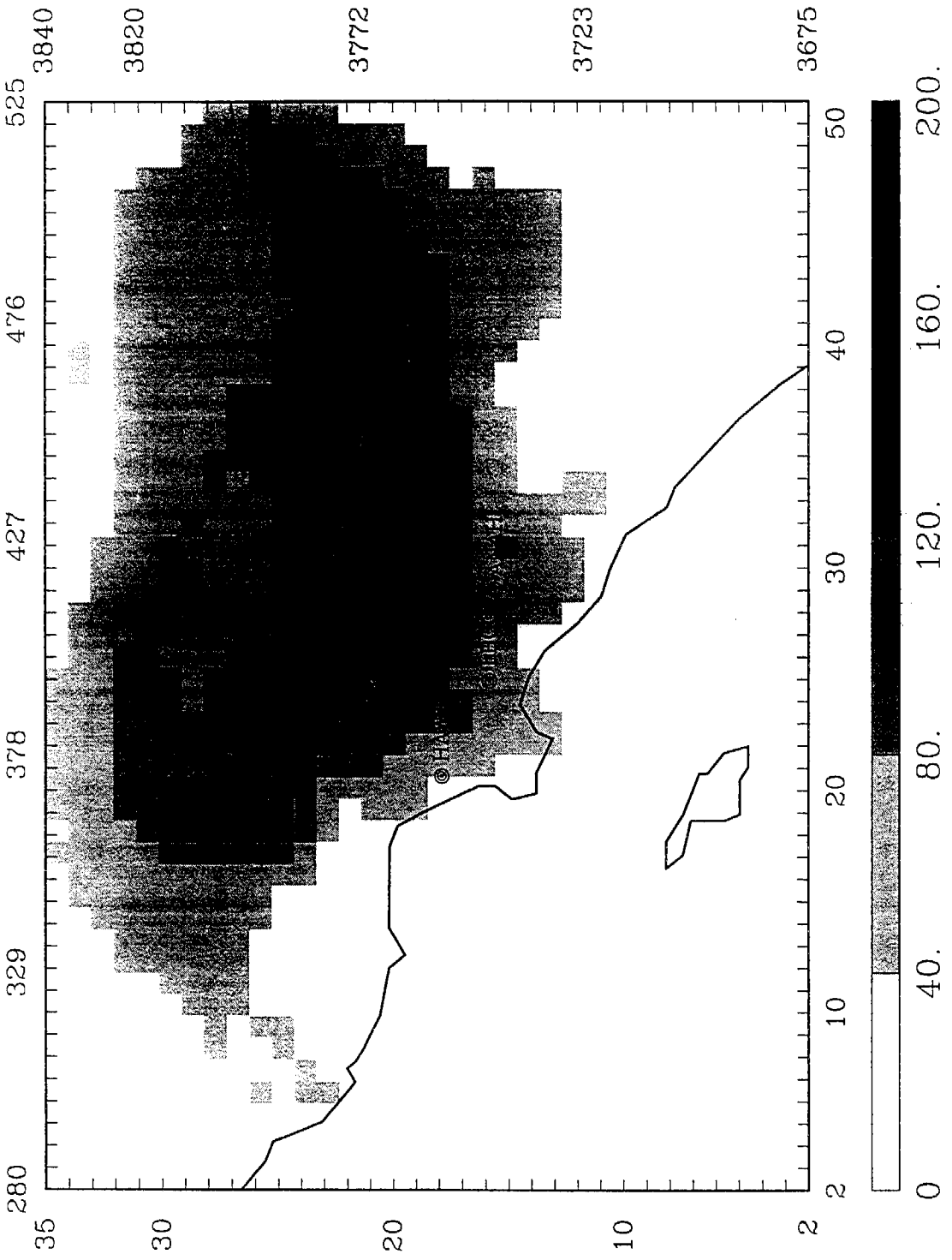

Figure 5-9. Predicted 24-hr average PM_{10} mass concentration ($\mu g/m^3$) on June 24, 1987 for baseline case.

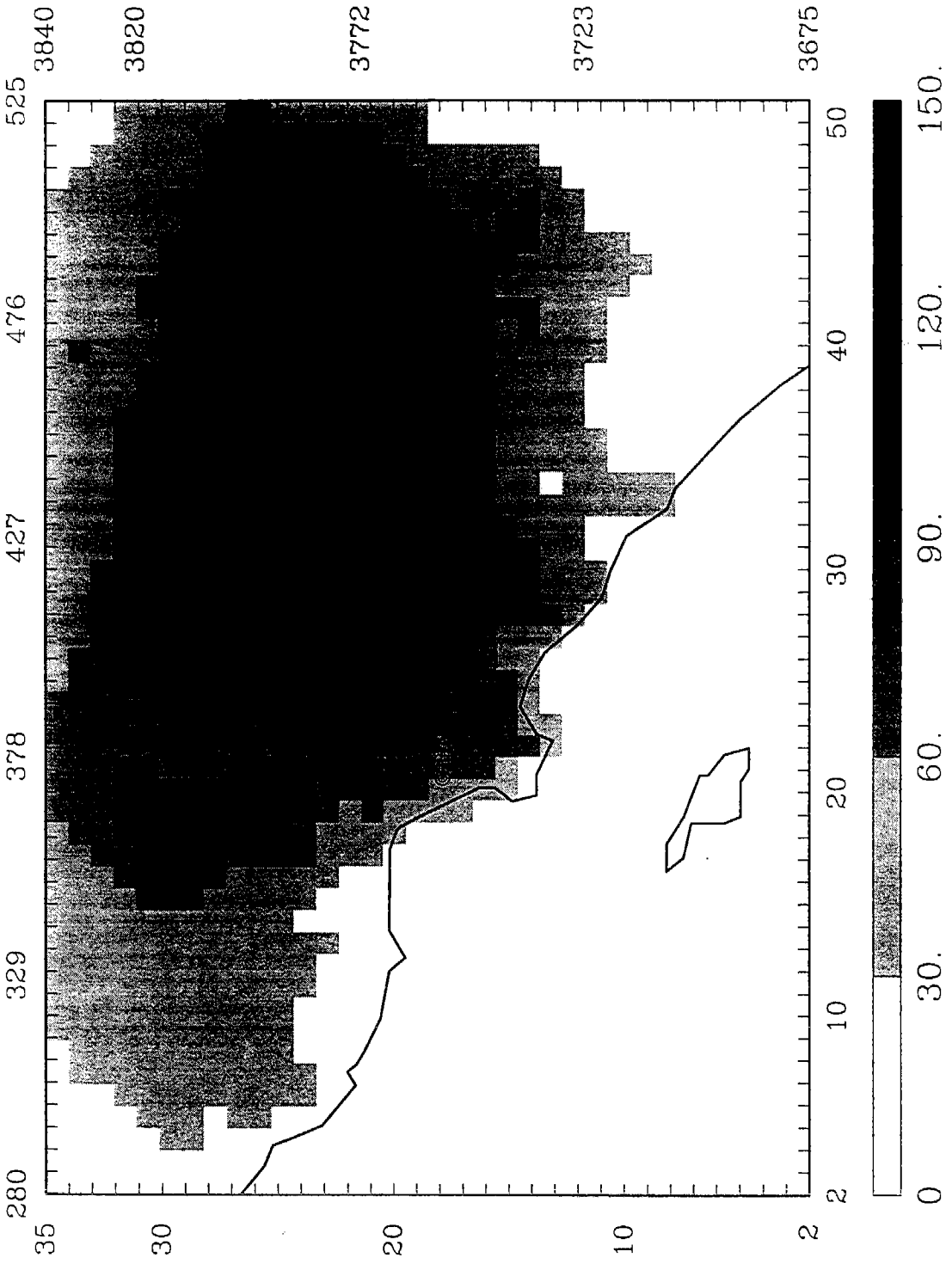

Figure 5-10. Predicted 24-hr average PM_{10} mass concentration ($\mu g/m^3$) on June 25, 1987 for baseline case.

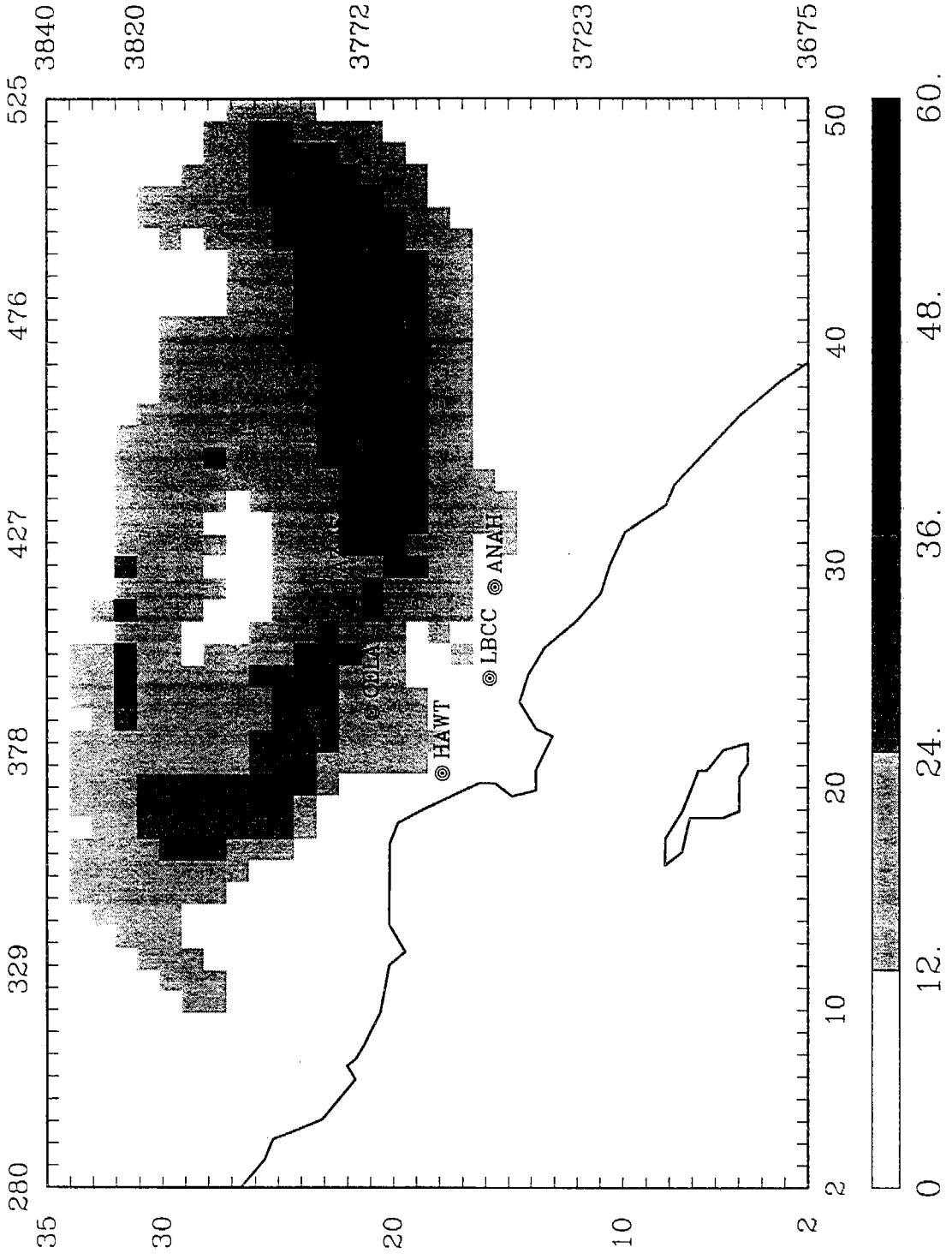

Figure 5-11. Predicted 24-hr average $PM_{2.5}$ NO_3 concentration ($\mu g/m^3$) on June 24, 1987 for baseline case.

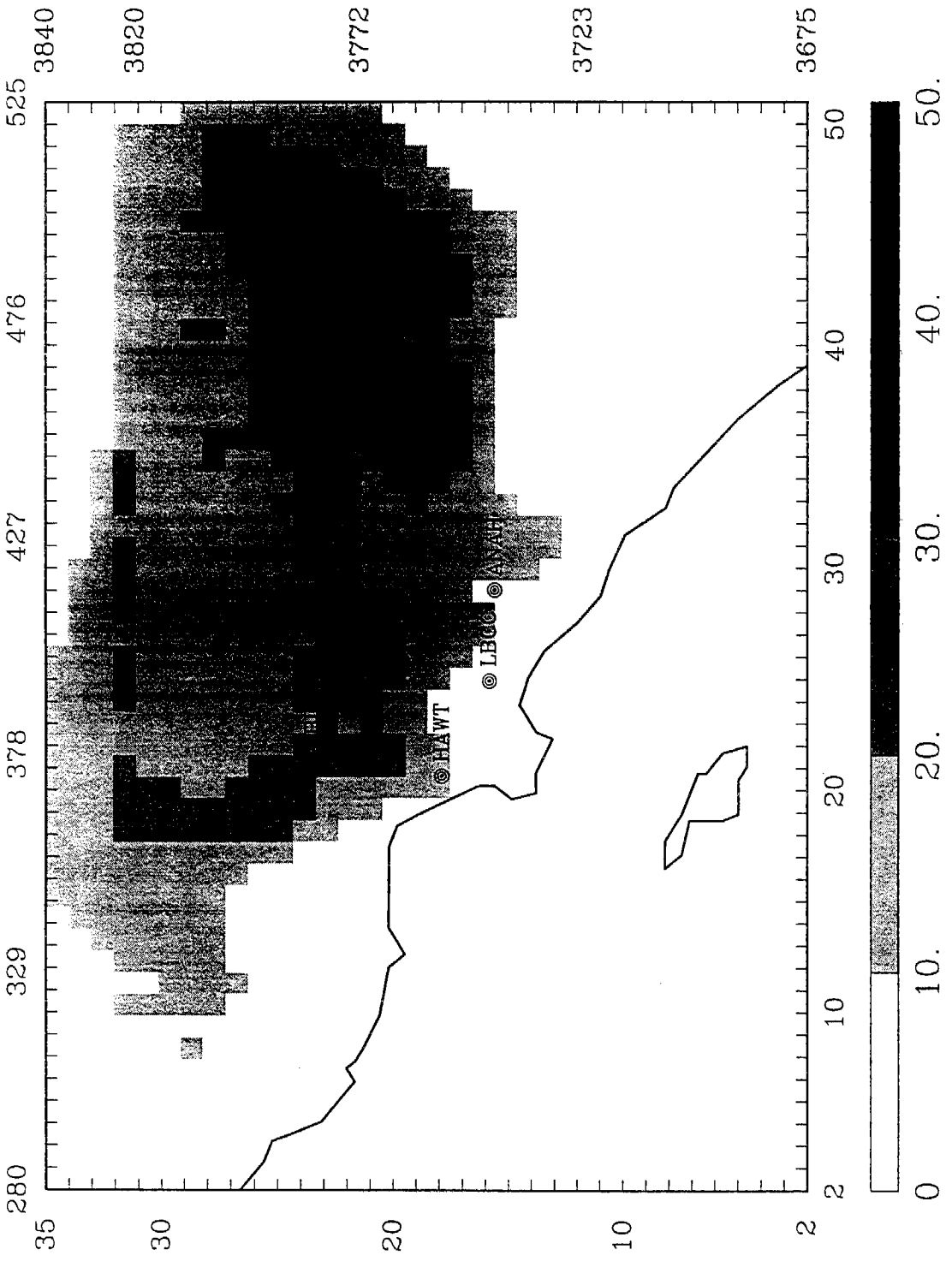

Figure 5-12. Predicted 24-hr average $PM_{2.5}$ NO_3 concentration ($\mu g/m^3$) on June 25, 1987 for baseline case.

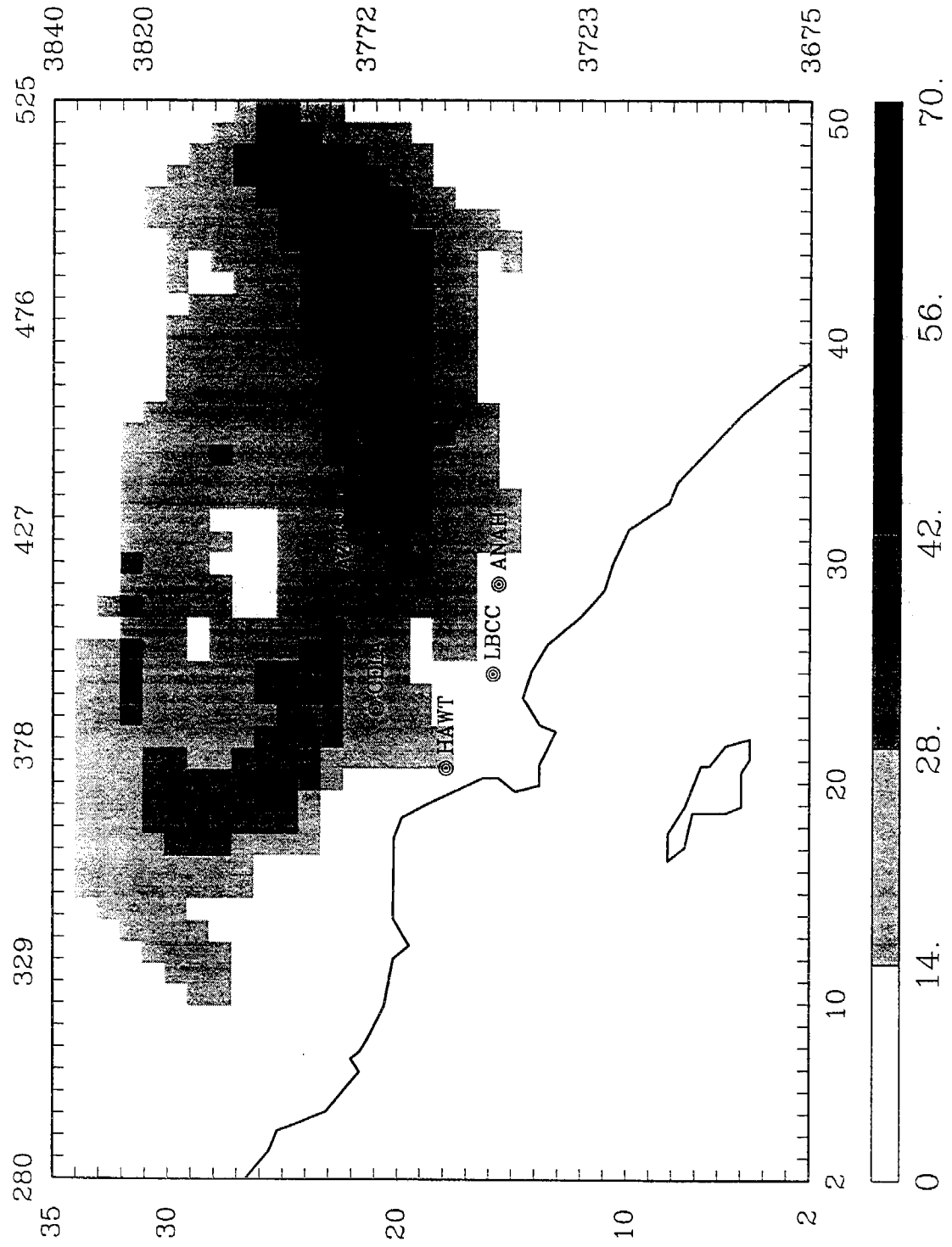

Figure 5-13. Predicted 24-hr average PM_{10} NO_3 concentration ($\mu g/m^3$) on June 24, 1987 for baseline case.

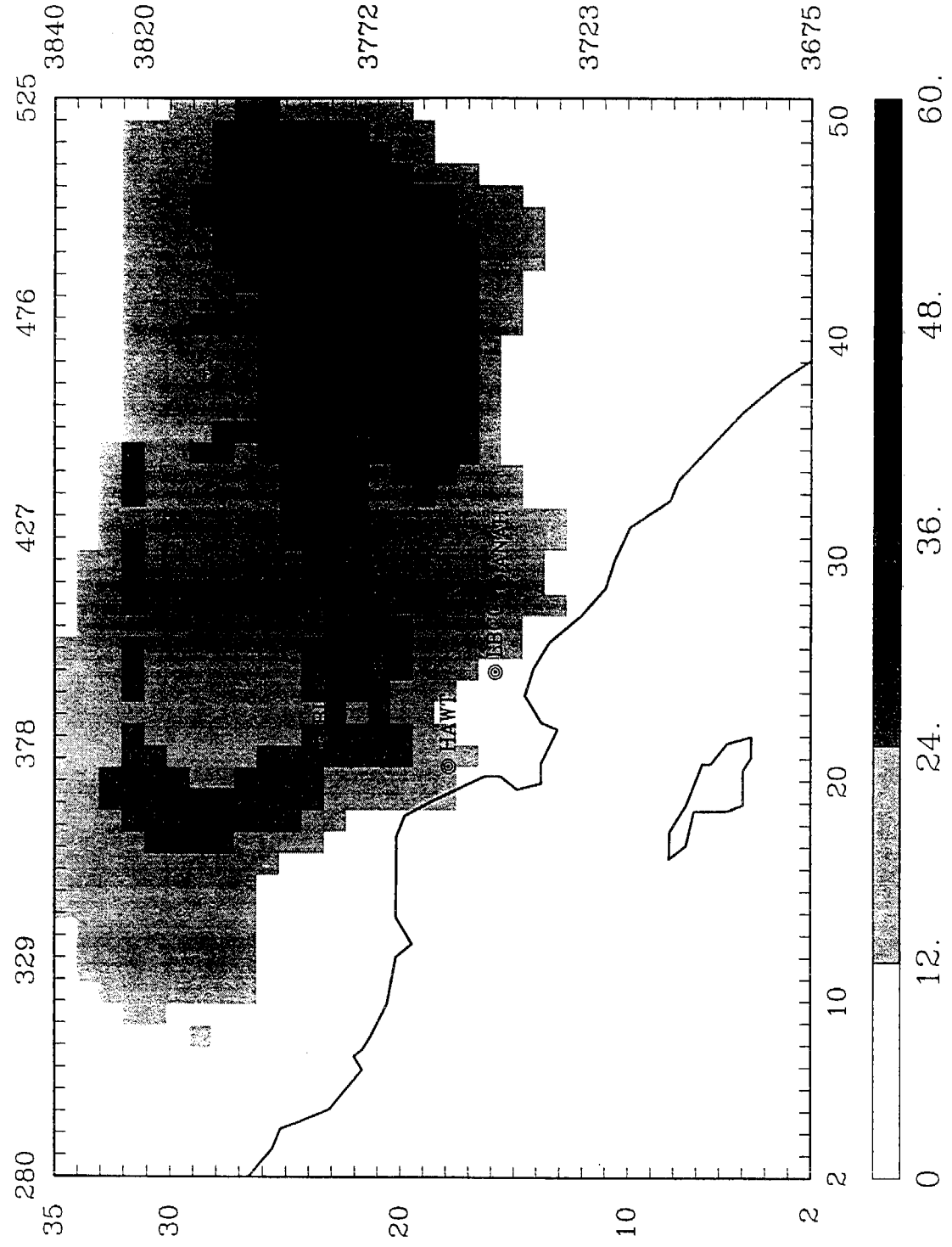

Figure 5-14. Predicted 24-hr average PM_{10} NO_3 concentration ($\mu g/m^3$) on June 25, 1987 for baseline case.

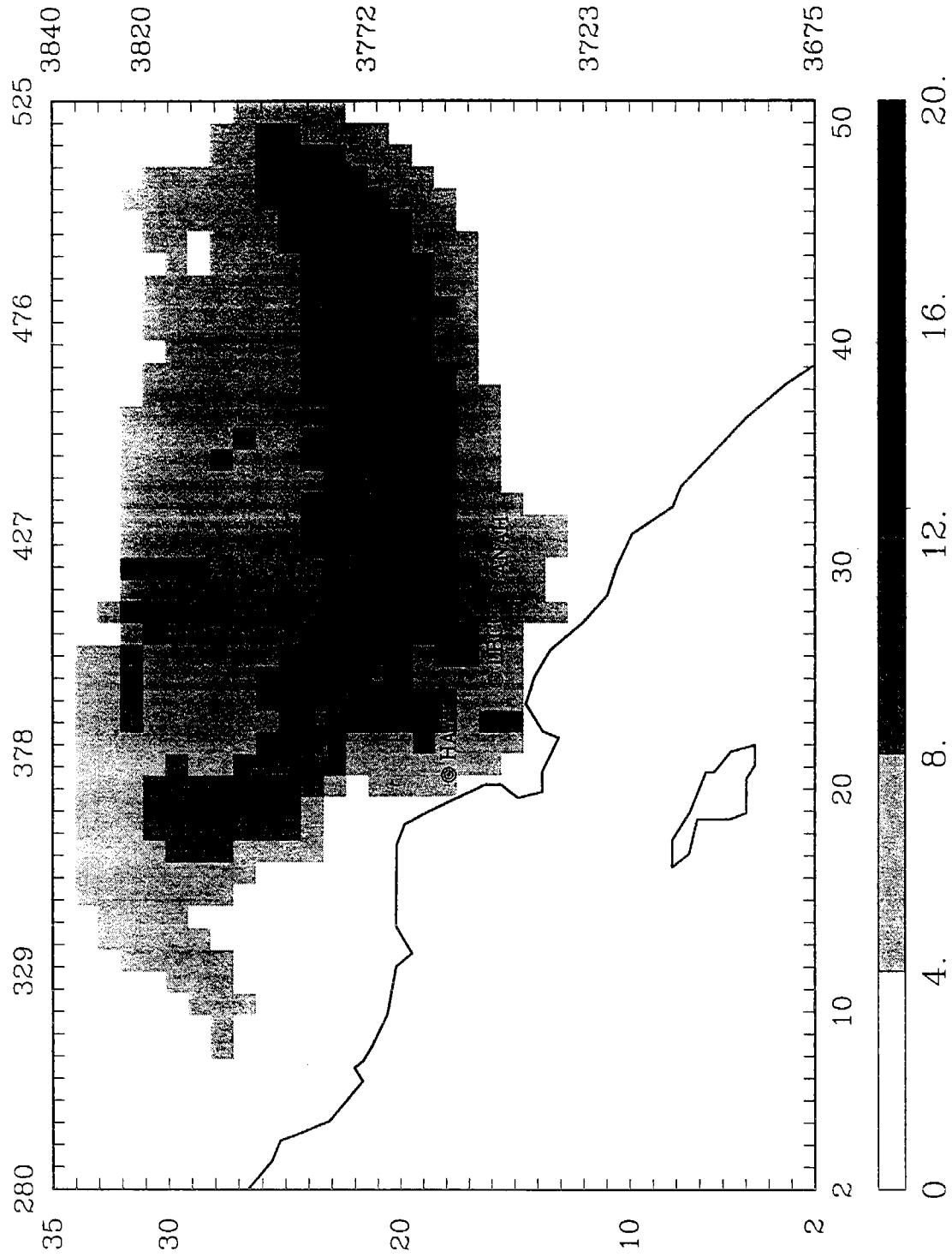

Figure 5-15. Predicted 24-hr average $PM_{2.5}$ NH_4 concentration ($\mu g/m^3$) on June 24, 1987 for baseline case.

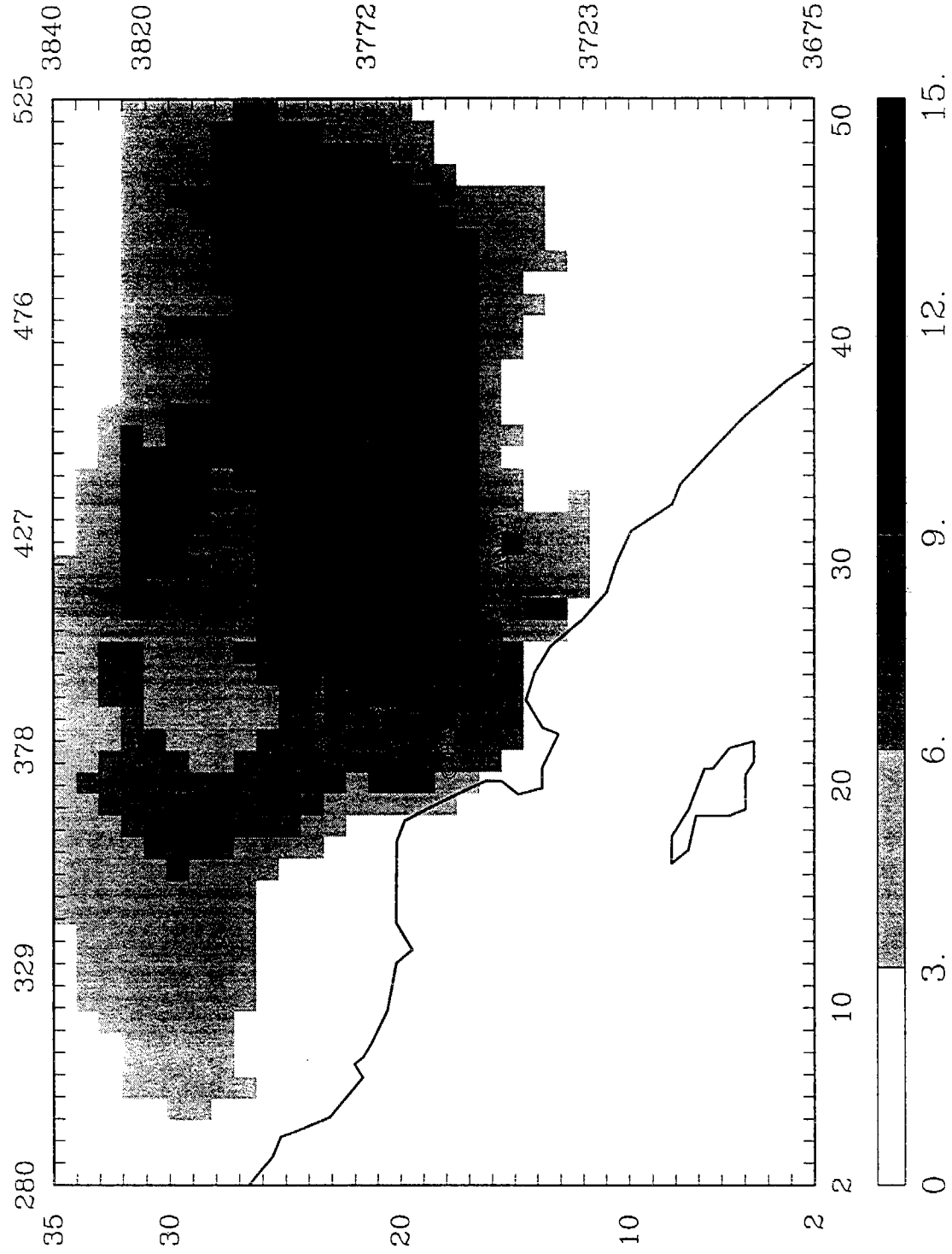

Figure 5-16. Predicted 24-hr average $PM_{2.5}$ NH_4 concentration ($\mu g/m^3$) on June 25, 1987 for baseline case.

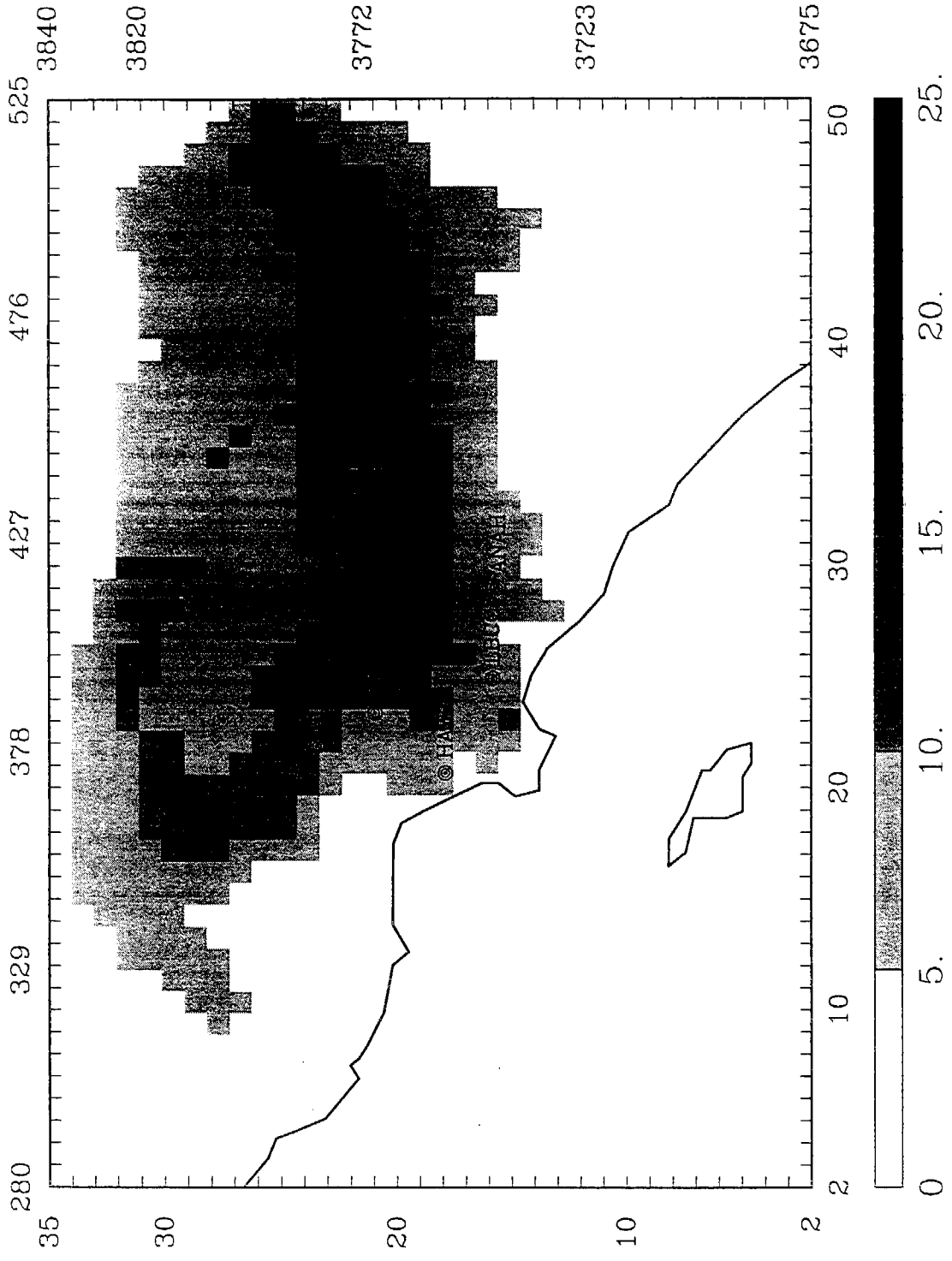

Figure 5-17. Predicted 24-hr average PM_{10} NH_4 concentration ($\mu g/m^3$) on June 24, 1987 for baseline case.

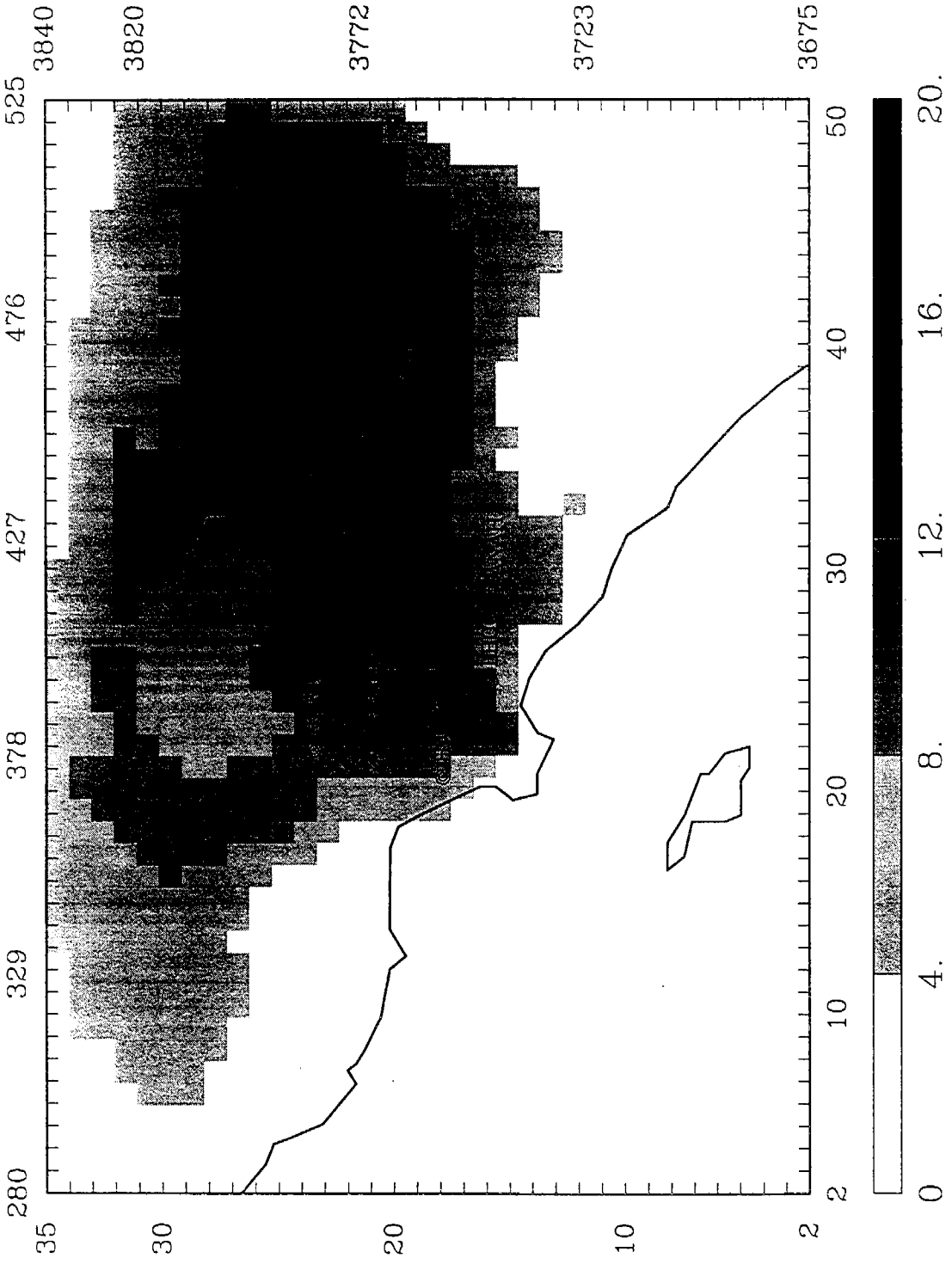

Figure 5-18. Predicted 24-hr average PM_{10} NH_4 concentration ($\mu g/m^3$) on June 25, 1987 for baseline case.

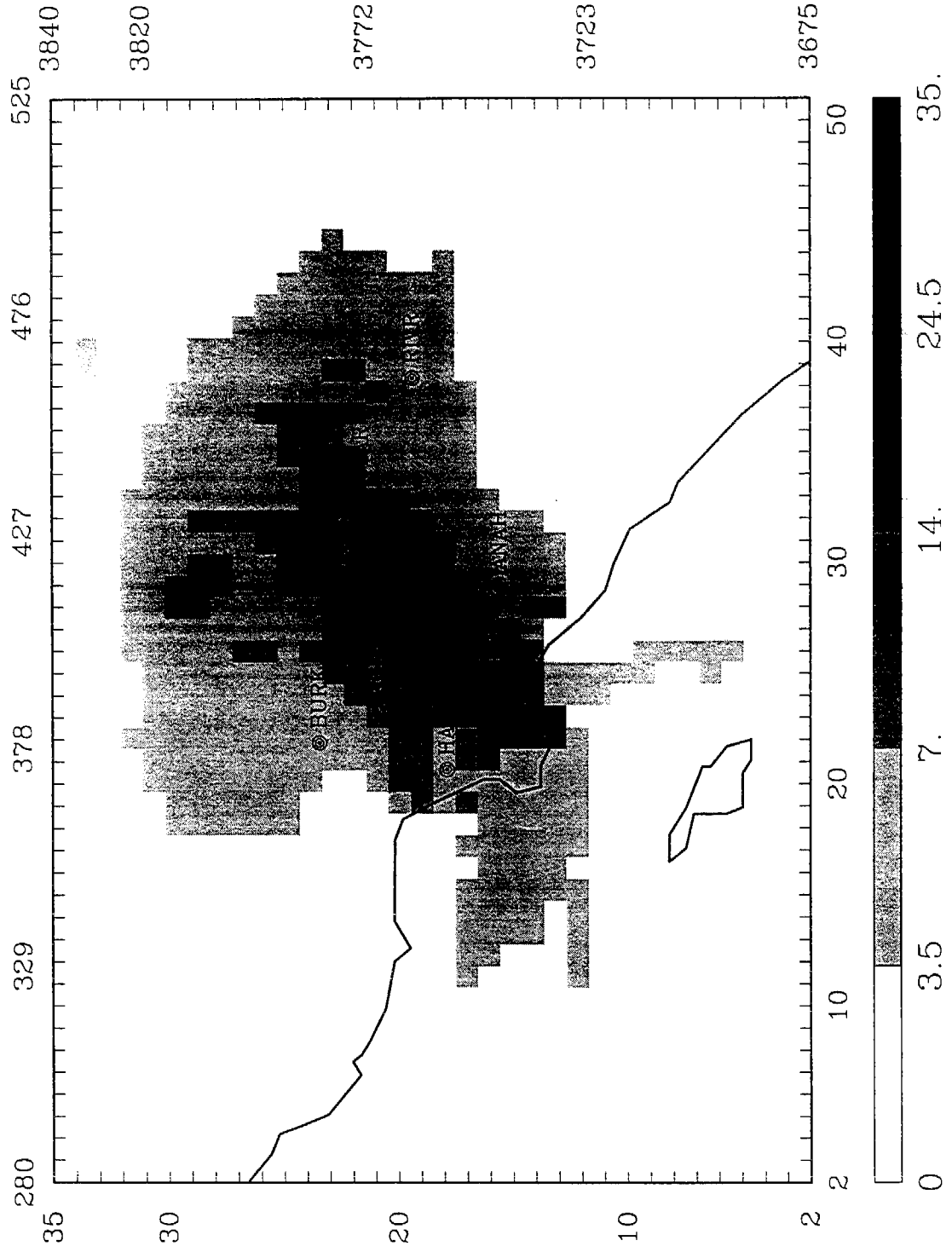

Figure 5-19. Predicted 24-hr average $PM_{2.5}$ SO_4 concentration ($\mu g/m^3$) on June 24, 1987 for baseline case.

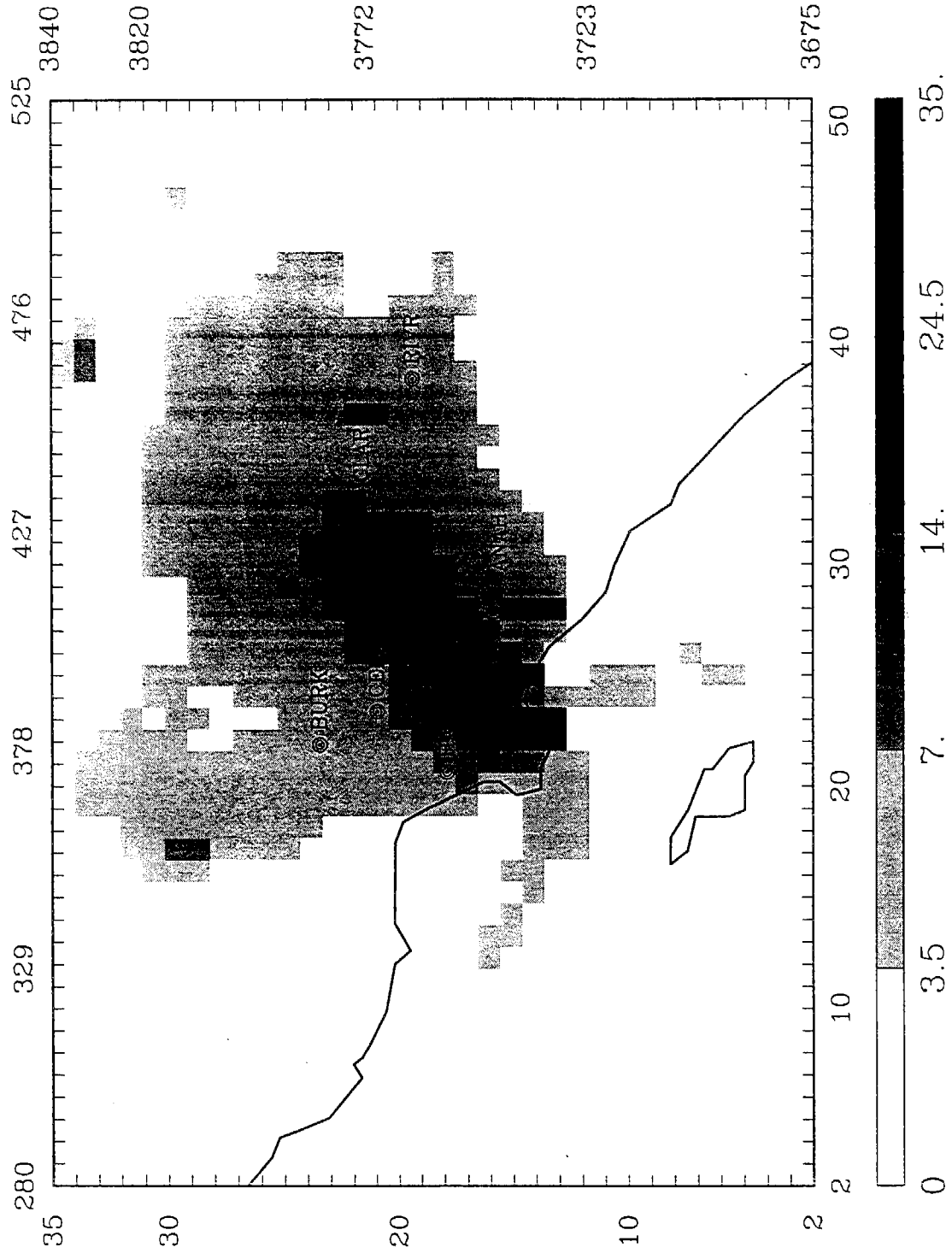

Figure 5-20. Predicted 24-hr average $PM_{2.5}$ SO_4 concentration ($\mu g/m^3$) on June 25, 1987 for baseline case.

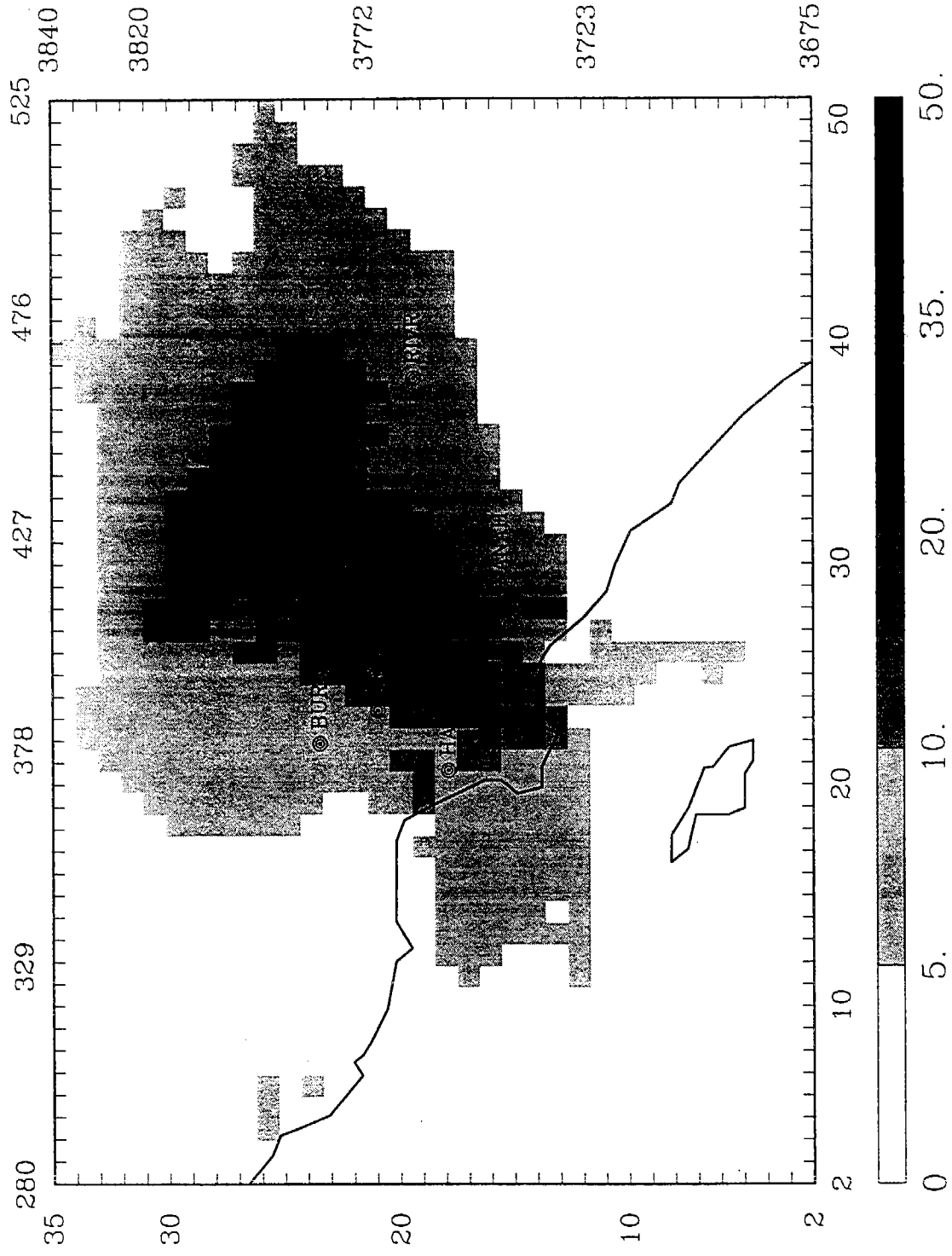

Figure 5-21. Predicted 24-hr average PM_{10} SO_4 concentration ($\mu g/m^3$) on June 24, 1987 for baseline case.

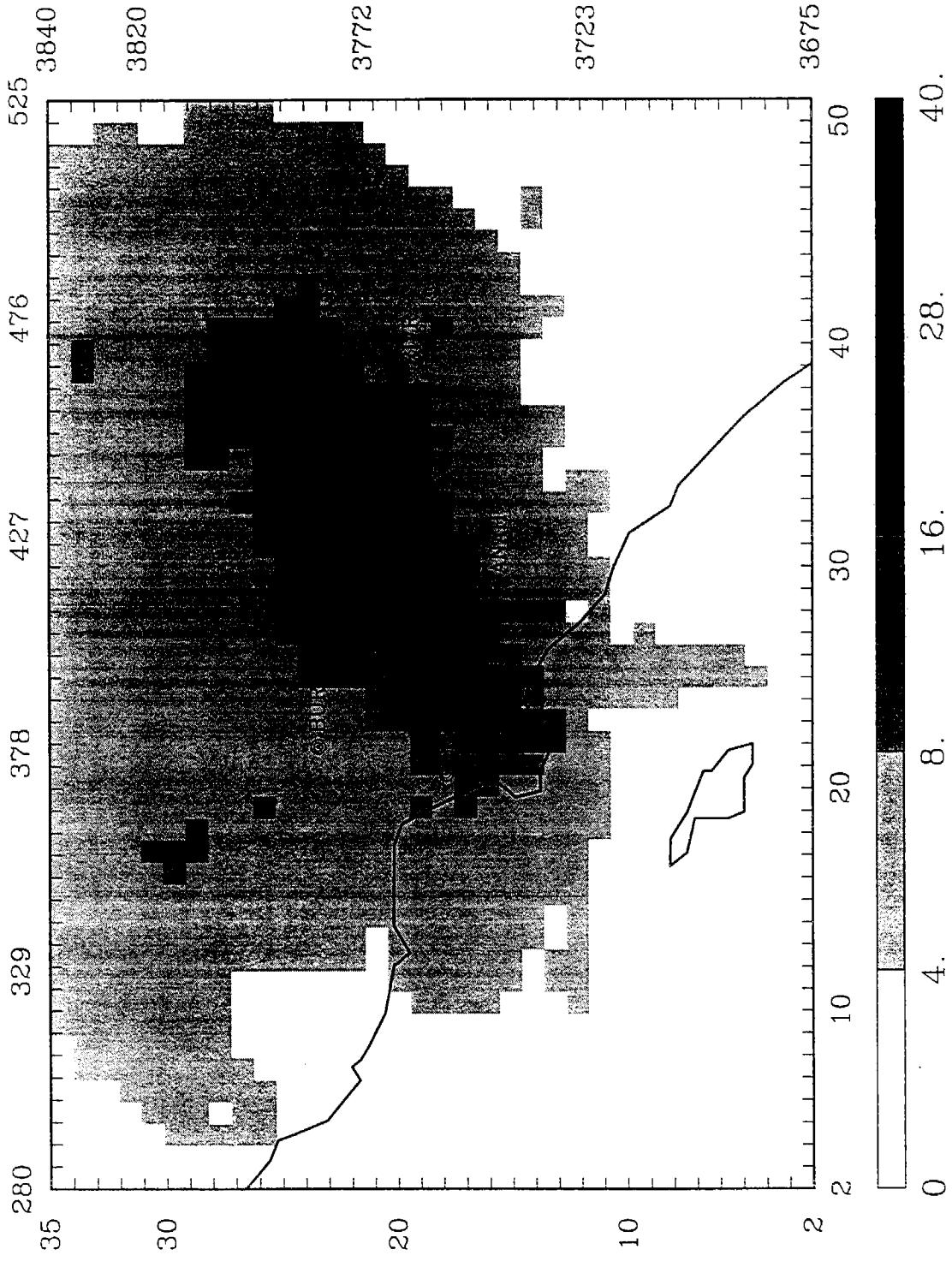

Figure 5-22. Predicted 24-hr average PM_{10} SO_4 concentration ($\mu g/m^3$) on June 25, 1987 for baseline case.

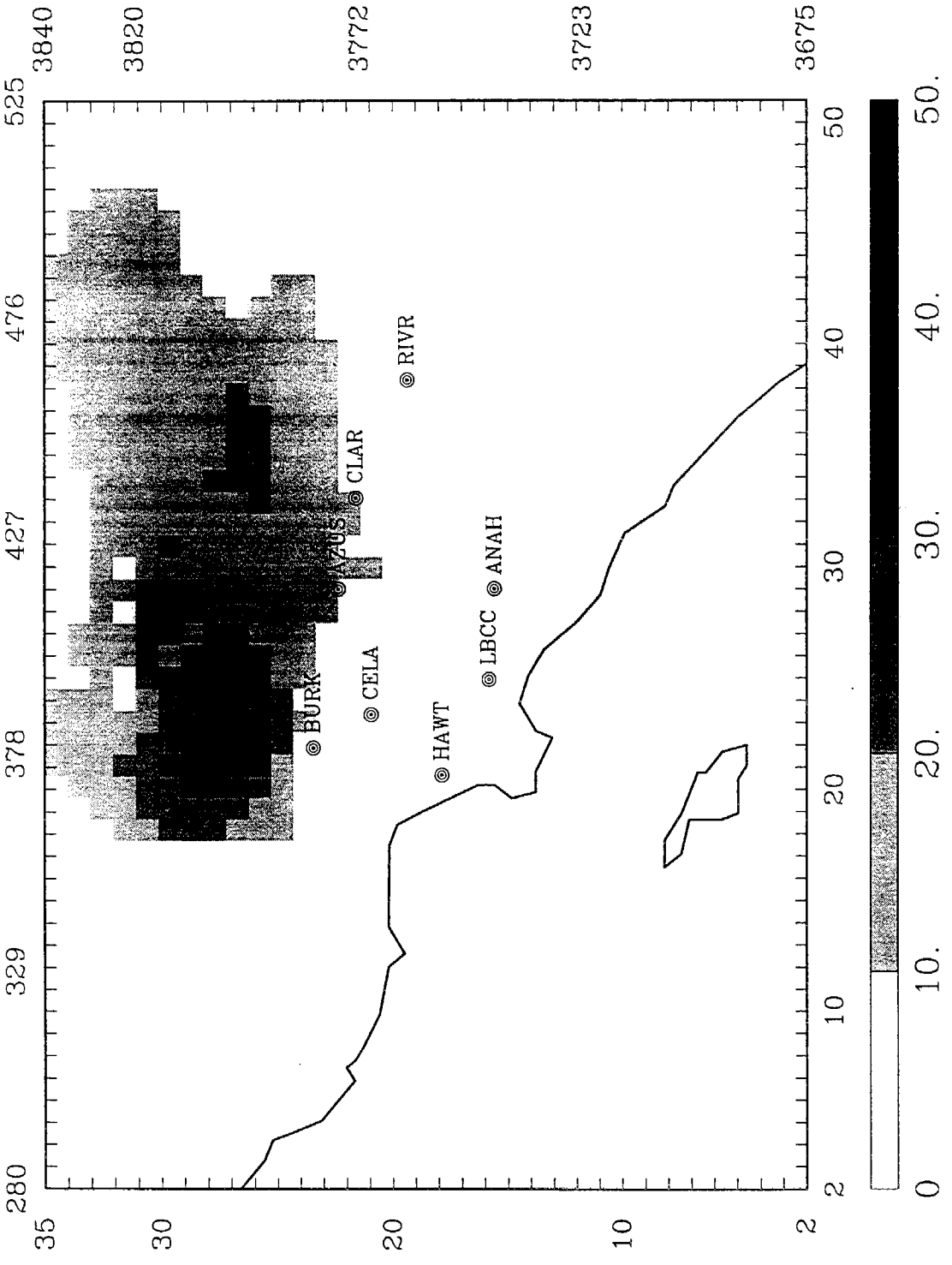

Figure 5-23. Predicted 24-hr average HNO_3 concentration (ppb) on June 24, 1987 for baseline case.

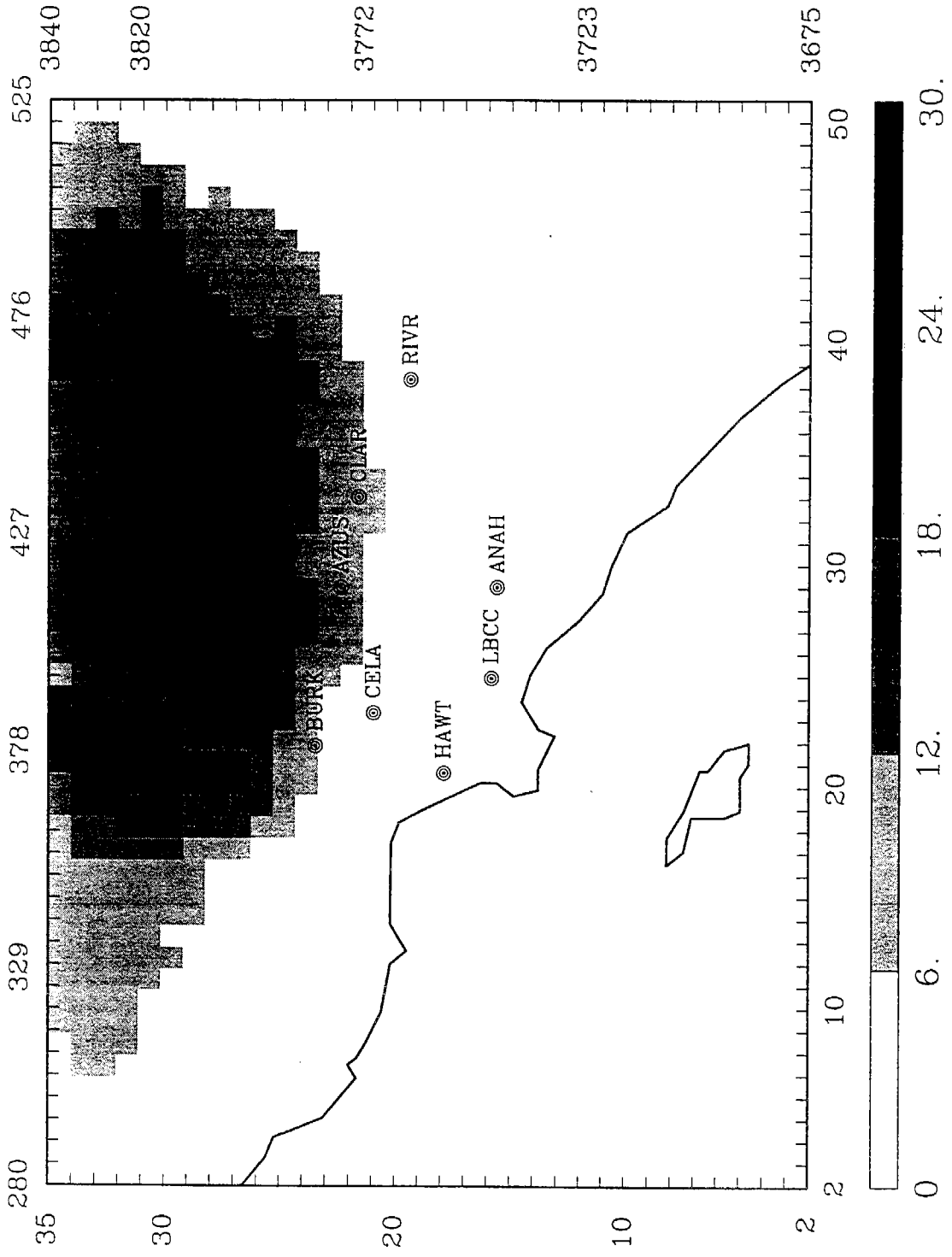

Figure 5-24. Predicted 24-hr average HNO_3 concentration (ppb) on June 25, 1987 for baseline case.